nagra National Cooperative for the Disposal of Radioactive Waste

TECHNICAL REPORT 91-34

GRIMSEL TEST SITE

OVERVIEW OF NAGRA FIELD AND MODELING ACTIVITIES IN THE VENTILATION DRIFT (1988 – 1990)

MARCH 1992

S. Vomvoris[1] and B. Frieg[1] (eds)

P. Bossart[2], C. Gmünder[3]
P. Heiniger[4], O. Jaquet[5], K. Watanabe[6]

1) NAGRA, Wettingen
2) Kellerhals & Häfeli AG; Bern Geotechnical Institute AG, Bern
3) Simultec AG, Meilen
4) Solexperts AG, Schwerzenbach; Suiselectra AG, Biel
5) Colenco AG, Dättwil
6) Saitama University, Urawa, Japan

GRIMSEL TEST SITE / SWITZERLAND
A JOINT RESEARCH PROGRAM BY

- NAGRA – National Cooperative for the Disposal of Radioactive Waste, Wettingen, Switzerland
- BGR – Federal Institute for Geoscience and Natural Resources, Hannover, Federal Republic of Germany
- GSF – Research Centre for Environmental Sciences, Munich, Federal Republic of Germany

Hardstrasse 73, CH-5430 Wettingen / Switzerland, Telephone +41-56-37 11 11

nagra National Cooperative for the Disposal of Radioactive Waste

TECHNICAL REPORT 91-34

GRIMSEL TEST SITE

OVERVIEW OF NAGRA FIELD AND MODELING ACTIVITIES IN THE VENTILATION DRIFT (1988 – 1990)

MARCH 1992

S. Vomvoris[1] and B. Frieg[1] (eds)

P. Bossart[2], C. Gmünder[3]
P. Heiniger[4], O. Jaquet[5], K. Watanabe[6]

1) NAGRA, Wettingen
2) Kellerhals & Häfeli AG; Bern Geotechnical Institute AG, Bern
3) Simultec AG, Meilen
4) Solexperts AG, Schwerzenbach; Suiselectra AG, Biel
5) Colenco AG, Dättwil
6) Saitama University, Urawa, Japan

GRIMSEL TEST SITE / SWITZERLAND
A JOINT RESEARCH PROGRAM BY

- NAGRA – National Cooperative for the Disposal of Radioactive Waste, Wettingen, Switzerland
- BGR – Federal Institute for Geoscience and Natural Resources, Hannover, Federal Republic of Germany
- GSF – Research Centre for Environmental Sciences, Munich, Federal Republic of Germany

Hardstrasse 73, CH-5430 Wettingen / Switzerland, Telephone +41-56-37 11 11

FOREWORD

Concepts for the disposal of radioactive waste in geological formations place a significant emphasis on acquiring extensive knowledge of the proposed host rock and the surrounding strata. For this reason, Nagra has, since May 1984, been operating the **Grimsel Test Site (GTS)** which is located at a depth of 450 m in the crystalline rock of the Aare Massif of the Central Swiss Alps. The general objectives of the research being carried out in this underground laboratory include

- the build-up of know-how in planning, performing and interpreting field experiments in various scientific and technical disciplines and

- the acquisition of practical experience in the development of investigation methodologies, measuring techniques and test equipment which will be of use during actual repository site explorations.

The GTS is operated by Nagra and, on the basis of a German-Swiss co-operative agreement, various experiments are carried out by Nagra, the "Bundesanstalt für Geowissenschaften und Rohstoffe, Hannover" (BGR) and the "Forschungszentrum für Umwelt und Gesundheit, München" (GSF). The Grimsel projects of both GSF and BGR are supported by the German Federal Ministry for Research and Technology (BMFT). NTB 85-46 (German version NTB 85-47) provide an overview of the German-Swiss investigation programme. In a special issue of the Nagra Bulletin 1988 (German version "Nagra Informiert 1+2/1988") the status of the programme up to 1988 is described.

VORWORT

Bei Konzepten, welche die Endlagerung radioaktiver Abfälle in geologischen Formationen vorsehen, ist die Kenntnis des Wirtgesteins und der angrenzenden Gesteinsschichten von grundlegender Bedeutung. Die Nagra betreibt deshalb seit Mai 1984 das **Felslabor Grimsel (FLG)** in 450 m Tiefe im Kristallin des Aarmassivs. Die generelle Zielsetzung für die Arbeiten in diesem System von Versuchsstollen umfasst

- den Aufbau von Know-how in der Planung, Ausführung und Interpretation von Untergrundversuchen in verschiedenen wissenschaftlichen und technischen Fachgebieten, und

- den Erwerb praktischer Erfahrung in der Entwicklung und der Anwendung von Untersuchungsmethoden, Messverfahren und Messgeräten, die für die Erkundung von potentiellen Endlagerstandorten in Frage kommen.

Im Felslabor der Nagra werden, auf der Basis eines deutsch-schweizerischen Zusammenarbeitsvertrages, verschiedene Versuche von den beiden deutschen Partnern Bundesanstalt für Geowissenschaften und Rohstoffe, Hannover (BGR) und Forschungszentrum für Umwelt und Gesundheit GmbH, München (GSF) durchgeführt. Das Deutsche Bundesministerium für Forschung und Technologie (BMFT) fördert die Arbeiten der BGR und der GSF im FLG. Der NTB 85-47 (englische Version NTB 85-46) enhält eine Uebersicht des FLG und die Zusammenfassung der Untersuchungsprogramme mit Status August 1985. In der Ausgabe 1+2/1988 des Heftes "Nagra informiert" bzw. der englischen Spezialausgabe "Nagra Bulletin 1988" ist der Stand der Arbeiten anfangs 1988 beschrieben.

Der vorliegende Bericht wurde im Rahmen der erwähnten Zusammenarbeitsverträge erstellt. Die Autoren haben ihre eigenen Ansichten und Schlussfolgerungen dargelegt. Diese müssen nicht unbedingt mit denjenigen der Nagra oder des beteiligten Partner übereinstimmen.

AVANT - PROPOS

Lors d'études de concepts de stockage de déchets radioactifs dans des formations géologiques, on attache une grande importance à l'acquisition d'informations étendues sur la roche d'accueil et les formations rocheuses environnantes. C'est pour cette raison que la Cédra exploite depuis mai 1984 son **laboratoire souterrain du Grimsel (LSG)** situé à 450 m de profondeur dans le cristallin du massif de l'Aar, situé au milieu des Alpes centrales. Les principaux objectifs des recherches effectuées dans ce réseau de galeries comprennent:

- l'acquisition de savoir-faire dans diverses disciplines techniques et scientifiques en ce qui concerne la conception, la réalisation et l'interprétation d'expériences in situ, ainsi que

- l'accumulation d'expériences pratiques dans la mise au point et l'application de méthodes d'investigation, de techniques et d'appareillages de mesure, qui pourraient être utilisés lors de l'exploration de sites potentiels de dépôts finals.

Le LSG est exploité par la Cédra et diverses expériences y sont réalisées par celle-ci et deux institutions allemandes: la "Bundesanstalt für Geowissenschaften und Rohstoffe, Hannover" (BGR) et le "Forschungszentrum für Umwelt und Gesundheit GmbH, München" (GSF) dans le cadre d'un traité de collaboration germano-suisse. Les projets poursuivis au Grimsel par la BGR et le GSF sont financés par le Ministère fédéral allemand de la recherche et de la technologie (BMFT). Les rapports NTB 85-46 (version anglaise) et NTB 85-47 (version allemande) présentent un aperçu du laboratoire souterrain et un résumé des programmes de recherches avec état au mois d'août 1985. L'état d'avancement de ce programme en 1988 est présenté dans la publication "Cédra informe 1+2/1988" (version française) et "Nagra informiert 1+2/1988" (version allemande), ainsi que dans une édition spéciale en anglais (Nagra Bulletin 1988).

ABSTRACT

The first phase of the Ventilation Test (VE) in the Grimsel Test Site (GTS) was mainly carried out by "GSF-Forschungszentrum für Umwelt und Gesundheit GmbH, Institut für Tieflagerung" between 1983 and 1987. During the phase 2 of the VE (1988 - 1990) Nagra participated actively in this test, contributing to the program with complementary field work and model development.

A short overview of Nagra's field- and modeling work as well as the corresponding results is presented in this report. Structural remapping of the ventilation drift assisted in an improved understanding of the flow path geometry. The effects of the observed heterogeneity of the deformation structures on water inflow variations into the drift and on the approach for macropermeability estimation are evaluated. Complementary methods for water inflow measurements are presented, with the emphasis on the newly developed evaporation-measurement method, where the evaporation rate at discrete points at the drift surface can be measured. Finally, highlights of the drilling campaign and the related hydrogeological tests are presented in chapter four. The objective of these tests was to investigate the geometry and deformation of the shear zone observed in the drift as well as to provide a hydrogeological characterisation of this discontinuity.

The modeling work was twofold: a validation experiment, where a prognosis of interval pressures is made prior to the drilling and compared to the results; the further development of inverse methodology in conjuction with geostatistical analysis. Both approaches give valuable information about the permeability variations in tectonically different deformed granitic host rocks.

The hydraulic conductivity and transmissivity derived by the different methods is compared in the last chapter. All methods converge to a permeability in the shear zone about one order of magnitude higher than that of the matrix. The latter however, especially if derived by the classical ventilation tests, may be affected by the drying out of the drift wall and may underestimate the actual saturated matrix permeability value. As a concluding remark, it appears that ventilation tests for the estimation of macropermeability (granitic host rocks), are best suited if inflow fluxes are of the order of $1\ mg \cdot m^{-2} \cdot s^{-1}$.

ZUSAMMENFASSUNG

Die erste Phase des Ventilationstests (VE) im Felslabor Grimsel (FLG) wurde zur Hauptsache vom "GSF-Forschungszentrum für Umwelt und Gesundheit GmbH, Institut für Tieflagerung" von 1983 bis 1987 durchgeführt. In der zweiten Phase von 1988 bis 1990 hat sich die Nagra mit zusätzlichen Feldarbeiten und mit Entwicklungsarbeiten zur Modellierung aktiv am VE-Test beteiligt.

Der vorliegende Bericht gibt einen kurzen Überblick über die Feld- und Modellierungsarbeiten der Nagra und stellt die entsprechenden Resultate vor. Die strukturgeologische Überarbeitung der Stollenaufname im VE-Abschnitt des Felslabors hat das Verständnis der Geometrie der Fliesswege verbessert. Im Untersuchungsabschnitt wird der Einfluss der beobachteten Heterogenität den Deformationsstrukturen auf die Variabilität des Wasserzuflusses und auf die Abschätzung der Makropermeabilität ermittelt. Es werden zusätzliche Methoden zur Messung des Wasserzuflusses vorgestellt. Dies im Hinblick auf die vor kurzem entwickelte Methode zur Bestimmung der Verdunstung, mit der die Verdunstungsrate an der Stollenwand punktuell ermittelt werden kann. In Kapitel 4 werden Hauptergebnisse der Bohrkampagne und der im Anschluss daran durchgeführten hydraulischen Tests vorgestellt. Ihr Ziel war es, die Geometrie und Deformation der Scherzone im VE-Abschnitt zu untersuchen und hydrogeologisch zu charakterisieren.

Die Modellierungsarbeiten hatten zwei Ziele: Im Validierungsexperiment die Prognose von Intervalldrücken vor Bohrarbeiten mit den effektiven Ergebnissen zu vergleichen sowie die Weiterentwicklung der inversen Modellierungmethodik unter Berücksichtigung geostatistischer Auswertungsverfahren. Beide Methoden liefern annehmbare Hinweise zur Variabilität der Durchlässigkeit in tektonisch unterschiedlich deformiertem kristallinen Wirtgestein.

Im letzten Kapitel werden hydraulische Durchlässigkeit und Transmissivität unterschiedlicher Ermittlungsverfahren miteinander verglichen. Für alle Methoden liegt die Durchlässigkeit in der Scherzone um eine Grössenordnung höher als in der umgebenden Matrix. Die Durchlässigkeit der Matrix ist wahrscheinlich durch die Austrocknung der Stollenwand beeinflusst und führt damit zu einer Unterschätzung der Durchlässigkeitswerte für die gesättigte Matrix, dies insbesondere bei Herleitung mit dem klassischen Ventilationstest. Abschliessend kann bemerkt werden, dass Ventilationstests zur Bestimmung der Makropermeabilität (kristallines Wirtgestein) anscheinend dann gut anwendbar sind, wenn der Zufluss eine Grössenordnung von 1 $mg \cdot m^{-2} \cdot s^{-1}$ aufweist.

RESUME

Des essais hydrauliques par ventilation (VE) ont été conduits au site d'essais du Grimsel (GTS). La première phase a été effectuée entre 1983 et 1987, principalement par une société allemande de recherche sur les rayonnements et l'environnement, la GSF (Forschungszentrum für Umwelt und Gesundheit GmbH, Institut für Tieflagerung). La Cédra a participé activement à la deuxième phase, conduite entre 1988 et 1990, avec des travaux de terrain complémentaires et le développement d'un modèle.

La contribution de la Cédra est présentée succintement dans le présent rapport. Un nouveau lever structural des déformations in situ a permis une meilleure compréhension de la géométrie des voies d'écoulement. On a ainsi pu évaluer les effets de l'hétérogénéité des structures de déformation sur les variations spatiales de l'écoulement dans la galerie ventilée, et sur l'estimation de la perméabilité en grand. On présente aussi des méthodes complémentaires de mesure de l'écoulement, notamment une nouvelle méthode de mesure de l'évaporation en un point précis de la surface de la galerie. Enfin, le chapitre 4 présente quelques aspects de la campagne de forage, et les essais hydrauliques correspondants. Ces essais avaient pour but d'étudier la géométrie et la déformation de la zone faillée observée dans la galerie, ainsi que de définir les paramètres hydrauliques de cette discontinuité.

Le travail de modélisation comportait deux aspects: d'une part une expérience de validation, les pressions pour un intervalle donné étant prévues avant forage et comparées aux observations après forage; d'autre part le développement de la méthode inverse en conjonction avec l'analyse géostatistique. Les deux approches fournissent une information utile sur les variations spatiales de la perméabilité dans des roches d'acceuil granitiques à déformation tectonique différenciée.

Les transmissivités et conductivités hydrauliques tirées des différentes méthodes sont comparées dans le dernier chapitre. Toutes les méthodes fournissent une valeur de perméabilité dix fois plus grande pour la zone faillée que pour la matrice. La perméabilité de la matrice saturée peut toutefois être sousestimée en raison de l'assèchement de la paroi de la galerie, spécialement lors des essais de ventilation classiques. On concluera en mentionnant que lors d'un test de ventilation le flux drainé le plus approprié pour l'estimation de la perméabilité en grand est de l'ordre de $1\ mg \cdot m^{-2} \cdot s^{-1}$.

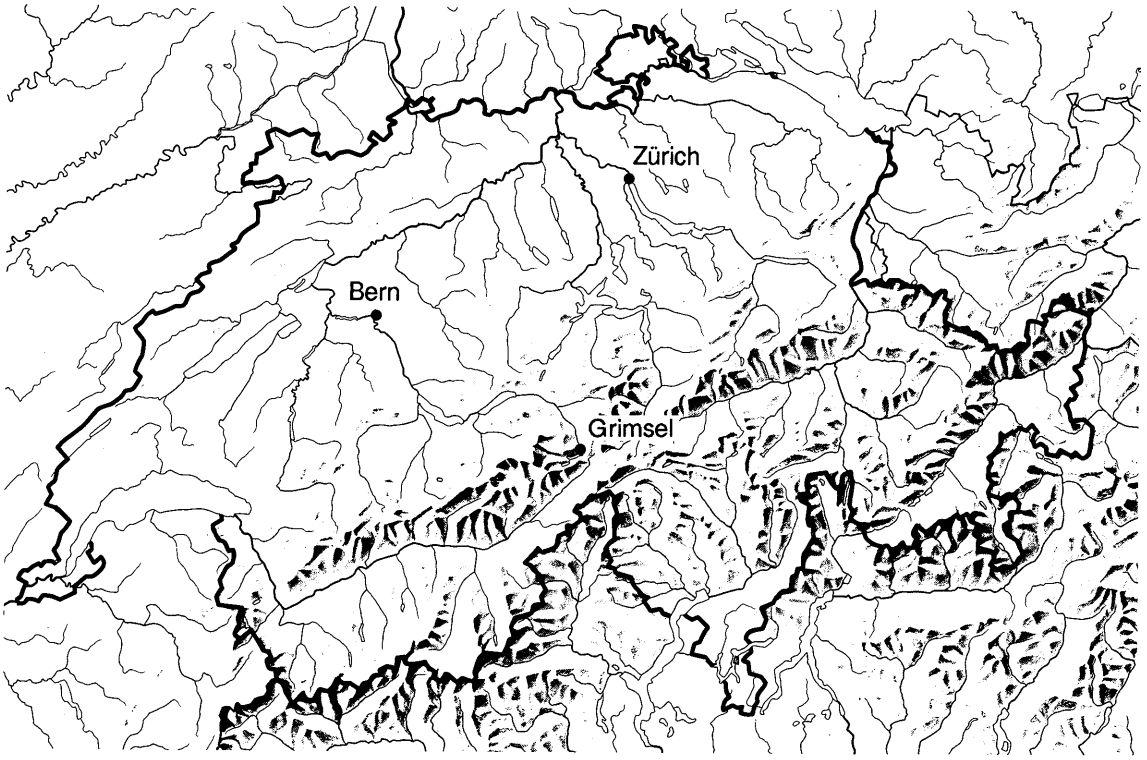

Location of Nagra's underground test facility at the Grimsel Pass in the Central Alps (Bernese Alps) of Switzerland (approximate scale 1 cm = 25 km).

Geographische Lage des Nagra Felslabors am Grimselpass (Berner Oberland) in den schweizerischen Zentralalpen (Massstab: 1 cm = ca. 25 km)

GRIMSEL-GEBIET

Blick nach Westen

1 Felslabor
2 Juchlistock
3 Räterichsbodensee
4 Grimselsee
5 Rhonetal

GRIMSEL AREA

View looking West

1 Test Site
2 Juchlistock
3 Lake Raeterichsboden
4 Lake Grimsel
5 Rhone Valley

FLG FELSLABOR GRIMSEL
GTS *GRIMSEL TEST SITE*

Situation

0 100 m

- Zugangsstollen/*Access tunnel*
- Fräsvortrieb/*by tunnel boring machine*
- Sprengvortrieb/*excavated by blasting*
- Zentraler Aaregranit ZAGR / *Central Aaregranite CAGR*
- Biotitreicher ZAGR / *CAGR with high content of biotite*
- Grimsel-Granodiorit / *Grimsel-Granodiorite*
- Scherzone/*Shear zone*
- Lamprophyr/*Lamprophyre*
- Wasserzutritt/*Water inflow*
- SB — Sondierbohrung/*Exploratory borehole*
- US — US Bohrung/*US borehole*

ZB	Zentraler Bereich/*Central facilities*
AU	Auflockerung/*Excavation effects*
BK	Bohrlochkranz/*Fracture system flow*
EM	El.magn. HF-Messungen/*-measurements*
FRI	Kluftzone/*Fracture zone investigation*
GS	Gebirgsspannungen/*Rock stresses*
HPA	Hydr. Parameter/*Hydr. parameters*
MI	Migration/*Migration*
MOD	Hydrodyn. Modellierung/*H. modeling*
NM	Neigungsmesser/*Tiltmeters*
UR	Untertageradar/*Underground radar*
US	Seismik/*Underground seismic testing*
VE	Ventilationstest/*Ventilation test*
WT	Wärmeversuch/*Heat test*

A — A Schnitt/*Section*

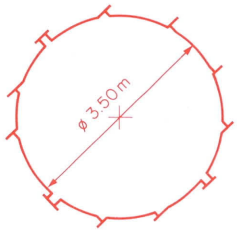

6/88

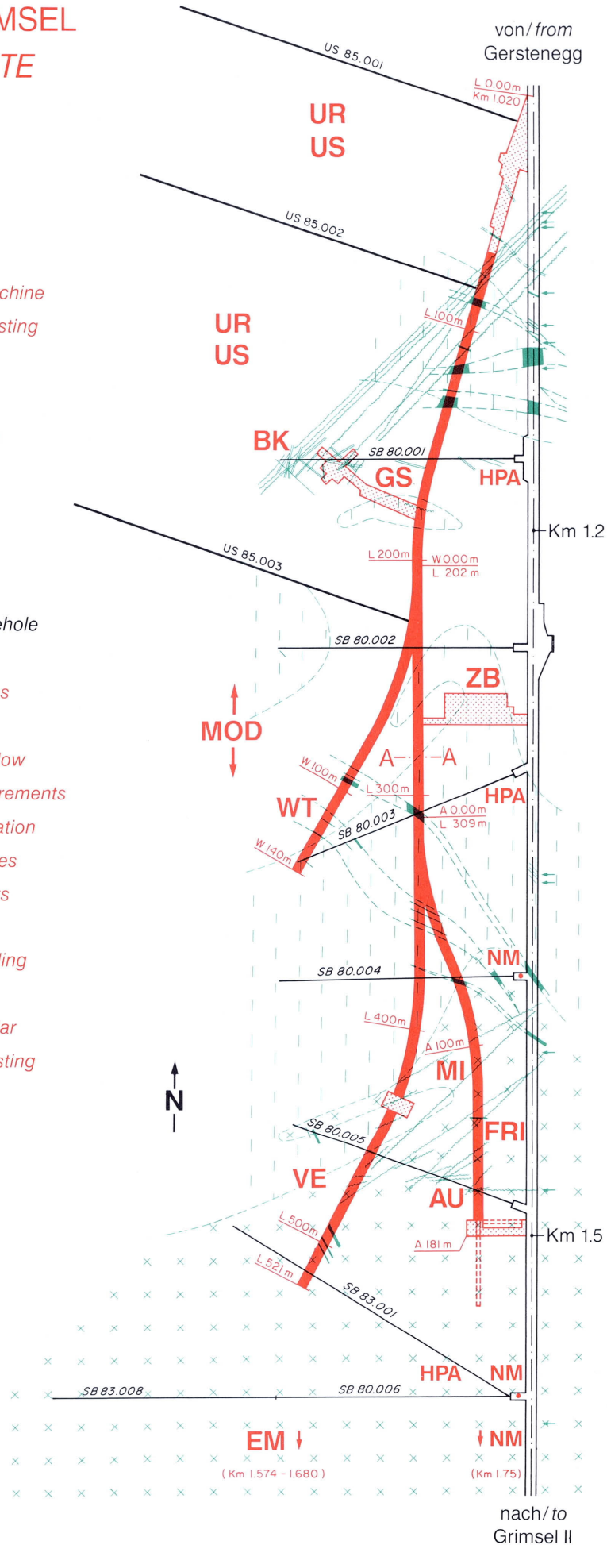

TABLE OF CONTENTS

LIST OF FIGURES page

LIST OF TABLES page

1 INTRODUCTION AND REPORT OVERVIEW

S. Vomvoris and B. Frieg (Nagra)

1.1 Background and Scope

The determination of hydraulic properties in low-permeability rocks as a basis for modeling possible nuclide migration from a deep underground repository is one of the key hydrogeological questions for site characterisation programs in such host formations. The Grimsel Test Site (GTS) offers a unique opportunity to investigate some of the relevant methodological and technical questions.

The Ventilation Test (Ventilationstest-VE) was originally conceived to focus on the question of determining the "macro"-permeability of low-permeability rock sections. As input one should use the inflow into sections of the drift with controlled ventilation, as well as measurements of the hydraulic head distribution in the formation. Figure 2 shows the location of the ventilation drift and the available boreholes.

The "GSF-Forschungszentrum für Umwelt und Gesundheit GmbH, Institut für Tieflagerung" in Braunschweig, Federal Republic of Germany, has been the Principal Investigator since 1985 at the VE-site focusing on the above mentioned topic. An overview of GSF's activities for Phase 1 and Phase 2 of GTS (1983-1990) and a list of the numerous publications can be found in NTB 91-02 (Brewitz & Kull, 1992). Currently GTS has entered its Phase 3 program of an overall duration of 3 years (1991-1993).

The present report focuses on the documentation of Nagra's activities during Phase 2, intended also partly as a preparation for the participation in the VE3 phase. Nagra's interests during this phase were:

- better geological characterisation of the drift;
- more detailed measurement of the inflows into the drift and their spatial variability;
- development of modeling capabilities, in particular with respect to inverse parameter estimation.

The inflow measurements and the hydraulical testing were carried out with assistance of GSF, namely Mr. H. Kull, by Prof. K. Watanabe (Saitama University) and the Nagra contractor Solexperts AG.

1.2 Report Organization

The form of this report as an edited volume was chosen to give credit to all persons involved in the particular subtasks; four relatively stand-alone chapters are included as described below.

Chapter 1 (P. Bossart) presents the geological and structural characterisation of the site. It covers a variety of scales, from mega- to micro-scale and it provides a geological explanation for the hydraulic properties estimated at different locations in the VE-site. The theoretical approach emphasises the strain analysis method.

Chapter 2 (K. Watanabe and P. Bossart) presents results from two additional methods for measuring inflows into the drift. In the first part data collected from the shear zone, after covering the whole zone with plastic sheets, are analysed for the estimation of "macro-transmissivity" of the zone. The second part focuses on the discrete evaporation measurement technique. Using micro-sensor the evaporation from the tunnel wall is measured - testing area is the first millimeter. With mobile sensors and different climate conditions, the temporal and spatial distribution of evaporation rates can be obtained.

Chapter 3 (P. Heiniger) describes the hydraulic testing performed in the various boreholes and a simple analysis of the obtained results. In addition, the head measurements are summarized.

Chapter 4 includes two major sections. The first one (C. Gmünder) describes the hydrodynamic modeling studies undertaken, following the direct approach, as part of the so called validation experiment. Based on observations in the two parallel boreholes (Figure 2) the modeller was called to predict head distribution in the four newly drilled boreholes. The second section of the chapter (O. Jaquet) was an exercise in inverse modeling approach. The focus was on the parameters of the shear zone which was modelled as a two-dimensional aquifer. Geostatistical methods were also used to estimate the a priori input values and their error.

Finally, in Chapter 5 the Nagra investigators S. Vomvoris and B. Frieg together with P. Bossart summarize and discuss the most important results of the Nagra activities and identify a few areas where additional investigations would be most useful.

2 GEOLOGICAL AND STRUCTURAL CHARACTERIZATION OF THE VENTILATION TEST SITE

P. Bossart (Geotechnical Institute AG, Bern)

2.1 Geology and petrography of the southern part of the Grimsel Test Site

The Grimsel Test Site (GTS) is located in the Aare Crystalline Basement, which is often termed the Aar Massif. This Crystalline Basement consists of a pre-Hercynian metasedimentary envelope which was intruded by Hercynian granitoids, Central Aare Granite and Grimsel Granodiorite. The latter is the host rock of the southern part of the GTS (Figure 1). The granodiorites are intersected locally by lamprophyre dykes. During the alpine orogeny, the rocks were buried to depths of about 8 km, with estimated pressures of 2.5 - 3 kbars and temperatures of 400° Celsius (CHOUKROUNE & GAPAIS, 1983; MARQUER et al., 1985). At these depths, the rocks were subjected to the peak of the greenschist facies metamorphism. This alpine metamorphic event has been dated at 19±3.9 Ma on granodiorites using an Rb-Sr total rock isochron (KRALIK et al., in preparation) (sample site in Figure 1). Tectonic deformation at this stage resulted in ductile structures such as granodioritic gneisses (formation of a cleavage and stretching lineation), shear zones and mylonites. During uplift and subsequent cooling, these ductile structures were reactivated by brittle processes, resulting in tectonic structures such as fractures and fault breccias. Table 1 shows the schematic relationship between the geological deformation processes, the corresponding structures and a rough timescale.

PROCESS	STRUCTURE	TIME
Brittle deformation (frictional sliding)	Fractures Brittle shear zones Fault breccias Fault gouge	5 Ma - recent
Reactivation of mylonites		10 - 5 Ma
Peak of metamorphism		19 + 3.9 Ma
Ductile deformation (viscous creep)	Mylonites Ductile shear zones Cleavage Stretching lineation	25 - 10 Ma
Granitic intrusion	Flow fabric	320 - 280 Ma

Table 1: Geological processes and resultant structures related to a timescale (for reference, see text)

The geology in the southern part of the GTS is dominated by a clearly visible cleavage (Figure 1). It is defined by the preferred orientation of grain shapes, for example the reorientation of biotites (passive rotation of biotite flakes) and the alignment of feldspars and quartz bands. The mean cleavage strike lies between a SW-NE and WSW-ENE trend with dip varying between 60° and 90° to the SE and SSE respectively. There are numerous ductile shear zones which strike parallel to the main cleavage. Three of the most characteristic ones are shown in Figure 1, with the corresponding tunnel intersections and the test sites. The thickness of the individual shear zones varies considerably. At location VE 470 they are around 10 m thick, while at AU 96 or AU 145 they are less than 1 m thick.

The shear zones 1 to 3 (Figure 1) are interpreted as thrusts. A weak stretching lineation which dips steeply to the SE can be observed in the cleavage planes of the mylonitic shear zones. It would seem reasonable that tectonic mass transport occurred parallel to these stretching lineations. Fabric analyses of mylonites suggest that the more southerly units were thrust over the northern ones.

The mineralogical compositions of granodioritic gneisses and mylonitic shear zones are given in BRADBURY (1989). The mineralogical composition varies considerably with the degree of ductile deformation. A weakly deformed granodiorite contains 28 vol% quartz, 29% plagioclase, 24% K-feldspar, 18% sheet silicates (biotite, muscovite, chlorite) and minor accessory minerals. The more advanced the mylonitization is, the higher is the proportion of sheet silicates; these reach over 50 vol% in mylonitic zones (mainly at the expense of feldspars). Because of this high proportion of sheet silicates and the marked decrease in grain size, these mylonitic zones represent areas of reduced mechanical competence. The lamprophyres are composed mainly of biotite (up to 70 vol%), followed by feldspars (plagioclase and K-feldspar up to 30 vol%) and minor epidote and amphibole (normally between 0-20 vol%).

2.2 Structural geology in the ventilation test drift

The ventilation test drift, together with the borehole configuration, is shown in Figure 2. Up till 1987, boreholes BOSB 80.005, BOSB 83.001 and the two parallel boreholes BOVE 84.011 and 84.018 were operational. In 1987, four new boreholes were drilled, namely BOVE 88.001 to BOVE 88.004. The main objective was to investigate the geometry and deformation of the dominant shear zone in the ventilation test drift as well as to obtain information on its hydraulic behaviour (see also chapter 4). Shear zone intervals and granodiorite intervals were separated by hydraulic-pneumatic packers.

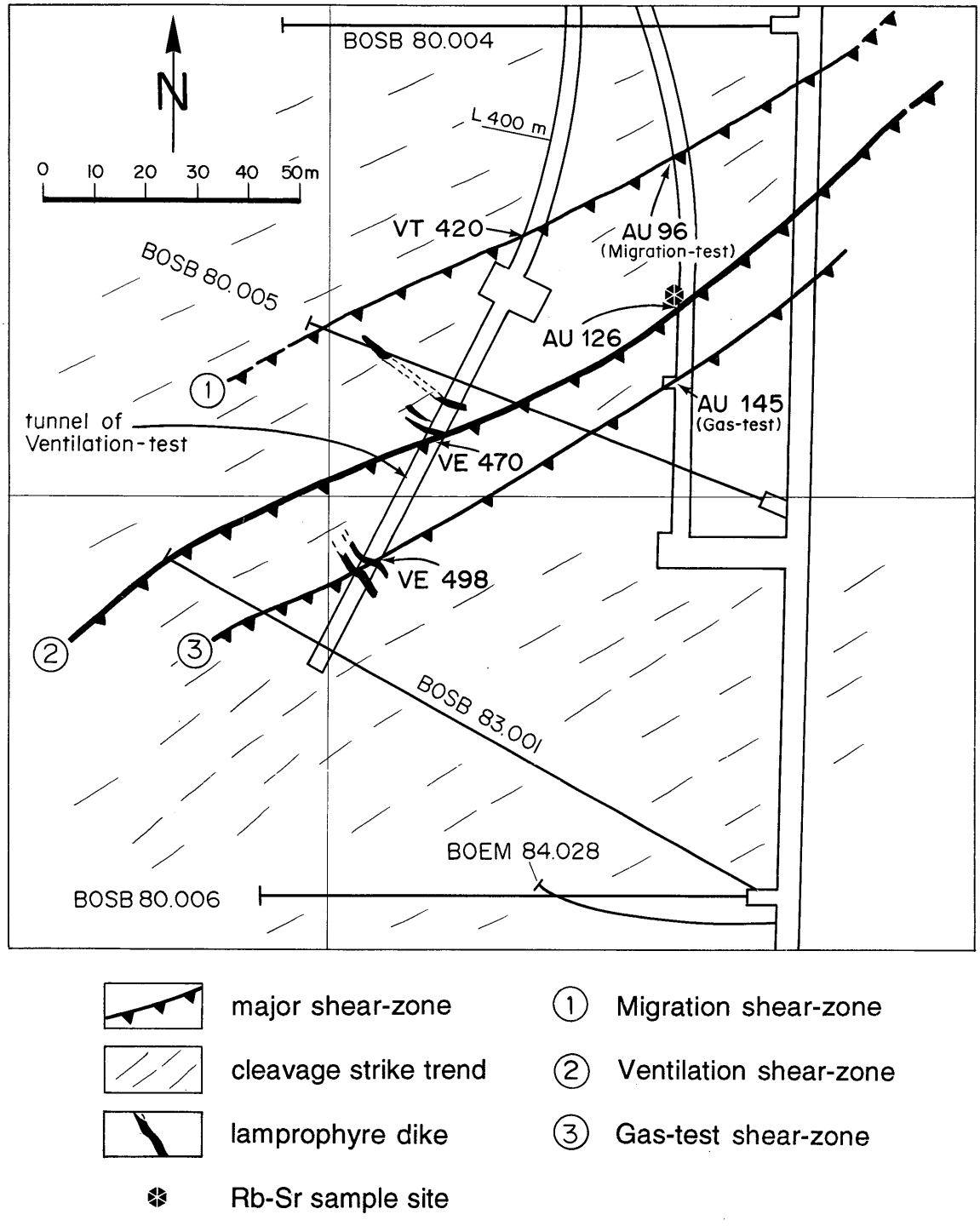

Figure 1: Structural map of the Southern part of the Grimsel Test Site

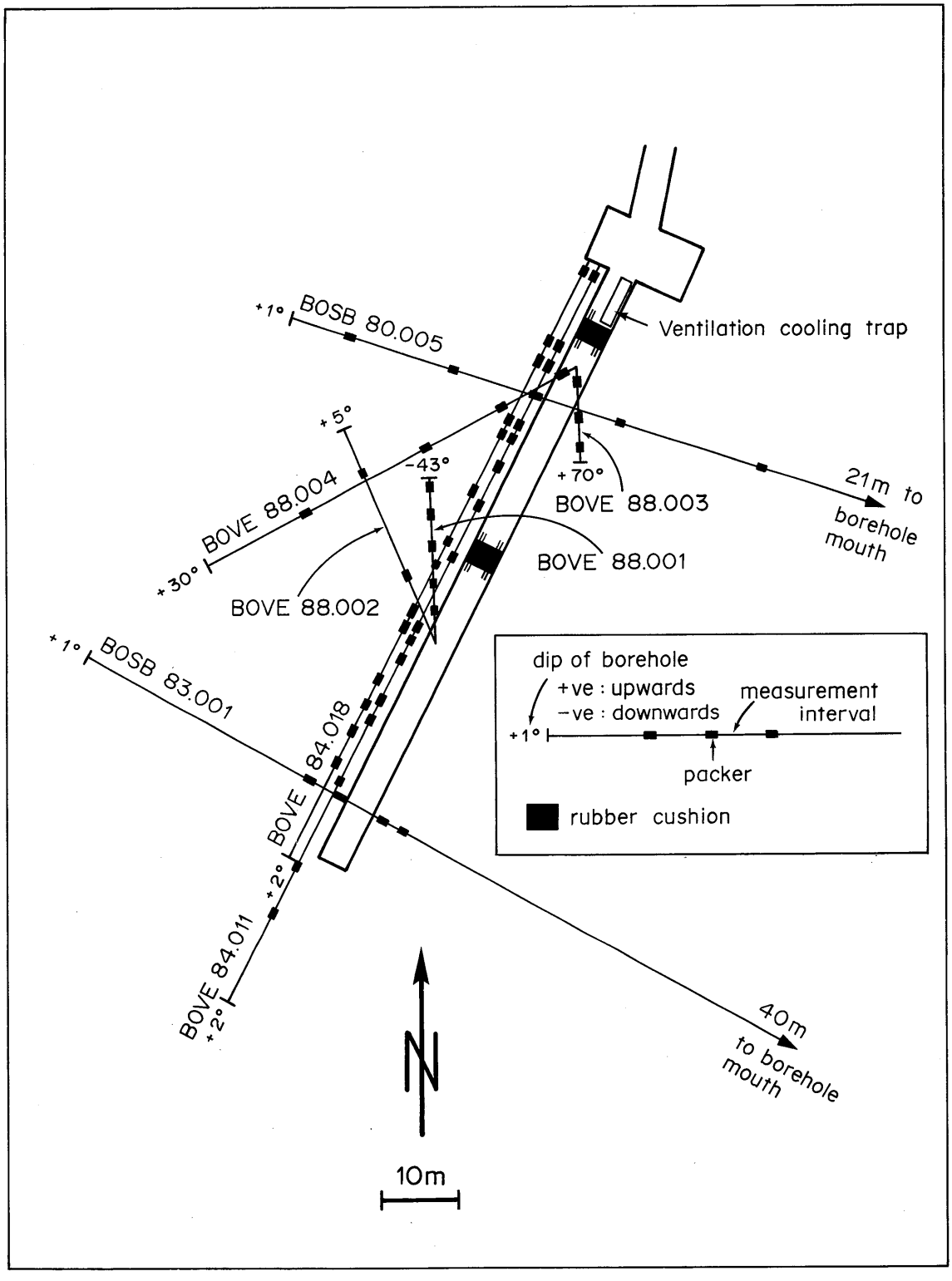

Figure 2: Ventilation test drift with drillcore net

2.2.1 Results from the new drillcores

Figure 3 shows the macroscopic geometry of the ventilation test shear zone. The shear zone was clearly identified in all eight boreholes and could be correlated from the main access tunnel to the ventilation test drift, altogether a distance of some 130 m (Figure 1). In the vicinity of the ventilation test drift, the mean azimuth of dip is 160° and the mean angle of dip is 75° (equivalent to strike 70° and dip 75° SSE). As shown in Figure 3, the shear zone strike is not a straight line but describes a smooth curve. Analysis of cores from the four new boreholes showed that the cleavage intensity in the mylonites is very high, but also that the fracture density is many times higher than in the granodiorites. These observations may be interpreted in terms of the significant contrast in mechanical competence between granodiorite and mylonite. The mechanically weak mylonitic shear zones may act as pre-existing discontinuities for subsequent brittle reactivation. Brittle deformation associated with the regional uplift was therefore accommodated preferentially in the mylonitic shear zones.

KEUSEN et al. (1989) reported three different sets of cleavages, namely S1, S2 and S3 systems with corresponding azimuths and dips of (142/77), (157/75) and (183/65) respectively. As an example the S2 and S3 systems are indicated in Figure 3. However analyses of the new drillcores have given the following results:

- the orientation and distribution pattern of cleavage orientations fluctuates around a mean orientation of (160/75)
- the cleavage geometry is controlled locally by shear bands (BERTHE et al., 1979). This seems to be the reason why the cleavage orientations can vary considerably on all scales (microscopic to outcrop).
- it is suggested to characterize the orientations of planar structures (cleavage and fractures) in terms of means and fluctuations. The division into different sets of planar structures seems to be somewhat arbitrary.

A useful approach to characterizing the spatial variability of cleavage and fracture planes in drillcores is to use a statistical description of their pole distributions. In our case, the BINGHAM statistical method is applied (WOODCOCK, 1979). With this methode for example, two populations of poles can be compared and related to each other. In the stereographic plots of Figure 4, cleavage and fracture poles from drillcores BOVE 88.001 to BOVE 88.004 are presented together with the so called lambda values, their orientations, and the cones of confidence (for the latter see ellipses around lambda points). The lambda values are used to categorise spatial distributions of pole data. In both plots of Figure 4 the lambda-max values (max stands for maximum) are about three times higher than the lambda-int values (int stands for intermediate), indicating a cluster distribution. Furthermore, the lambda-max values for both cleavage and fracture poles results in more or less identical orientations and cones of confidence, although considering only the data points in the stereonet of Figure 4 the fracture poles cluster much more than the cleavage poles.

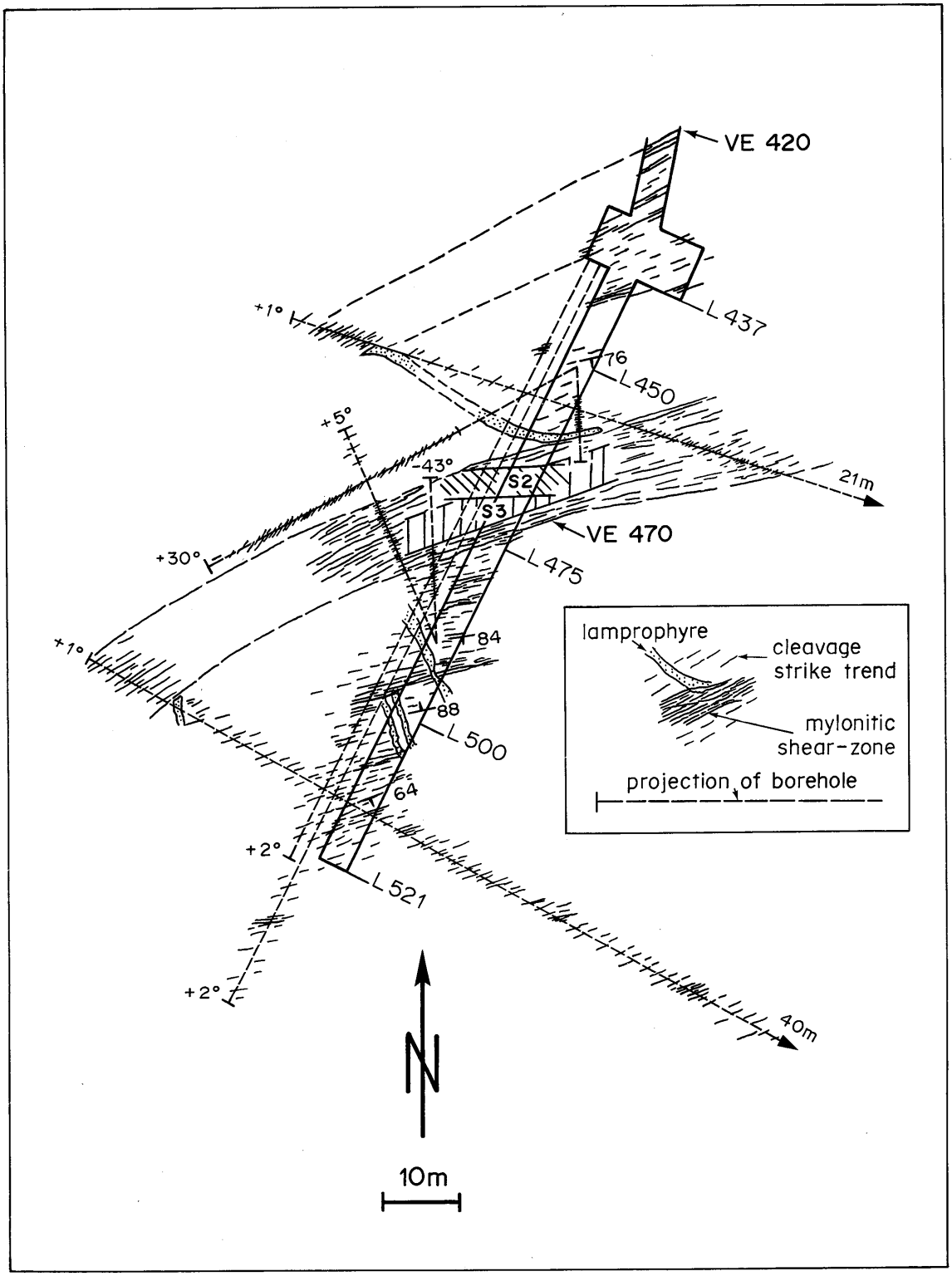

Figure 3: The main geologic structure in and around the ventilation test drift

cleavage poles (shear-zone and matrix)

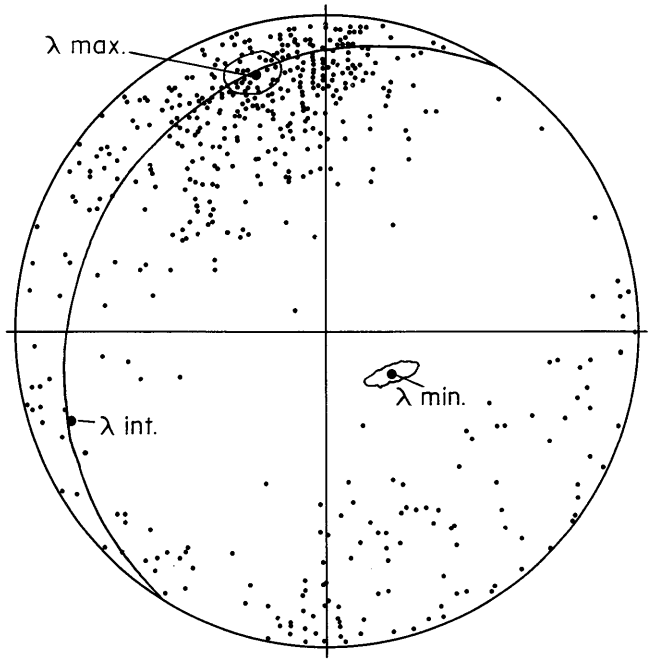

611 data

λ values	orientation
0.732 max.	344 / 16
0.165 int.	250 / 13
0.103 min.	122 / 69

fracture poles (shear-zone and matrix)

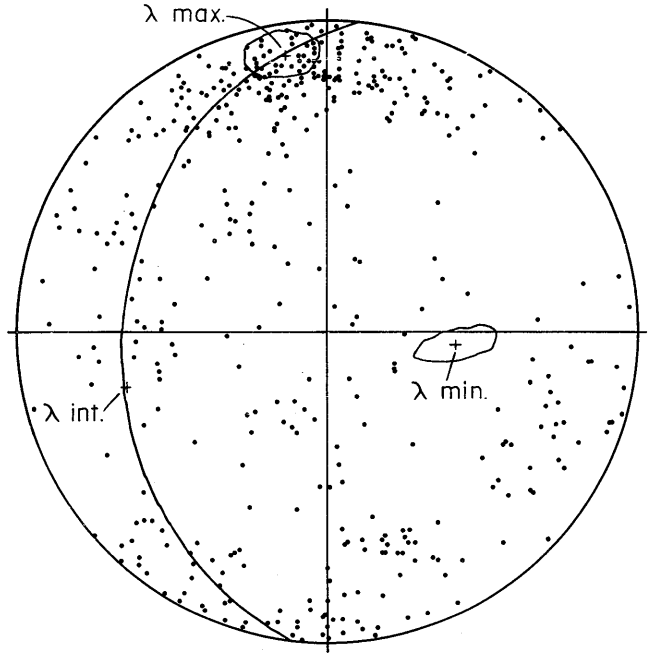

475 data

λ values	orientation
0.613 max.	351 / 10
0.218 int.	254 / 33
0.169 min.	96 / 55

Figure 4: Orientations of cleavage and fractures, stereoplots, lower hemisphere

2.2.2 Revised geological and structural map of the ventilation test drift

Figure 5 presents the tectonic structures occurring in the ventilation test drift between 445 m and 521.5 m (layout of the curved tunnel surface). The division of the ventilation drift into a forward and rear section coincides with the two ventilation chambers selected by the GSF (see chapter 3.1).

The main lithological units are the fairly light granodiorites (or granodioritic gneisses, depending on the formation of a clearly visible cleavage), with local deformed dark xenoliths and lamprophyre dykes cutting through the granodiorites. The initial magmatic fabric is generally well-preserved in the granodiorites. The ductile shear zones are represented by zones of very high cleavage intensity. In these highly deformed zones, the original granodiorite fabric is generally recrystallized, with a grain size reduction of feldspars and quartz and a clear increase in sheet silicate minerals (mainly biotite). Such zones are termed mylonitic shear zones and occur mostly in dark bands ranging in thickness from a few cm up to several m.

Four lamprophyre dykes intersect the ventilation test drift. They generally strike NW-SE, oblique to the cleavage. These lamprophyres behave as incompetent layers which are embedded in the more competent granodioritic host rock. This is supported by 1) a cleavage intensity which is higher than in the surrounding granodiorites, 2) a cleavage refraction at the granodiorite-lamprophyre transition, and 3) a cuspate-lobate fold pattern (ductile deformation) at the lamprophyre borders (RAMSAY & HUBER, 1987). The borders of the lamprophyres are frequently overprinted by later brittle reactivation (formation of fault gouge layers).

Brittle structures such as fractures and fault gouges (where visible at outcrop) were superimposed onto the ductile structures on the map in Figure 5. The map shows that the fractures (in blue) are mainly associated with ductile shear zones (in red). This observation is in agreement with the analysis of the drillcores which indicated that 1) the fracture density was found to be highest in the mylonites and 2) the fracture planes have the same mean orientation as the cleavage planes in the shear zones. The high fracture density in the shear zones is also the reason why the tunnel surface is usually wet on the surface of ductile shear zones (see chapter 2.3).

In the following, the mapped structures in the ventilation test drift (Figure 5) are described:

- **445 - 466 m:** Slightly deformed, massive, generally homogeneous granodiorite, initial magmatic fabric well-preserved. Small ductile shear zones (few cm thick) with fractures at 455 m and 463 m. Fracture at 463 m with counterclockwise splays (indication of brittle fault zone; MARTEL & PETERSON, 1991). Lamprophyre dyke at 462 m with higher cleavage intensity than surrounding granodiorite, cleavage refractions and borders with cusps and lobes, indicating reduced competence compared with the granodiorite. Start of boreholes BOVE 88.003 (eastern tunnel wall) and BOVE 88.004 (western tunnel wall) at 450.3 m and 451.8 m respectively.

frontal chamber

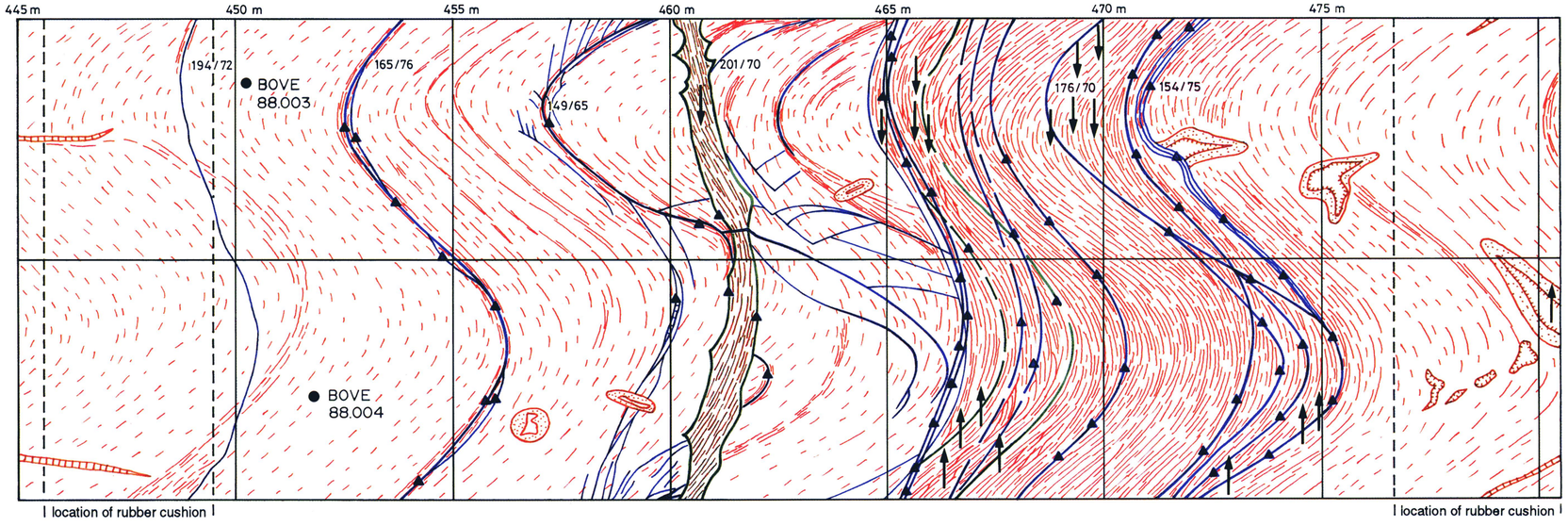

rear chamber

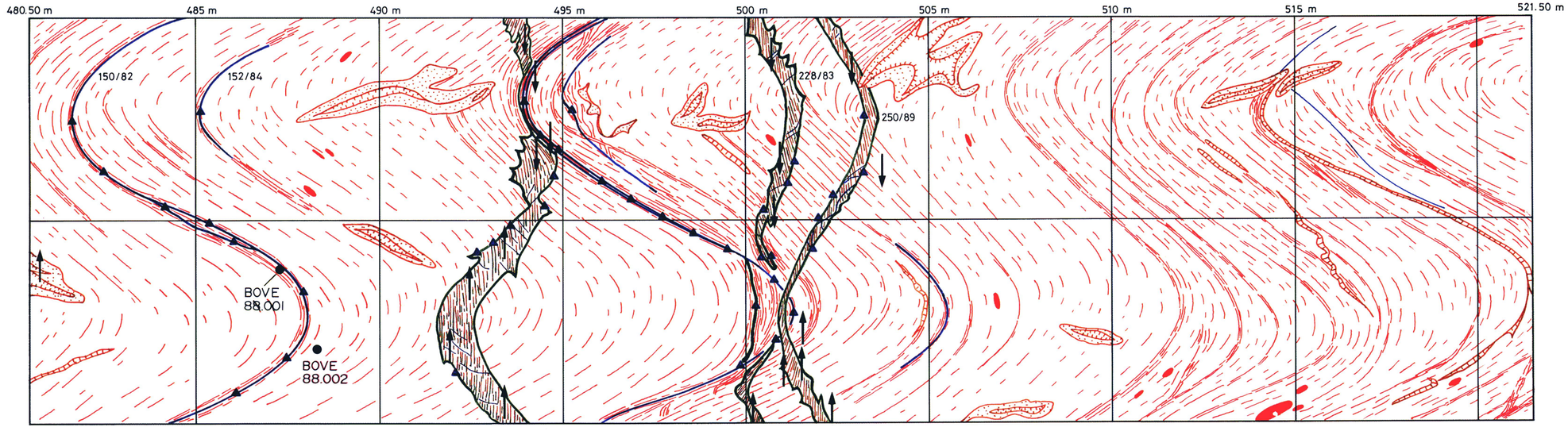

ductile structures

- cleavage trace of mildly deformed granodiorite (low cleavage intensity)
- cleavage trace of granodiorite gneiss (moderate cleavage intensity)
- cleavage trace of mylonitic shear-zone (high cleavage intensity)
- deformed xenolithe
- lamprophyre dike with cleavage trace (cusp, lobe)

brittle structures

- fracture s.l.
- fault gouge (visible by eye)

- quartz-vein
- extension fracture
- bleached border
- locations with permanent water inflow

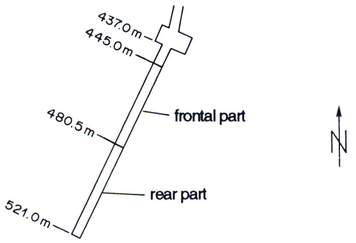

Figure 5: Structural map, surface of the ventilation test drift

- **466 - 476 m:** "Ventilation shear zone" (see Figure 1). Huge ductile mylonitic shear zone. Mean azimuth of dip (160°), mean angle of dip (80°), mean thickness 10 m. High fracture density. Clear fault gouge horizon at northem boundary (466 m). Two deflected and pinched-out lamprophyre dykes at 467 m and 468 m respectively, locally altered to fault gouges. Numerous water inflow points (arrows in Figure 5).

- **476 - 493 m:** Slightly to moderately deformed granodiorite gneisses. Ductile shear zones at 478 m, 485 m, 489 m. Shear zone at 485 m shows brittle reactivation. Many flat-lying extension fractures ("Zerrklüfte") with bleached but compact borders. BOVE 88.001 and BOVE 88.002 (both western tunnel wall) are found at around 490 m.

- **493 - 503 m:** Three lamprophyre dykes striking NW-SE (oblique to the cleavage). Sharp cusps and deep lobes at their borders, high cleavage intensity and cleavage refraction indicating clearly reduced competence compared with the surrounding gneisses. Borders and, locally, centres of lamprophyres show brittle reactivation (fault gouge) with increased water flow. Pronounced ductile and brittely reactivated shear zone at 498 m (correlated with gas test shear zone, see Figure 1) which displaces the lamprophyres vertically rather than horizontally.

- **503 - 520 m:** Slightly to moderately deformed granodiorite gneisses with tight (non reactived) ductile shear zones (5 mylonitic shear zones between 510 m and 515 m) Many flat-lying extension fractures with bleached borders. Between 514 m and 516 m (near tunnel top) nice examples of deformed xenoliths.

2.3 Microstructural characterization of GTS shear zones

The ventilation shear zone (Figure 5, 466 m - 476 m) initially appears to reflect a fairly homogeneous state of deformation. However, even on the outcrop scale, the tectonic strains in this shear zone show a very heterogeneous pattern. High strain gradients (mylonites lying next to lightly deformed granodiorites) seem to be common in all the ductile shear zones of the GTS. In order to characterize these tectonic strains more adequately, the finite strain ellipsoids were derived and precise mapping carried out for a characteristic ductile shear zone.

2.3.1 Derivation of the finite strain ellipsoid

The finite strain ellipsoid is defined by the shape and orientation of an ellipsoid which was originally a sphere. During tectonic deformation, this sphere was transformed into an ellipsoid which is termed the finite strain ellipsoid. In the GTS we assume that, in tectonically undeformed granodiorites, the xenoliths (dark inclusions in the cm to dm scale) have a more or less spherical shape. If these xenoliths are deformed, they therefore directly reflect the finite strain ellipsoid. Because of the contrast in competence between xenoliths and surrounding granodiorites, the finite strain ellipsoid can only be derived in a qualitative manner.

The orientations and shapes of tectonically deformed xenoliths which are embedded in moderately to highly deformed granodiorites were measured and the results presented in Figure 6a. The stereonet shows that the long axes of the finite strain ellipsoids (X) are subvertically inclined and parallel to the steeply dipping mineral stretching lineations. The field of the short axes (Z) plunges subhorizontally to the NW and SE respectively, and these axes coincide with the orientation of the cleavage poles (see Figure 4). The intermediate Y-axis is constructed. The XY-planes of the finite strain ellipsoids (planes defined by the X- and Y-axes) are parallel to the cleavage planes. The shapes of the finite strain ellipsoids were derived in a Flinn diagram (FLINN, 1962)(Figure 6a). The deformed xenoliths in the Flinn diagram show that the finite strain ellipsoids belong to the apparent flattening field. This means that the ellipsoids have a pronounced "pancake" shape (in contrast to a cigar form). It seems that the higher the ductile deformation in the granodiorites is, the more flattened the finite strain ellipsoids are. Unfortunately no xenoliths could be measured in mylonitic shear zones.

As a result, the variability of orientations and shapes of the finite strain ellipsoids in Figure 6a characterizes the heterogeneity of ductile strains in slightly to highly deformed granodiorite gneisses. This heterogeneity could not be evaluated in the mylonites of the ductile shear zones using the same approach. In order to characterize the heterogeneous strain pattern in shear zones, which also include mylonites, the technique of precise shear zone mapping was selected.

2.3.2 Tectonic strain heterogeneity in ductile shear zones

Figure 6b represents a precise map of a ductile GTS-type shear zone. The mapping was carried out on a horizontal surface outcrop on the shore of the Raterichsboden reservoir, in a plane parallel to the YZ-strain plane of the finite strain ellipsoid (BOSSART & MARTEL, 1990). In the GTS, horizontal plane mapping is restricted due to the circular tunnel cross-section.

The map in Figure 6b shows that in a thick "ventilation-type" shear zone there are many small mylonitic shear zones surrounded by slightly to strongly deformed granodiorites. Two geometric types of small mylonitic shear zones were identified and are termed S- and K-zones in the following. The S-zones are more pronounced and thicker, and strike and dip parallel to the regional alpine cleavage. The shear sense in S-zones is counterclockwise when looking onto the mapping plane. The K-zones are less pronounced and generally less thick and strike oblique to the regional cleavage in a NW-SE direction. They also lie close to the orientation of the lamprophyre dykes. The shear sense in the K-zones is clockwise when looking onto the mapping plane. The shear sense of S- and K-zones can clearly be derived from the rectangular, slightly deformed granodiorite lenses (see Figure 6b, "bookshelf lenses", upper right).

In Figure 6b, examples can be found where S-zones are deflected by K-zones, but also where K-zones are deflected by S-zones or both S- and K-zones deflect one another. This geometric deflection pattern is a good argument for relating the formation of S- and K- zones to the same deformation event. Such shear zones are termed conjugate ductile shear zones. Conjugate shear zones are also found in the GTS, e.g. north of VT

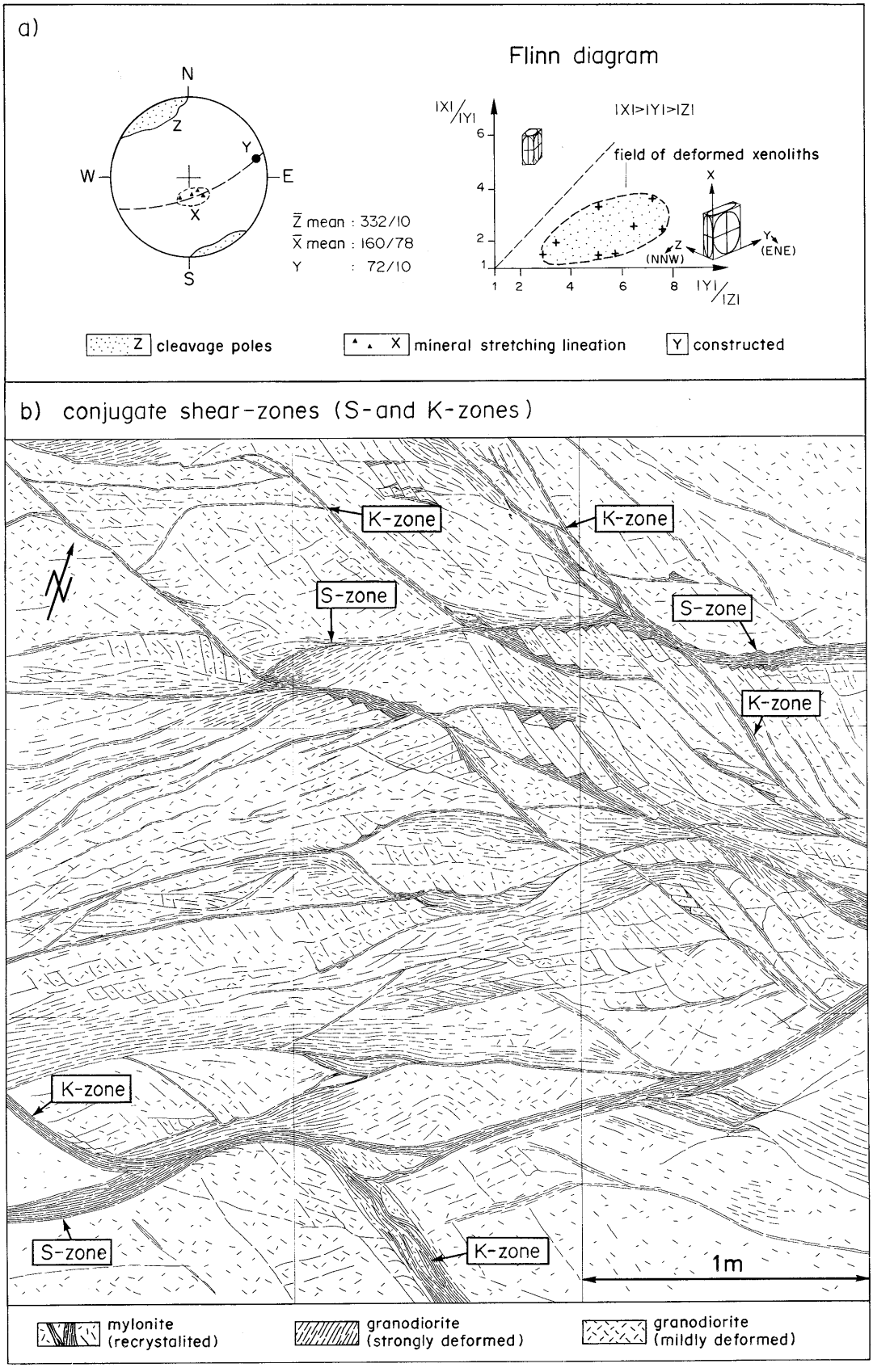

Figure 6: *a) Definition of the finite strain ellipsoid*
b) Tectonic strain heterogeneity in a ductile shear zone

420 on the western tunnel wall (for location see Figure 1). However, the geometric relationship of conjugate shear zones is complicated due to the circular cross-section in the GTS.

The spatial variability of tectonic strains appears to be very high in ductile shear zones where slightly deformed granodiorites lie close to mylonite bands. Although the cleavage determines the main structural anisotropy, there are shear zones such as the K-zones which are clearly obliquely orientated to these anisotropy planes. In the granodiorites and granodiorite gneisses, the spatial variability of tectonic strains is much lower compared to that of ductile shear zones.

2.4 Finite strain, open porosity and hydraulic permeability

In order to study qualitatively the relationship between the deformed fabric of the different lithologies (granodiorites, gneisses, lamprophyres, mylonites) and the hydraulic permeability, it is necessary to identify the appropriate open rock porosity and flow path. The drillcore analysis (chapter 1.2.1) and the structural mapping of the ventilation drift (chapter 1.2.2) have shown that, in particular, the mylonites in the ductile shear zones have undergone brittle reactivation due to cataclastic processes. One important resulting structure is the network of fault gouges (BOSSART & MAZUREK, 1991) (Figures 7a and b). These fault gouge layers are several mm thick and consist of a fine, micaceous rock flour matrix with low cohesion. Embedded in this matrix are coarse angular mylonite components. Fault gouge material, which has been isolated out of a fracture in the GTS and analysed in the laboratory resulted in an estimated porosity of about 20 vol% (KRALIK et al., in preparation). Fault gouges occur mainly in zones of high ductile (mylonitic) deformation in shear zones, although they are often found along the borders of the lamprophyres. Other types of porosities, such as sheet silicate pores in the mylonites and grain boundary-, transgranular- and solution pores in the granodiorites, were identified and investigated. It can be said that different pore types will predominate depending on the degree of ductile deformation of the lithologies. Fault gouge and sheet silicate porosities dominate in zones of higher ductile deformation (mylonites), while grain boundary pores are important in the granodiorite gneisses. It is important to note that all these pore spaces are interconnected and basically represent an open porosity.

In Figure 8a, the tectonic deformation is related to the characteristic lithological units occurring in the ventilation drift. Figure 8a has been transformed into a pore space cartoon which results in Figure 8b (not to scale). The highest open porosity or highest hydraulic permeability is found in the fault gouges of the mylonitic shear zones and the borders of the lamprophyres. The grain boundary pores of the granodiorites have a lower porosity and the compact, non-reactivated mylonites have the lowest porosity. This is consistent with microscopic investigations which show that recrystallized, fine-grained and non-reactivated mylonites have a denser structure than the granodiorites. These important results have to be taken into account when interpreting tests, e.g. hydrotests (chapter 4).

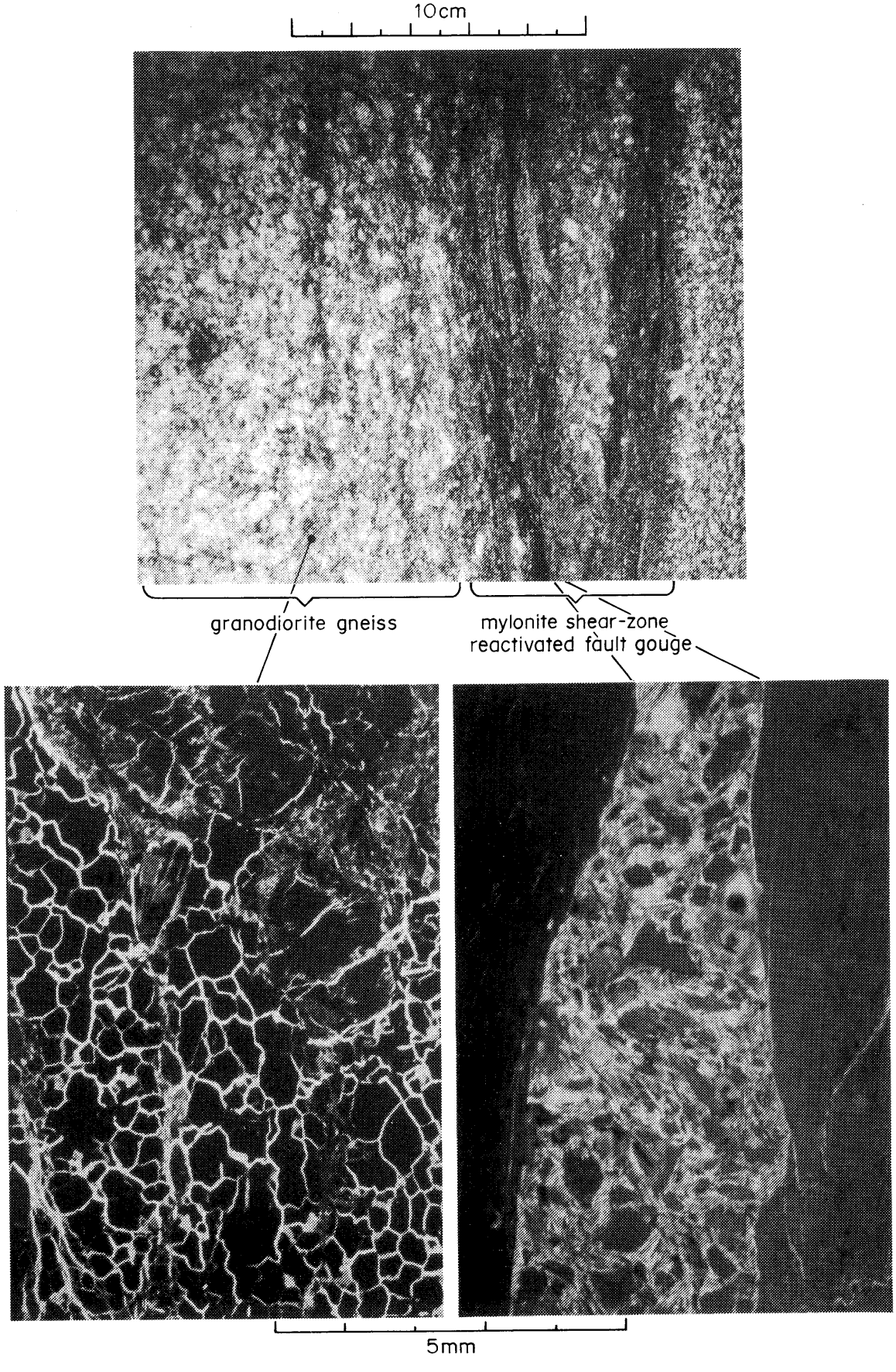

Figure 7: Network of grain boundary pores in a granodiorite gneiss (left). Fault gouge porosity in a mylonite shear zone (right)

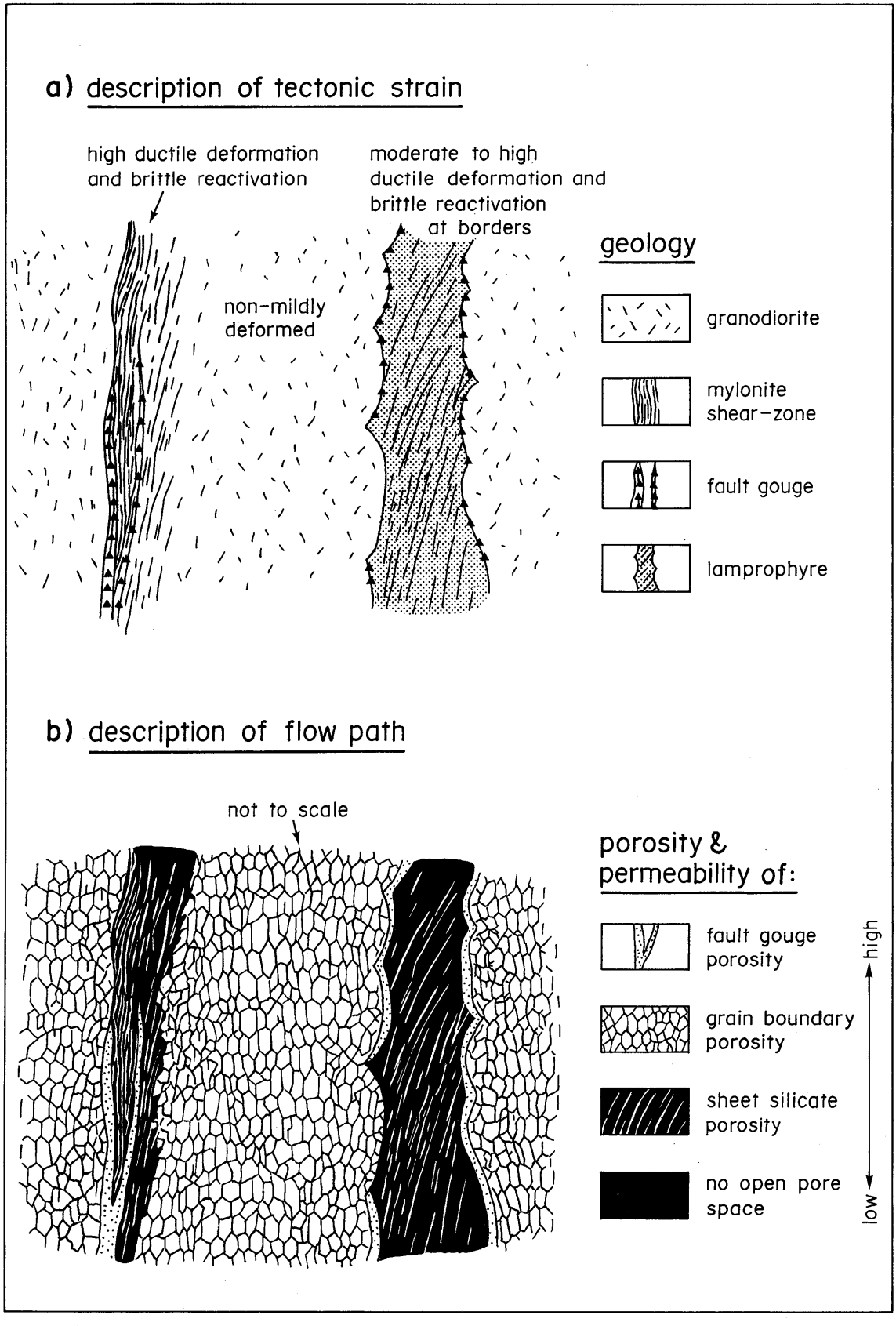

Figure 8: Cartoon of tectonic strain a) and flow path b)

3 COMPLEMENTARY METHODS FOR MEASURING WATER INFLOW INTO THE VENTILATION DRIFT

K. Watanabe (Saitama University, Urawa, Japan) and
P. Bossart (Geotechnical Institute, Bern)

3.1 Introduction

In many respects, the permeability of the intact host rock surrounding a waste repository is an important parameter in safety analysis. The permeability in the rock formation surrounding a tunnel or a gallery cannot be measured directly, but is estimated from the hydraulic gradient near the tunnel surface and the water and vapor inflow into the tunnel. Measurement of hydraulic gradient and water inflow is therefore the main aim of the so called ventilation experiment (VE-test).

The concept of the VE-test is described in BREWITZ & PAHL (1986) and BRASSER (1987). The ventilation drift at the GTS is divided into two chambers (Figure 9), which are sealed off using two mobile, inflatable rubber cushions. Ventilation pipes passing through these cushions are used to regulate the humidity and temperature of the two chambers. Air with a defined temperature and relative humidity is pumped into one of the chambers using a closed air-circulating system; it then becomes saturated with rock formation moisture. This saturated air is returned via the closed air-circulating system to a cooling trap, where it is cooled to around 1°C. The quantity of water extracted from the condensed air is taken as being equal to the natural water inflow from the rock mass into the drift.

Water pressure measurements are simultaneously conducted in the two boreholes running parallel to the drift (Figure 9), in order to estimate the hydraulic gradient. Other measured parameters include temporal temperature distribution in the test chambers and in the parallel boreholes and the air flow through the ventilation tubes.

An overview of the ventilation phases is given in Table 2. For further details, reference should be made to the GSF "F+E-Jahresberichte" (BRASSER & KULL, 1986, 1987; KULL, 1988, 1989) and the final test report NTB 91-02 (BREWITZ & KULL, 1992). The mean quantity of extracted water in the two chambers is:

- The mean quantity of water extracted in the **forward** section of the ventilation drift (chamber 1, 1985-1987) is 1.40 ± 0.25 liters per hour (BREWITZ & KULL, 1992). With a rock surface area of 297 m^2 in the forward chamber, the equivalent flux amounts to 1.36 ± 0.24 $mg \cdot m^{-2} \cdot s^{-1}$.
- The mean quantity of water extracted in the **rear** section of the drift (chamber 2, 1987-1988) varies between 0.35 and 0.90 liters per hour (BREWITZ & KULL, 1992). The rock surface area in the rear chamber is 440 m^2 and the corresponding flux varies then between 0.23 and 0.57 $mg \cdot m^{-2} \cdot s^{-1}$.

The temporal variations in the quantities of water extracted in the two sections of the ventilation drift may be found in KULL (1988).

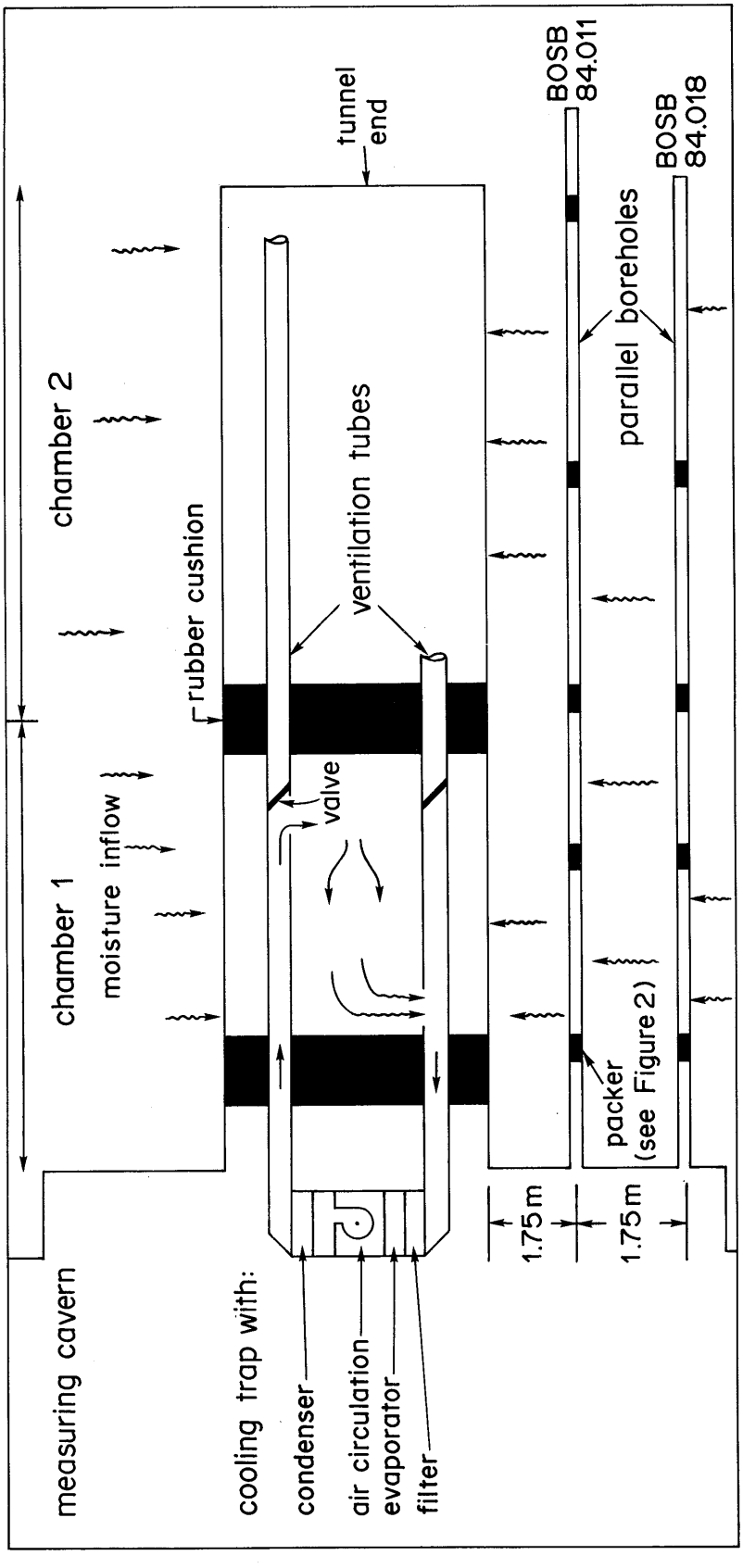

Figure 9: Test design of the ventilation experiment applied in the Grimsel Test Site (not to scale) (cf. BRASSER, 1987)

Frontal part of VE-tunnel (chamber 1)	1985	1986	1987	1988
Phase 1				
(60%<RH<70%)		----------		
(12°C<T<14°C)		----------		
Phase 2				
(45%<RH<50%)			----------	
(14°C<T<15°C)			----------	
Phase 3				
(30%<RH<50%)			----	
(20°C<T<23°C)			----	
Rear part of VE-tunnel (chamber 2)	**1985**	**1986**	**1987**	**1988**
Phase 1				
(60%<RH<70%)			-----	
(T=12°C)			-----	
Phase 2				
(50%<RH<70%)				--------
(T=17°C)				--------
Phase 3				
(25%<RH<30%)				-------
(23°C<T<24°C)				-------

Table 2: Ventilation phases.RH-relative humidity [%], T-Temperature [°C]

The application of a VE-test is suitable for fairly homogeneous and isotropic rocks surrounding a tunnel. However, in the case of the ventilation drift at the GTS, the structure of the surrounding rock mass is heterogeneous and has a distinct fabric anisotropy (see chapter 2). This explains why water inflow into the drift is not homogeneously distributed (see Figure 5), and why the permeability varies with location. In order to take into account the variability of inflow, two methods (performed by Nagra) are also used:

- Covering the tunnel wall with plastic sheeting and collecting the water at the base of the wall (see chapter 3.2).
- Calculating the evaporation rate at the tunnel surface by measuring gradients of relative humidity and temperature (see chapter 3.3).

These two methods should be viewed as complementary to the "traditional" VE-test for determining the spatial variability of water inflow in a heterogeneous rock mass with a greater degree of accuracy.

One assumption of the performed VE-test in the GTS is, that the amount of water extracted from the tunnel wall is equal to the natural inflow from the rock matrix into the drift (see also Figure 12). Another interpretation is that a part of the measured discharge has been removed from storage in the grain boundary pores of the granodiorite and that the matrix close to the surface of the drift is slowly drying out. If this process occurs, removal of stored water will create an unsaturated zone around the drift. When the true natural water inflow is lower than the measured one, then also the true macropermeability would be lower than the estimated one.

3.2 Rock macropermeability in homogeneous rock sections

If the rock mass surrounding a tunnel is homogeneous and isotropic and the lowered water table is symmetric (Figure 10), then only one permeability value will result. This implies that the aquifer has a constant thickness with an infinite lateral extent, and that there is no skin (no disturbed zone, all pores saturated) around the tunnel. Such a permeability can be defined as a macropermeability because it is valid for the entire host rock surrounding the tunnel. If these assumptions are valid, there are two methods for calculating the macropermeability under steady state conditions: equation [1] which is the formula of THIEM (1906), and equation [2] which is the formula of GOODMAN et al. (1965). The required geometric parameters and estimated hydraulic parameters are given in Figure 10.

$$K = \frac{Q \ln (r_2/r_1)}{2 \pi (h_2-h_1)} \qquad [1]$$

$$K = 5.3E-11 \quad [m/s]$$

where:

K	=	Hydraulic conductivity	[m/s]
Q	=	Flow from host rock into drift per tunnel meter	$[m^3 \cdot s^{-1} \cdot m^{-1}]$
r_2, r_1	=	Radial distances of two parallel boreholes	[m]
h_2-h_1	=	Head difference between the two parallel boreholes	[m]

Strictly speaking equation [1] can be applied only for the case of vertical boreholes. However in the ventilation test, it was used for the horizontal ventilation tube (in a horizontal tube, the heads on the surface are not equal).

$$K = \frac{2.3\, Q \log (2H_o/R)}{2 \pi H_o} \qquad [2]$$

$$K = 2.0E-11 \quad [m/s]$$

where:

K	=	Hydraulic conductivity	[m/s]
Q	=	Flow from host rock into drift per tunnel meter	[$m^3 \cdot s^{-1} \cdot m^{-1}$]
R	=	Radius of tunnel	[m]
H_o	=	Water pile above tunnel	[m]

The parameter H_o in equation [2] is estimated from interval pressures of boreholes which are far removed from the tunnel and are thus only slightly influenced by the tunnel pressure sink. Such pressures are in the order of 40 bars (corresponding to a water pile of 400 m). The direct location of a water table near the surface was not investigated. Equation [2] is analougous to equation (68) in BIDAUX & TSANG (1991), the latter additionally implementing a possible skin around the underground opening.

Another approach is to calculate the permeability in sections of the ventilation drift where more or less homogeneous conditions prevail. As shown in chapter 2.2.2, there are five sections in the ventilation drift, each of which can be described in terms of more or less homogeneous tectonic strains. If the water inflow in each of these five sections is known, and the corresponding gradients can be evaluated (pressure differences in the corresponding five sections in the parallel boreholes), then the resulting permeabilities can also be calculated. In the following, such an exercise is performed for the forward section (chamber 1) of the ventilation drift.

The forward section of the ventilation drift is divided into a matrix part (granodiorites with grain boundary porosities) and a shear zone part (mainly mylonites with fault gouge porosity)(see chapter 2.4). The granodiorite section occupies approximately 2/3 of the drift surface, and the shear zone the remaining 1/3.

Due to the fault gouge porosity, there is clear water inflow from the shear zone into the drift, even under varying climatic conditions. This water inflow was measured by covering the shear zone with plastic sheeting and collecting the water at the base of the drift wall (BOSSART & HUFSCHMIED, 1989). The amount of water measured from the shear zone is presented in Figure 11. Over a period of four months (in 1989) the water inflow amounted to 1.1 ± 0.2 l/hour (Figures 11 and 12). This corresponds to a flux of 2.97 ± 0.54 $mg \cdot m^{-2} \cdot s^{-1}$.

During the ventilation periods (1985-1988), an amount of 1.40 ± 0.25 l/hour was measured in the forward section of the ventilation drift. This amount is composed of shear zone and matrix flows into the drift (see chapter 3.1). When ventilation was stopped, the matrix remained dry (under normal climatic conditions) and only the shear zone component of the water inflow continued at a rate of 1.1 l/hour. This implies that, during ventilation, around 0.3 l/hour are removed from the matrix section (Figure 12), corresponding to a flux of 0.37 $mg \cdot m^{-2} \cdot s^{-1}$ from the granodiorite matrix into the drift.

The hydraulic conductivities of the shear zone part and the matrix part are calculated using the formula of THIEM (1906), as it was done in chapter 3.2. The input parameters are given in Figure 12 and the results listed in Table 3.

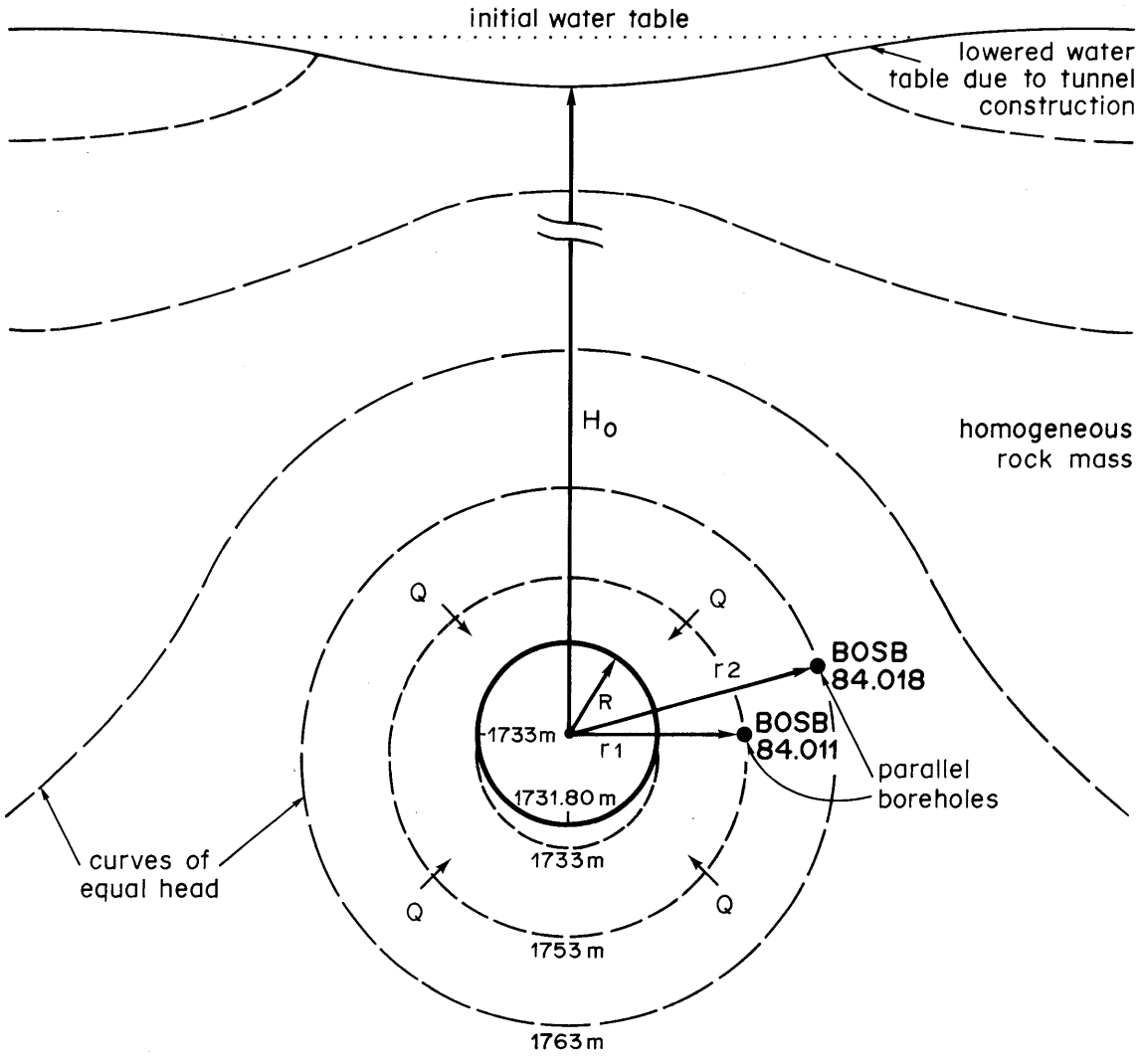

Geometric parameters	Hydraulic parameters *
R = 1.80 m (Radius of tunnel)	h_2-h_1 = 10 m (head difference between boreholes BOSB 84.018 and BOSB 84.011)
r_1 = 3.55 m (radial distance of BOSB 84.011)	H_0 = 400 m (depth of tunnel centre line below water table)
r_2 = 5.30 m (radial distance of BOSB 84.018)	Q = 0.03 l/hour per m of tunnel = 8.3 E-9 $m^3 \cdot s^{-1} \cdot m^{-1}$ of tunnel
	* hypothetical values (expected range)

Figure 10: Idealized hydraulic situation around the ventilation test drift

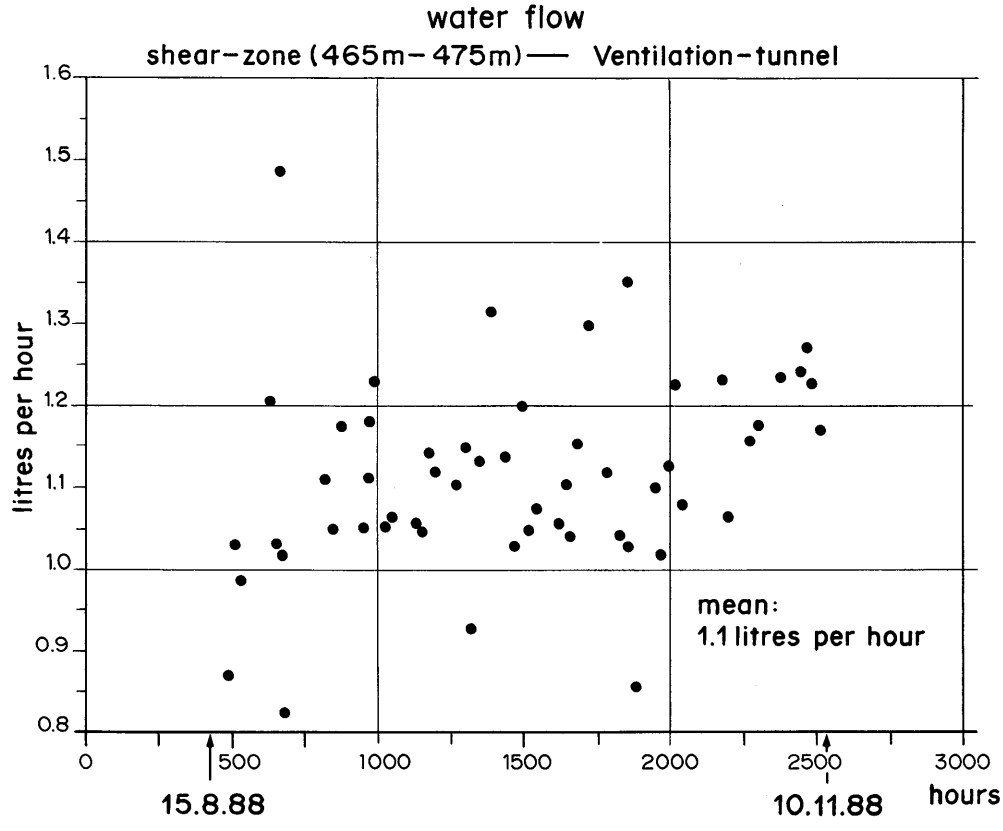

Figure 11: Inflow measurements by plastic sheeting

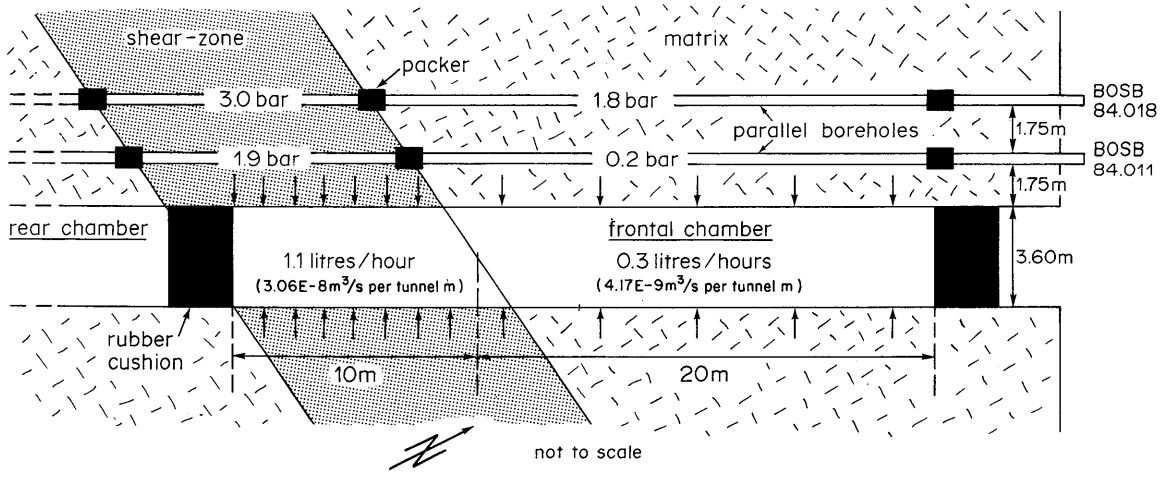

Figure 12: Water balance and parallel borehole pressure, frontal chamber

	q	Q	h_2-h_1	T	K
Shear zone	2.97	3.06E-8	11	1.78E-9*	1.78E-10
Matrix	0.37	4.17E-9	16	---------	1.66E-11

Parameters:

q	=	flux (rock --> tunnel)	[mg·m^{-2}·s^{-1}]
Q	=	Inflow (rock --> tunnel) in m^3/s per m of tunnel	[m^3·s^{-1}·m^{-1}]
h_2-h_1	=	Head difference of parallel boreholes (observation data: Sept. 86)	[m]
T	=	Transmissivity	[m^2/s]
K	=	Hydraulic conductivity	[m/s]
*	=	Thickness of shear-zone: 10 m	

Table 3: Hydraulic conductivity and transmissivity in shear-zone and matrix, respectively, forward section of ventilation drift

The difference in hydraulic conductivity between the shear zone and the matrix is around one order of magnitude. This is in agreement with the findings of structural investigations (chapter 2.4) where it was shown qualitatively that the permeability of (reactivated) shear zones is higher than that of granodioritic gneisses.

It must be mentioned that the calculated transmissivity of 1.78E-9 m^2/s is valid for a homogeneous 10 m-thick shear zone. The high variation in permeability within the shear zone itself is not considered here (e.g. highly permeable fault gouges in contact with low-permeability mylonites).

3.3 Discrete evaporation measurements at the surface of the drift

3.3.1 Program objectives

The geological and small-scale structural investigations carried out (chapter 2) have shown that the rock mass around the ventilation drift is characterized by a highly heterogeneous deformation pattern. This heterogeneity in tectonic strain on all scales is also reflected by variations in permeability and by a non-uniform flow field from the drift wall towards the drift or vice versa.

Under normal ventilation conditions (75% relative humidity, 14° Celsius), the surface of the drift along zones of high permeability is wet (e.g. fault gouges in mylonitic shear zones), while zones of low permeability are dry (e.g. granodiorite matrix). This implies that fluxes of water in both liquid and gaseous phase from the drift wall into the drift are occurring simultaneously. Furthermore, small changes in the climatic conditions (i.e. temperature, relative humidity) in the drift result in transient changes in water and vapor fluxes into the drift.

a) measurement method

RH.....relative humidity
T.....temperature

measurment of T_A, T_B and RH_A, RH_B
at sensors [A] and [B]

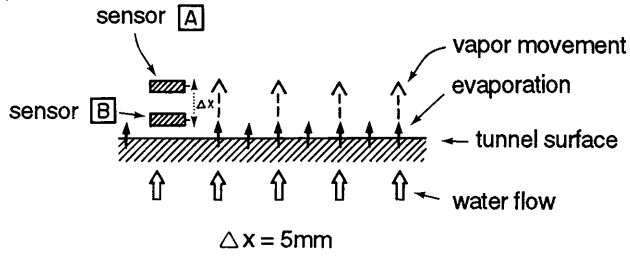

b) assumptions

- laminar flow at tunnel surface
- D = > constant close to the tunnel surface

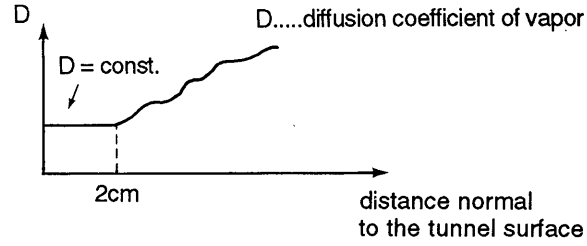

c) equations

$$\frac{\partial Q}{\partial t} = -D \cdot \frac{\partial c}{\partial x} \qquad [1]$$

$\frac{\partial Q}{\partial t}$: vapor flux; $\frac{\partial c}{\partial x}$: concentration gradient of vapor

approximation of equation [1]

$$\frac{\Delta Q}{\Delta t} = -D \cdot \frac{\Delta C}{\Delta x} = \frac{-D}{\Delta x} \cdot \frac{}{R} \cdot \left(\frac{P_{SB} \cdot RH_B}{T_B} - \frac{P_{SA} \cdot RH_A}{T_A} \right) \qquad [2]$$

$\frac{\Delta Q}{\Delta t}$ in $kg \cdot m^{-2} \cdot s^{-1}$

diffusion coefficient of vapor: $D = f\ (T_A, T_B, \text{air pressure})$ (UEDA, 1956) .....D in m^2/s

saturation pressure: $P_{SA} = f\ (T_A)$, $P_{SB} = f\ (T_B)$ (BOSEN, 1960) .....P_{SA}, P_{SB} in Pascal

Δx.....distance between sensor [A] and [B]

R.....gas constant 461.89 Joule / o Kelvin

T_A, T_B ...measured temperatures at sensor [A] resp. [B].....in deg. Celsius

RH_A, RH_B measured relative humidity at sensor [A] resp. [B].....in % divided by 100

Figure 13: Evaporation methode: measurements (a), assumptions (b) and equations (c)

Measurements taking into account both the high spatial variability in vapor flux at the drift surface and transient changes in vapor flux due to changing climatic conditions were performed using a newly developed evaporation technique (WATANABE et al., 1989). This technique was applied in the ventilation drift during October 1989 and April 1990. The technique and the results are presented in the following.

3.3.2 Evaporation measurement technique

The test concept and measurement technique are presented in Figure 13a. A section through a small volume of rock mass, drift surface and drift atmosphere is considered. In the quasi-homogeneous rock mass (volume several cm^3), there is an uniform water flow towards the drift, normal to the drift surface. At the surface, the water evaporates and, due to molecular diffusion, vapor moves uniformly towards the centre of the drift. Molecular diffusion implies that there is a temperature and/or humidity gradient. In the following, temperature is abbreviated with T and relative humidity with RH. If T- and RH-gradients are known, then the vapor flux can be calculated. The T- and RH-gradients are approximated by T- and RH- differences at two locations in the drift, close to the surface. These are measured using temperature and relative humidity sensors (Figure 13a), with resulting T- and RH-values at locations A and B. The sensor units are shown in Figure 14.

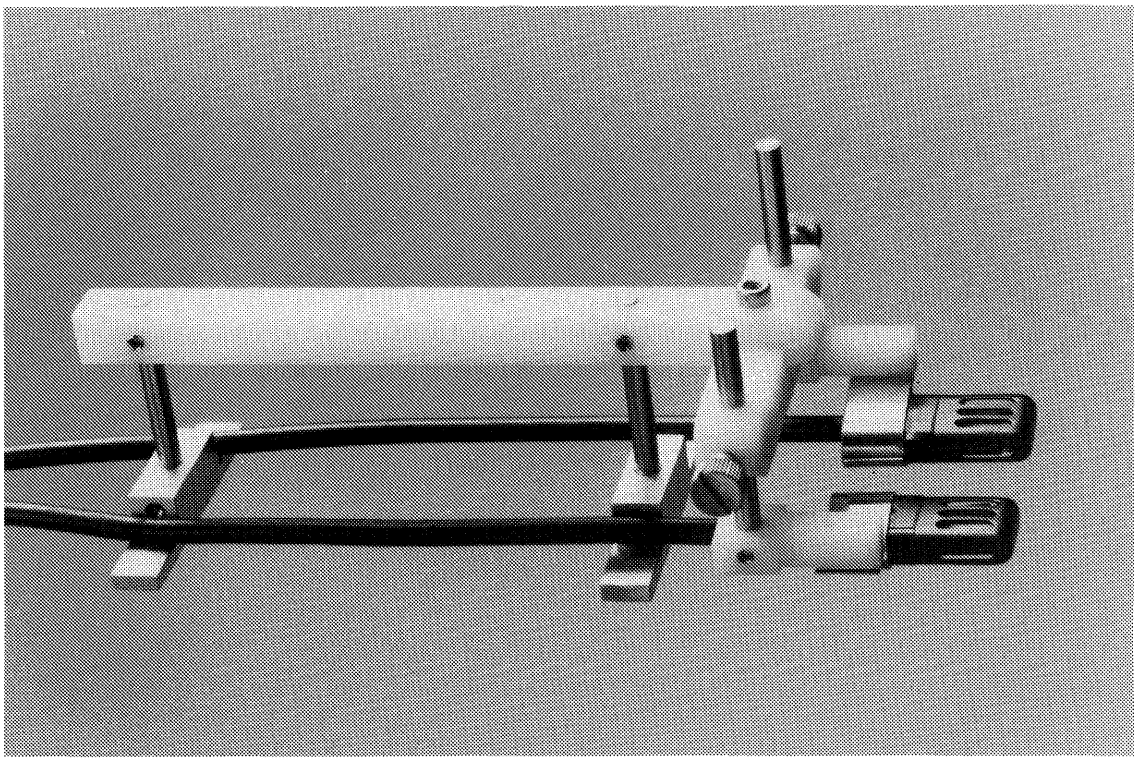

Figure 14: Sensor units (black boxes on the right)

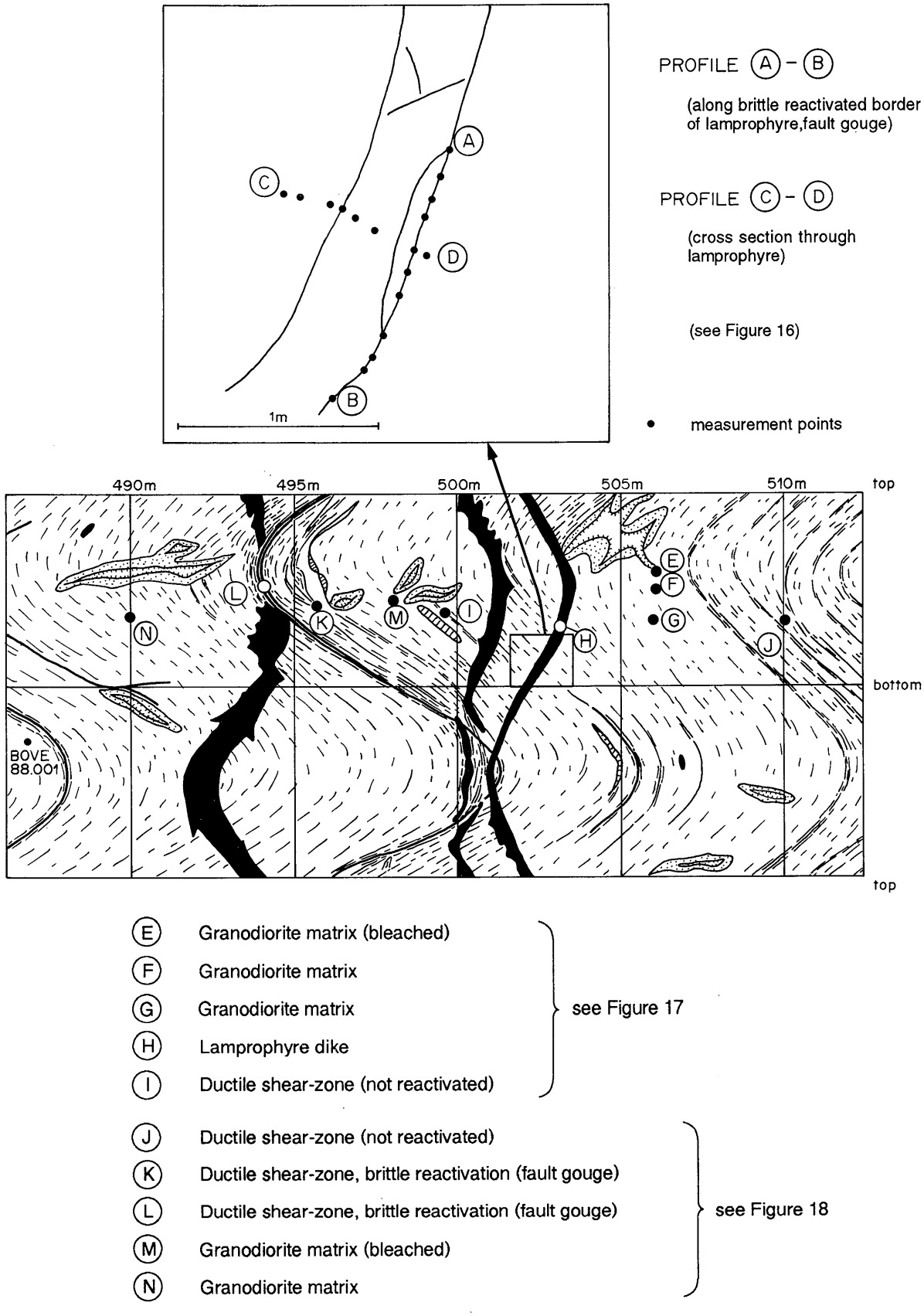

Figure 15: Measurement locations

A thin laminar flow layer exists just above the surface of the drift; the thickness of this layer is dependent on the air velocity in the drift. It was shown experimentally that, for calculating the flux accurately with the evaporation equipment, a laminar flow layer of about 1 cm is needed (WATANABE et al., 1989). In this laminar flow layer, the diffusion coefficient of vapor is assumed to be constant (Figure 13b). The wind velocities in the ventilation drift suggest a laminar flow layer above the surface of at least 1 cm. This is also the reason why T and RH measurements were performed at radial distances of 0.3 and 0.9 cm above the drift surface.

Equation [1] in Figure 13c describes the vapor flux due to a one- dimensional concentration gradient normal to the rock surface. It can be approximated by equation [2] of the same figure where the concentration gradient is expressed in terms of an absolute humidity difference invoking the BOYLE-MARIOTTE law for ideal gases. This equation contains all the measured quantities: T_A and RH_A at sensor A, T_B and RH_B at sensor B. Finally the diffusion coefficient of vapor and the vapor saturation pressure required in equation [2] have been determined experimentally.

Detailed information on the performance of the measurements, the accuracy and calibration of the sensors and the resolution and accuracy of calculated fluxes may be found in WATANABE (1991a, 1991b). A summary is presented below:

Performance of measurements:

T_A, RH_A, T_B and RH_B are measured simultaneously every 20 seconds. The recorded values are 2-minute averages of the 20-second values.

Accuracy and calibration of sensors:

The manufacturer confirms that RH and T can be measured with an accuracy of ± 3%, if RH is lower than 90%. During measurements, a clear temporal T- and RH-drift of the sensors was observed. The sensors were therefore calibrated both before and during measurement in order to correct the calculation of flow.

Resolution and accuracy of calculated fluxes:

The resolution of the calculated fluxes is around 0.1 $mg \cdot m^{-2} \cdot s^{-1}$. Laboratory experiments in which the evaporation rate is known suggest a relative error in the calculated flux of not more than 20%. If movement of the vapor away from the rock surface is not only radial but also parallel along the drift wall (as is the case of strong air circulation), then the relative error is in the order of 30%.

3.3.3 Presentation and discussion of results

The evaporation measurements were performed in the VE drift between tunnel meter 480 and 520 at the locations shown in Figure 15. Profiles A-B and C-D were measured in October 1989, and points E to N were measured in April 1990. The results are shown in Figures 16, 17 and 18.

In Figure 16 the fluxes across and along a lamprophyre dyke are shown. There is a clear positive flux along the lamprophyre wall (profile A-B). The highest fluxes in profile C-D also correspond to the lamprophyre walls. These high fluxes are the result of the fault gouges at the boundary between the lamprophyre and granodiorite matrix, where a zone of increased hydraulic conductivity exists. Small fluxes are measured in the granodiorite matrix and in the lamprophyre dyke. It is not clear whether the negative values are true fluxes from the drift into the rock-wall or whether they represent only very small positive fluxes (from the rock-wall into the drift) which fall within the error interval. A comparison is also made with water inflow values measured using the ventilation experiment and the plastic sheeting method (see Figure 16, top). Although these fluxes were measured over a large area and a long period of time, the values are of the same order of magnitude and compare favourably to the "point" fluxes calculated using the evaporation technique.

Figure 17 shows the transient behaviour of vapor fluxes due to changing climatic conditions at sites E to I in the ventilation drift. The letters E to I correspond to the locations in Figure 15. The initial climate conditions in the VE drift consisted of a relative humidity of 100% over one week and a temperature of around 13 degrees Celsius. There is a general tendency for fluxes to increase just after the introduction of each new climatic condition, and then to gradually decrease (see peaks in Figure 17). This rapid increase in flux may be explained by an increase of the pressure gradient which leads to removal and evaporation of the water stored close to the drift surface (e.g. water stored in the grain boundary pores of the granodiorite). Once this stored water has been removed, a new vapor equilibrium is slowly reached. A further increase in the humidity gradient (e.g. change from climatic condition 1 to 2) repeats this process but extends the "unsaturated" zone deeper into the rock. Under steady-state conditions, the evaporation rate should be constant and should theoretically equal the natural inflow rate. The evaporation rate should then be independent of air humidity. This can partly be seen in Figure 17 (i.e. F and G) where the vapor fluxes evaluated during climatic conditions 2 and 3 are more or less the same. On the other hand, some fluxes at climate condition 3 were clearly higher (see H and I in Figure 17). This indicates that true steady-state conditions are not reached and the unsaturated zone is still extending. The measuring periode during a constant climate condition should therefore be increased from about one day to several weeks.

In Figure 18 (top), fluxes from a mylonitic ductile shear zone are compared with fluxes in brittely reactivated shear zones (fault gouges). It can be seen that the calculated evaporation rate in the fault gouges is up to 6 times higher than in the non-reactivated shear zone. These fault gouge fluxes probably do not represent steady-state conditions (high variability of the fluxes during the three climatic phases) and therefore cannot be related to natural inflows. The granodiorite matrix (Figure 18, bottom) shows a flux in the order of 1 $mg \cdot m^{-2} \cdot s^{-1}$, which seems to be slightly higher than the flux in non-reactivated shear zones. The latter give calculated fluxes of less than 1 $mg \cdot m^{-2} \cdot s^{-1}$. These results are confirmed structurally by the flow path geometry (chapter 2, Figure 8). It was shown that hydraulic conductivity is highest in the fault gouges of the reactivated shear zones and lowest in the compact, mylonitic (non-reactivated) shear zones.

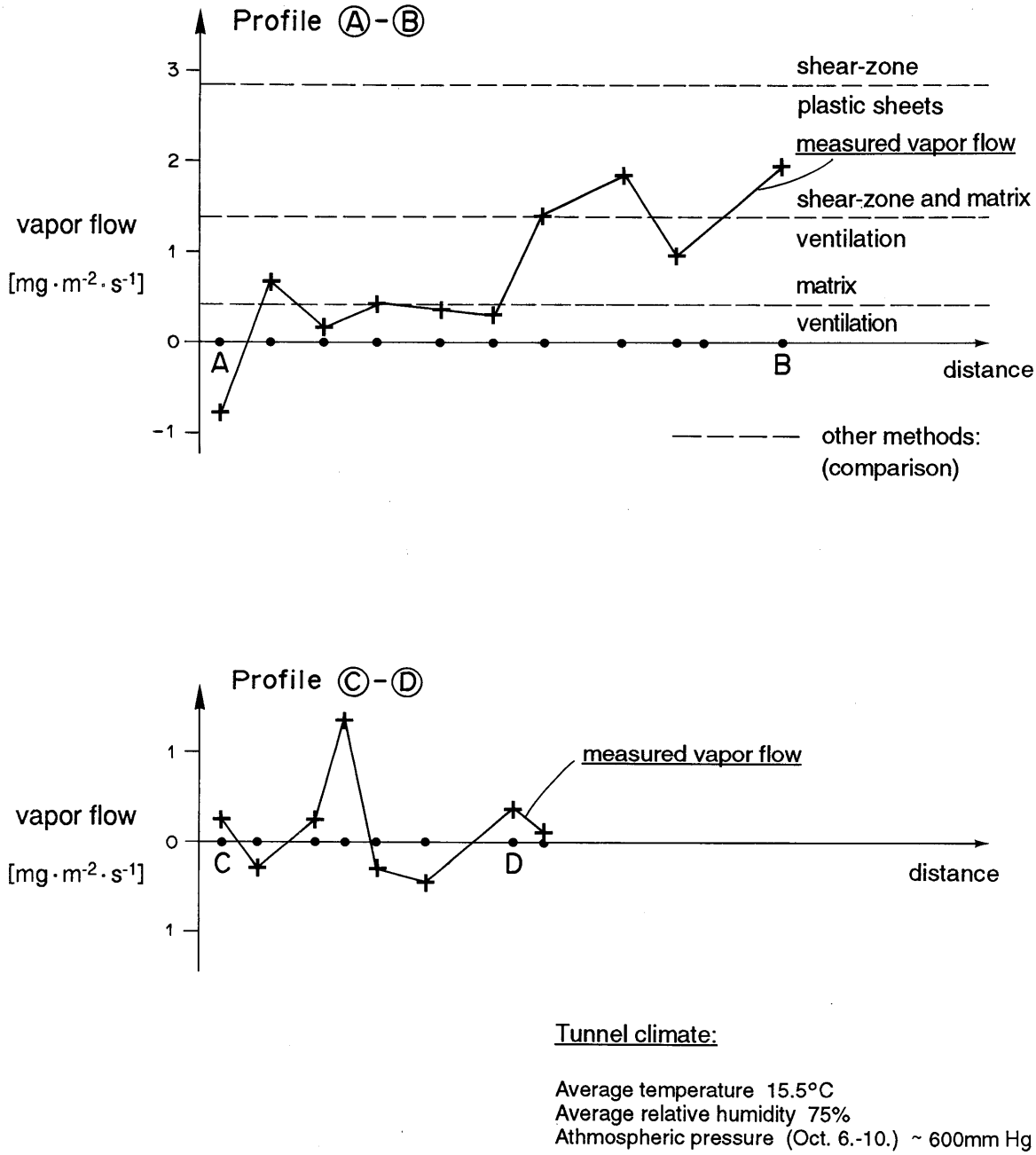

Tunnel climate:

Average temperature 15.5°C
Average relative humidity 75%
Athmospheric pressure (Oct. 6.-10.) ~ 600mm Hg

Figure 16: Evaporation rate along and across lamprophyre

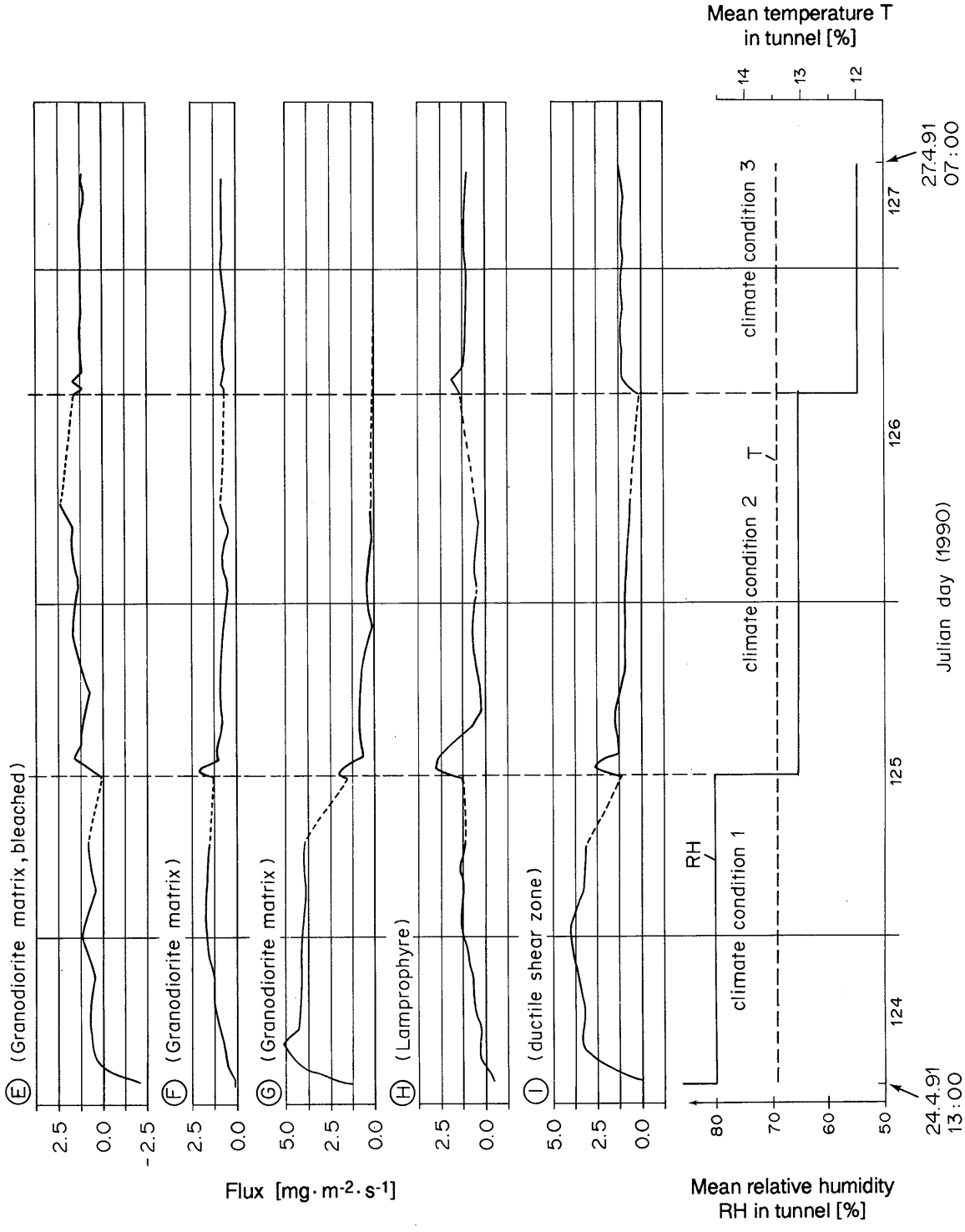

Figure 17: Temporal variations of evaporation rate due to changing climate conditions in the drift

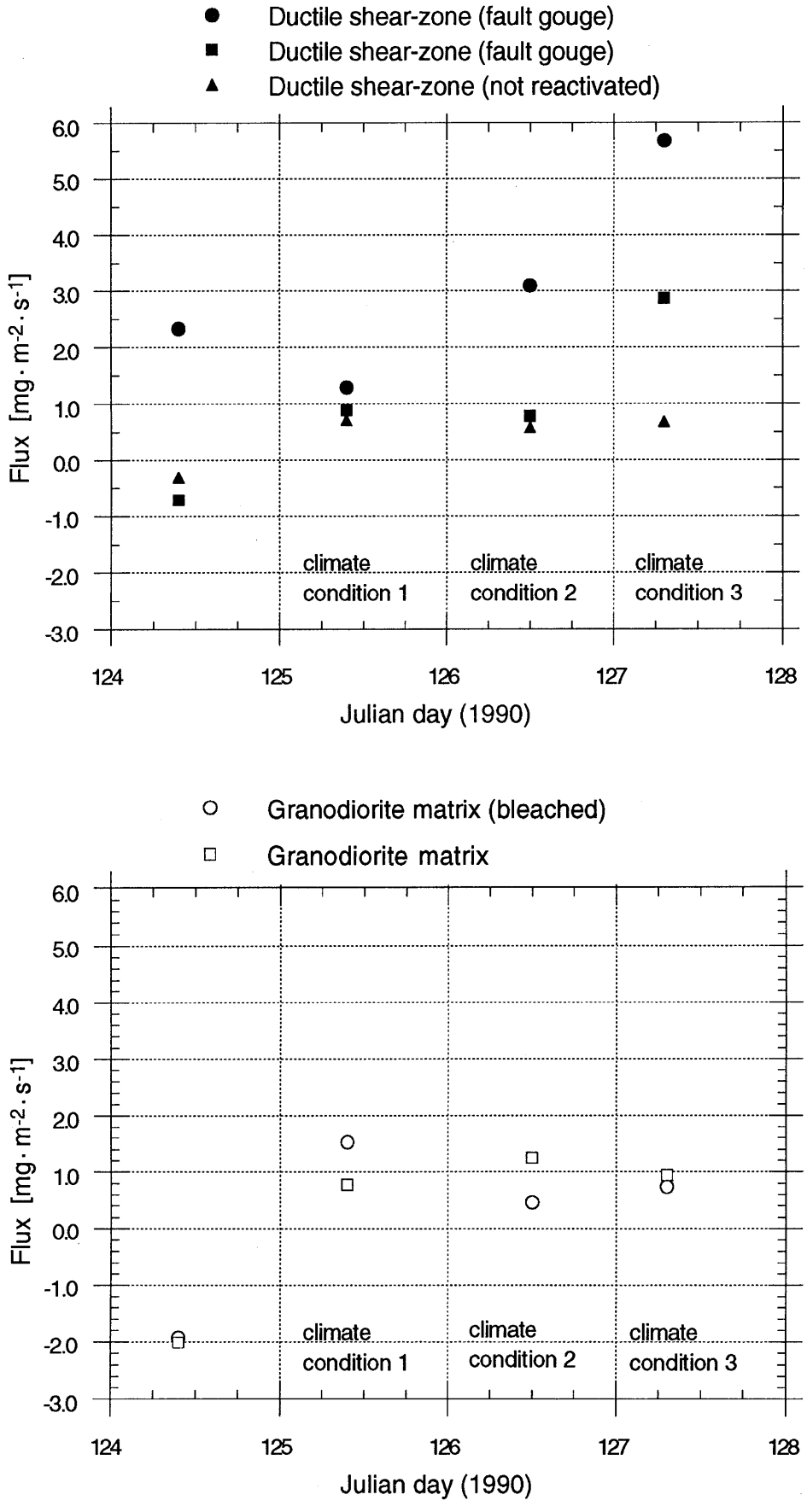

Figure 18: Evaporation rates related to geologic structure

4. ACTIVE AND PASSIVE HYDROGEOLOGICAL TESTING IN THE VE DRIFT

P. Heiniger (Suiselectra AG, Biel)

4.1 Introduction

In the forward section of the VE drift, the boreholes BOVE 88.001, 88.002, 88.003 and borehole BOSB 80.005 intersect both the granodiorite matrix and a 10 m-thick shear zone (cf. Figures 3 and 5, chapter 2). The hydrogeological investigations carried out in these boreholes had the following objectives:

- measuring the spatial distribution of hydraulic pressure in the vicinity of the VE drift
- determining the hydraulic parameters transmissivity (T), permeability (K) and storage coefficient (S) of the matrix and the shear zone
- identifying hydraulic connections (interference reactions)

4.2 Hydraulic head measurements

Once the multipacker systems had been installed, pressure build-up was registered continuously in the individual measuring intervals over a period of several weeks. Long-term monitoring of the spatial pressure distribution in the vicinity of the VE drift assisted in the calibration of the hydrodynamic modeling work (see chapter 5). The observed steady-state relative pressures and corresponding heads are shown in Table 4 in relation to the VE drift.

In borehole BOVE 88.001 it proved impossible to measure pressure build-up due to leakage of the packer system. This borehole was equipped with hydraulically inflatable packers in 1990.

Unexpectedly low heads were measured in the intervals near the drift, which indicates that the potential field is strongly influenced by the VE drift in zones near the drift (unsaturated zone). Two open fracture systems were identified clearly during the pressure build-up phase:

- In borehole BOSB 80.005, interval 5.5, there was no pressure build-up. The rock formation in this area is drained by an open fracture directly into the AU tunnel.
- In the matrix intervals of boreholes BOVE 88.003 (interval 3.3) and BOSB 80.005 (interval 5.3), a temporally absolutely parallel pressure build-up and, therefore, the same steady-state head were measured (approx. 27.0 m); this indicates a direct hydraulic connection between these two intervals.

These two intervals are located to the north of the 10 m-thick shear zone, where there is increased fracture density on both sides of a lamprophyre dyke (cf. Figure 5, tunnel meters 455-465). A hydraulic link is therefore plausible.

Borehole	Interval	Rel. Pressure [bar]	Head [m]	Geology
88.002	2.1	12.9	131.5	Matrix
	2.2	4.8	48.9	Shear zone
	2.3	1.35	13.8	Matrix/Shear zone
88.003	3.1	5.4	55.0	Matrix
	3.2	3.6	38.7	Shear zone
	3.3	2.65	27.0	Matrix
88.004	4.1	23.0	234.5	Matrix
	4.2	13.1	133.5	Shear zone
	4.3	12.5	127.4	Shear zone
	4.4	1.75	17.8	Matrix
88.005	5.1	19.75	207.0	Matrix
	5.2	7.6	83.2	Matrix
	5.3	2.8	26.9	Matrix
	5.4	2.55	31.7	Shear zone
	5.5	---	---	Shear zone

Table 4: Pressure and head measurements relative to the drift surface (1733.0 m asl.)

4.3 Hydrogeological testing

4.3.1 Test programme

In order to determine the hydrogeological parameters transmissivity T and storage coefficient S, and to investigate the presence of hydraulic connections, hydrotests were performed in the intervals shown in Figure 19. The aim of these tests was to obtain estimated parameter values for the shear zone and the matrix which are spatially homogeneously distributed, and to investigate interference reactions between the individual boreholes.

Constant head injection tests or constant flow injection tests were used to determine the hydrogeological parameters transmissivity T and storage coefficient S. Interference reactions could also be observed using the constant head injection tests (see chapter 4.4).

Pressure recovery after the injection tests was also evaluated to give an additional measurement of transmissivities.

The test performance and evaluation methods can be summarized as follows:

- **Constant head injection test (QCH):**
  - Principle: Measuring injection rate as a function of time with constant injection pressure
  - Evaluation: Straight-line method after JACOB & LOHMAN (1952)

- **Constant flow injection test (QCF):**
  - Principle: Measuring pressure as a function of time with constant injection rate
  - Evaluation: Straight-line method after COOPER & JACOB (1946)

- **Pressure recovery following QCH and QCF:**
  - Principle: Measuring the temporal evolution of pressure recovery following constant head or constant flow tests
  - Evaluation: Horner-Plot after HORNER (1951)

In addition to these test methods, the "steady-state" approximation (MOYE, 1967) allowed a rough estimate of transmissivity. This particular method will not be discussed further in the following chapters.

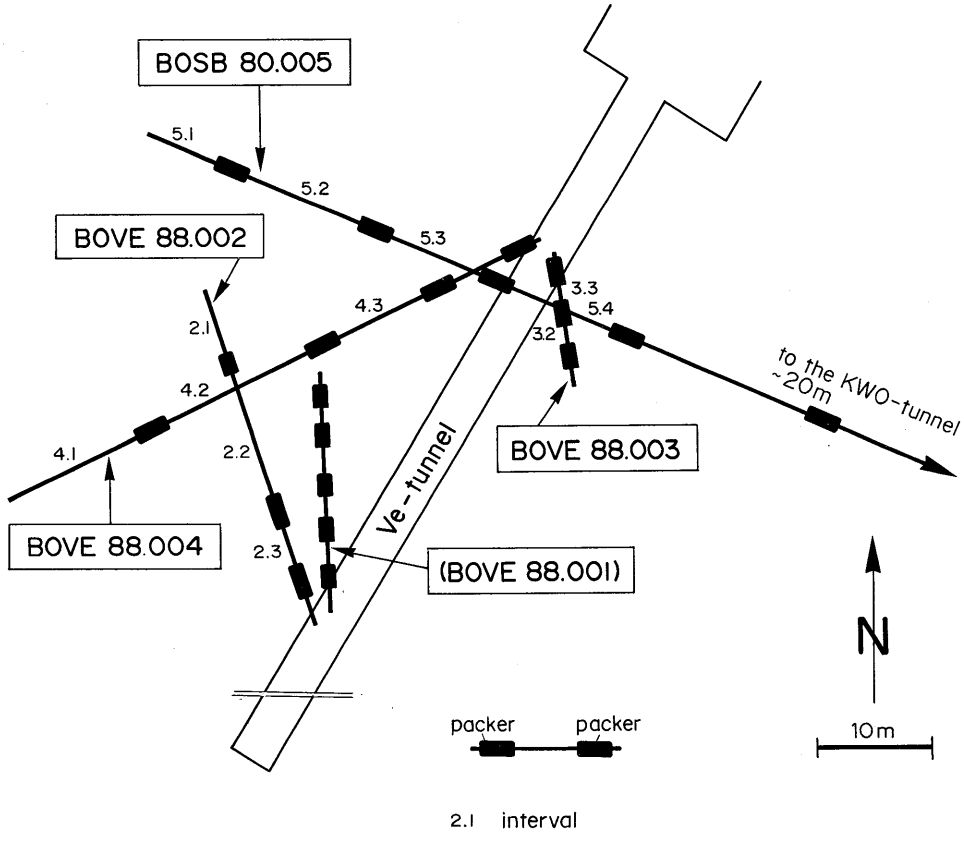

Figure 19: Instrumentation of BOVE 88.001, 88.002, 88.003, 88.004 and BOSB 80.005. Numerical orders of the measurement intervals

Measuring values for transmissivity and storage coefficient using the straight-line method after JACOB & LOHMAN (1952) and COOPER & JACOB (1946), and determining transmissivity on the basis of the pressure recovery phase (HORNER, 1951) following injection tests, both assume that a number of boundary conditions will be observed (infinite, homogeneous, isotropic aquifer, radially symmetric flow, constant injection pressure, constant injection rates, etc.).

4.3.2 Test equipment

The equipment used in the tests consists of the following components (cf. also Figure 20):

- **Multipacker systems type Solexperts:**
  - These packer systems consist of pneumatic-hydraulic packers (length = 1000 mm).
  - The packers are inflated with gas or water using separate inflation lines. An observation line and an injection line lead into each measuring interval. Measurement of pressure in the intervals is performed outside the borehole using electric pressure sensors.

- **Multipacker system type GSF-Braunschweig:**
  - Borehole VE 88.001 was equipped with this system consisting of mechanically inflatable packers.

- **Injection unit:**
  - Rotary pump for T > 1E-9 m^2/s, formation pressure < 17 bars
  - Pressure vessel for T < 1E-9 m^2/s, formation pressure > 17 bars
  - Constant flow injection pump (type Shimadzu HPLC-SP pump) for formation pressures > 17 bars.

- **Flow measurements:**
  - Electronic weighing cell (type Mettler PE22) for Q < 30 ml/min
  - Flow-meters (type Micromotion D6 and D25) for Q > 30 ml/min.

- **Data acquisition system:**
  - A/D converter (type Thermodac 32)
  - Personal computer.

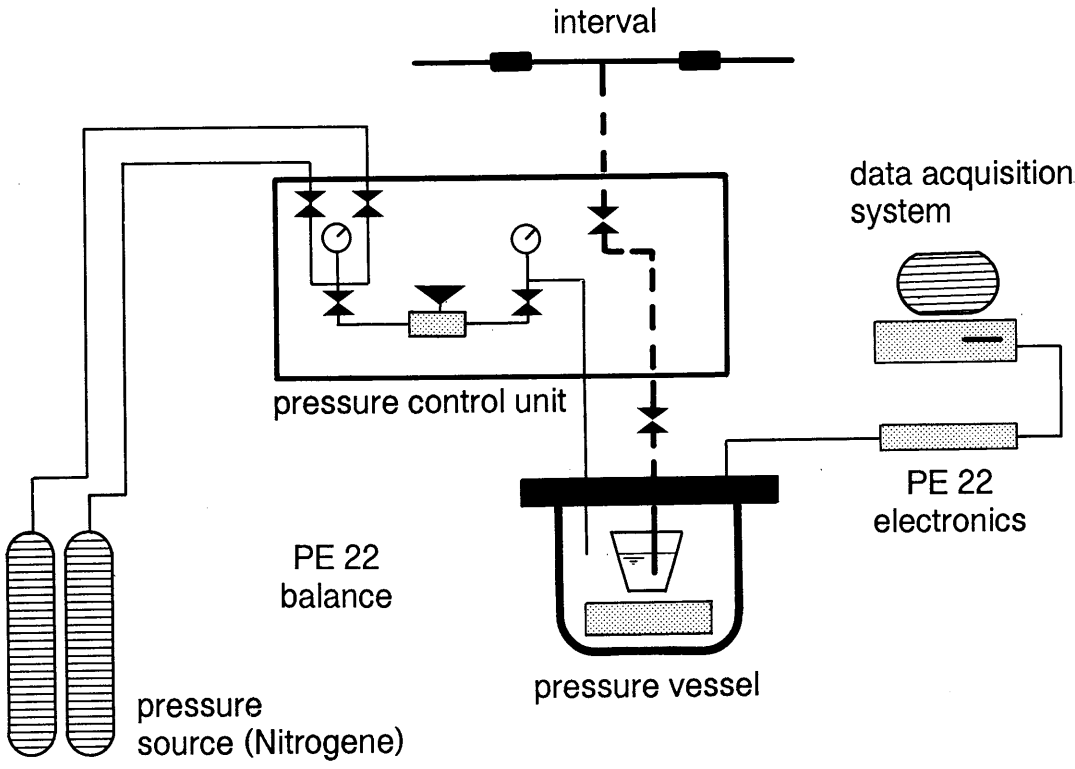

Figure 20: Test equipment for constant head injection test for T < 1E-9 m^2/s, P < 17 bar

For performing the relevant tests and measurements, the boreholes were equipped with multipackers as outlined in Table 5a+b.

Boreholes BOSB 80.005, BOVE 88.002, BOVE 88.003 and BOVE 88.004 were equipped with hydraulically inflatable multipacker systems (type Solexperts), and borehole BOVE 88.001 with a mechanically expanding packer system from GSF-Braunschweig. The layout of the borehole instrumentation is shown in Figure 19.

The entire hydrogeological investigation campaign (borehole instrumentation, measurement of pressure distribution, hydrotesting) was carried out between February 1989 and November 1989, and is documented in detail in HEINIGER (1989a, 1989b).

Borehole BOVE 88.001

Total length : 28.25 m
Inclination : -43° 20'
Top of borehole : 1732.81 m asl.
Shear zone : 10.00 - 22.90 m
Type of instrumentation : Multipackers (type GSF)

Test interval	Start	End	Geology
1.1	26.40 m	28.25 m	Matrix
1.2	20.70 m	25.95 m	Shear zone
1.3	17.50 m	20.25 m	Shear zone
1.4	11.80 m	17.05 m	Shear zone
1.5	7.10 m	11.35 m	Matrix/Shear zone

Borehole BOVE 88.002

Total length : 29.91 m
Inclination : 5° 27'
Top of borehole : 1734.84 m asl.
Shear zone : 09.48 - 20.43 m
Type of instrumentation : Multipackers (type SOLEXPERTS)

Test interval	Start	End	Geology
2.1	23.00 m	29.91 m	Matrix
2.2	11.00 m	22.00 m	Shear zone
2.3	3.00 m	10.00 m	Matrix/Shear zone

Borehole BOVE 88.003

Total length : 34.50 m
Inclination : 173° 43'
Top of borehole : 1734.84 m asl.
Shear zone : 13.32 - 24.10 m
Type of instrumentation : Multipackers (type SOLEXPERTS)

Test interval	Start	End	Geology
3.1	26.00 m	34.50 m	Matrix
3.2	11.50 m	25.00 m	Shear zone
3.3	4.00 m	10.50 m	Matrix

Table 5a: Instrumentation of borehole VE 88.001, 88.002 and 88.003

Borehole BOVE 88.004

Total length : 59.15 m
Inclination : 30° 55'
Top of borehole : 1734.26 m asl.
Shear zone : 19.44 - 41.00 m
Type of instrumentation : Multipackers (type SOLEXPERTS)

Test interval	Start	End	Geology
4.1	59.15 m	44.00 m	Matrix
4.2	27.80 m	43.00 m	Shear zone
4.3	15.50 m	26.80 m	Shear zone
4.4	4.50 m	14.50 m	Matrix

Borehole BOVE 88.005

Total length : 100.00 m
Inclination : 2° 00'
Top of borehole : 1738.45 m asl.
Shear zone : 35.00 - 55.00 m
Type of instrumentation : Multipackers (type SOLEXPERTS)

Test interval	Start	End	Geology
5.1	94.00 m	100.00 m	Matrix
5.2	81.00 m	93.00 m	Matrix
5.3	60.00 m	80.00 m	Matrix
5.4	48.50 m	47.50 m	Shear zone
5.5	31.20 m	47.50 m	Shear zone

Table 5b: Instrumentation of borehole VE 88.004 and 88.005

4.3.3 Field data

The hydrotests were carried out in two phases. In the first phase, boreholes BOVE 88.002, 88.003 and 88.004 were tested. Figure 21 shows the pressure evolution in the tested intervals in phase I. In the second phase, hydrotests were performed in borehole BOSB 80.005.

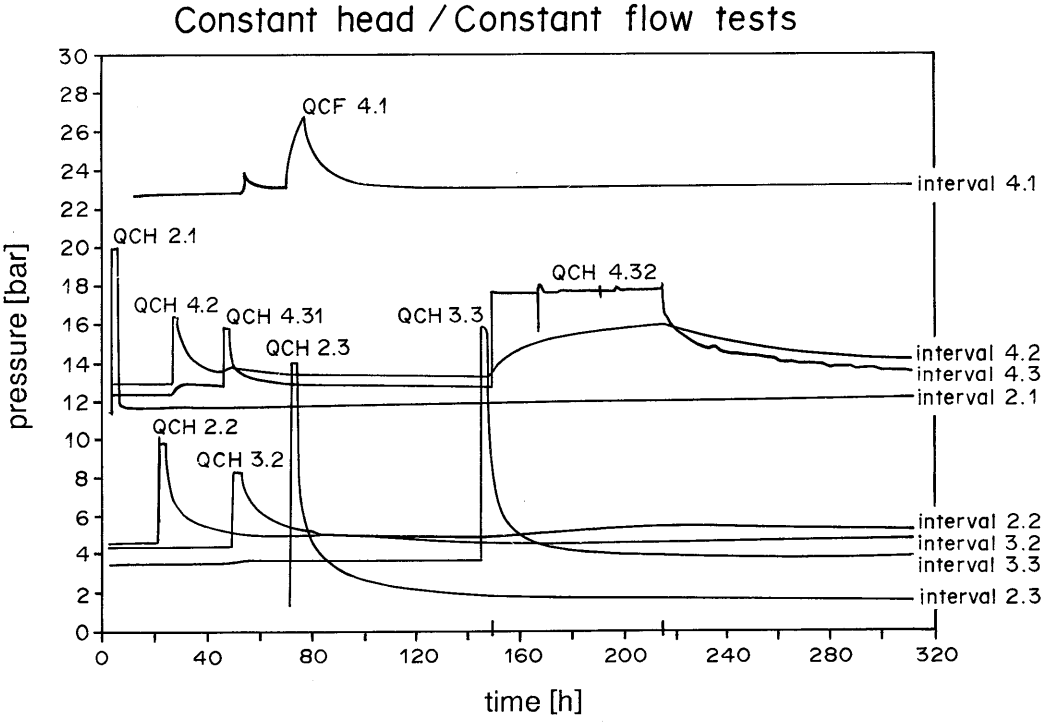

Figure 21: Constant head and constant flow injection tests

4.3.4 Test interpretation

By way of an example the test performance and interpretation is presented in the following section. A constant head injektion test followed by a pressure recovery period was carried in borehole BOVE 88.003, interval 3.2 (shear zone) (cf. Figures 22 and 23).

Based on mentioned two interpretation methods, the following transmissivity values were obtained for the shear zone in borehole BOVE 88.003:

- Constant head injection test T = 2.7E-9 [m^2/s]
- Pressure recovery T = 6.7E-10 [m^2/s]

The values therefore correlate well and the deviation is less than half an order of magnitude ($T_{QCH} : T_{PR} = 1:4$).

The results of all the tests are presented in detail in HEINIGER (1989b). The determined hydrogeological parameters are summarized in the following table 6.

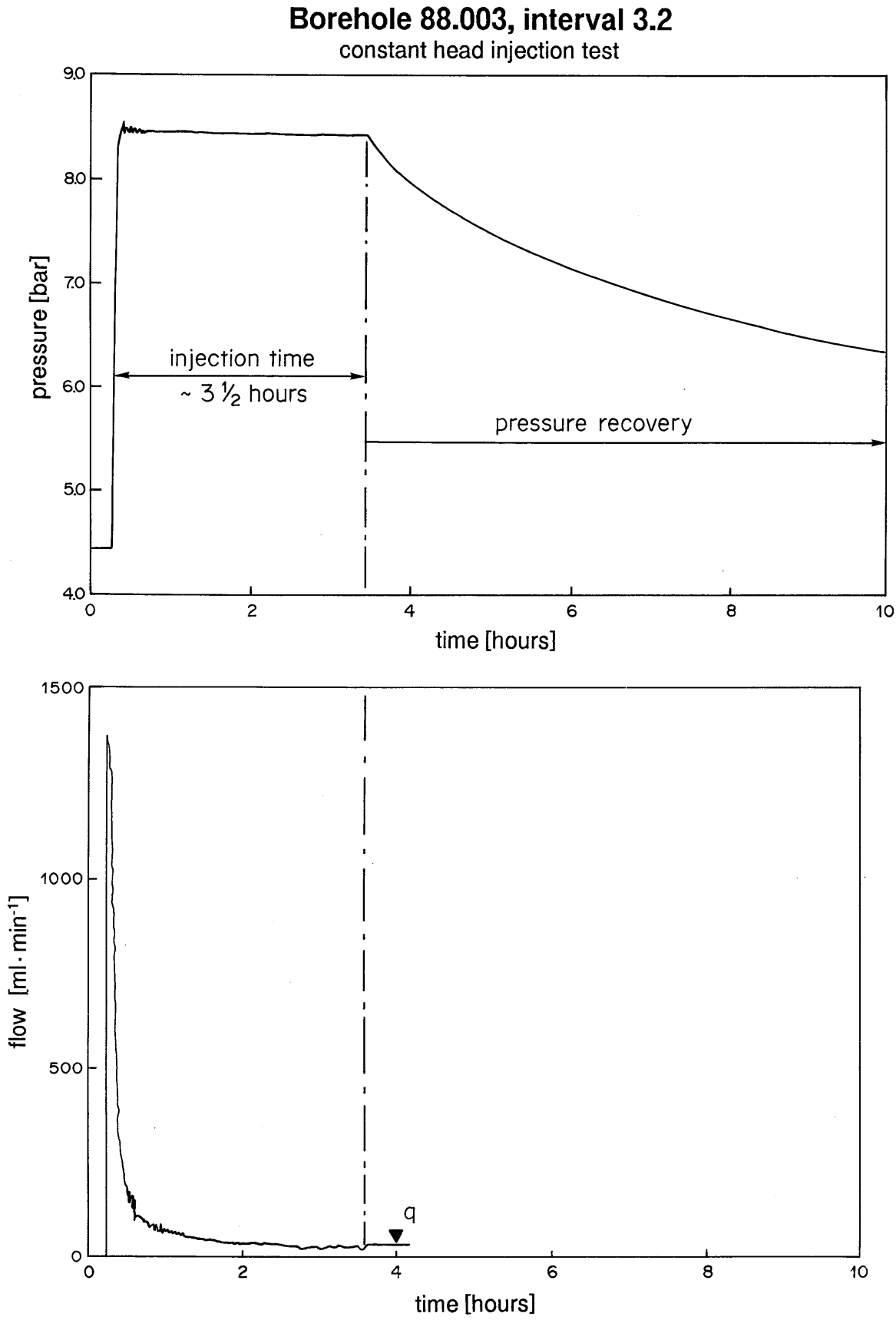

Figure 22: Constant head injection test with pressure recovery BOVE 88.003, interval 3.2

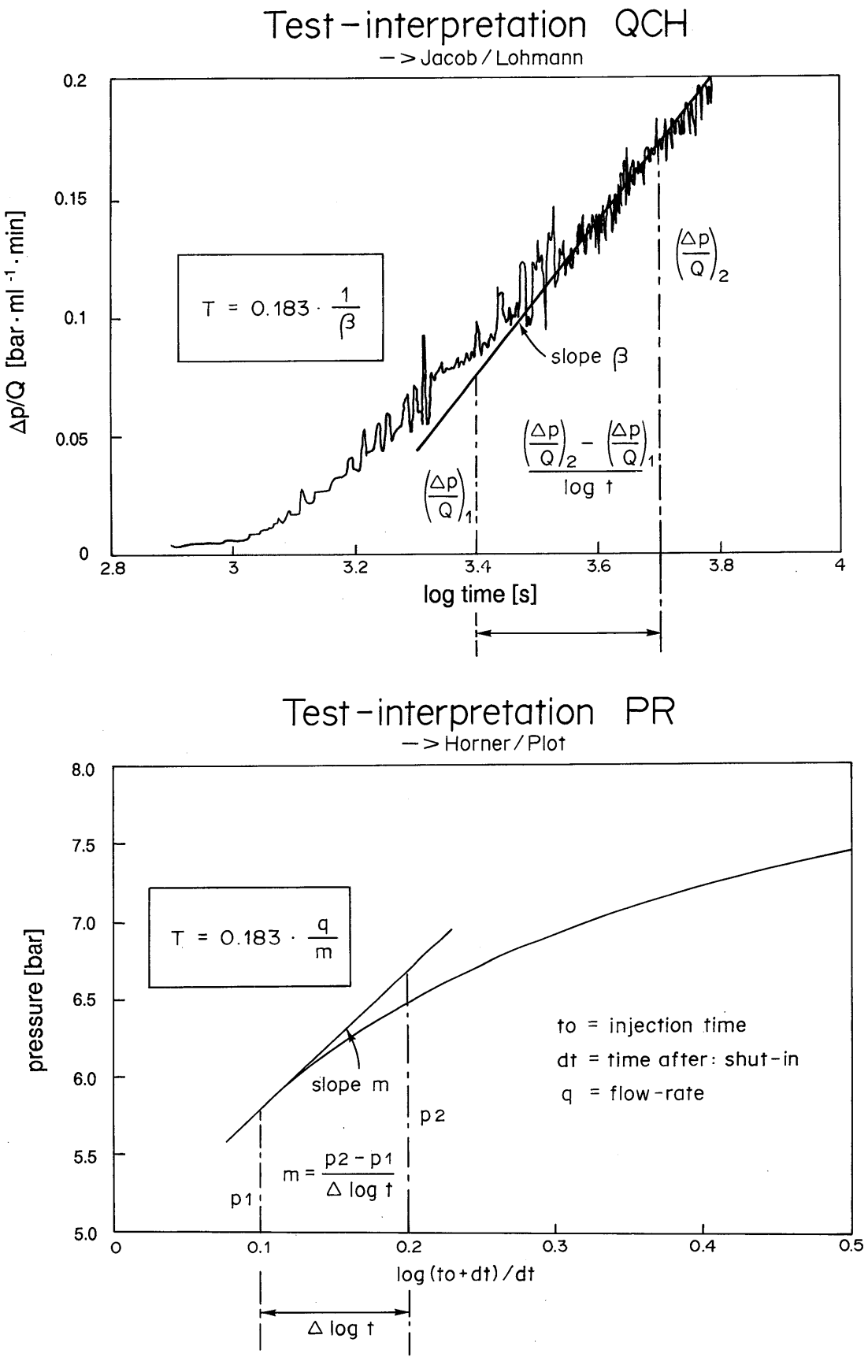

Figure 23: Test evaluation

Intervals of matrix:

Borehole	Interval	length [m]	T [m^2/s]	S	K [m/s]	S_s [m^{-1}]
88.002	2.1	6.9	1.5 E-9	3.3 E-7	2.2 E-10	4.8 E-8
	2.3	7.0	7.2 E-10	2.6 E-3	1.0 E-10	3.7 E-4
88.003	3.3	6.5	6.6 E-11	3.7 E-5	1.0 E-11	5.7 E-6
88.004	4.1	15.2	6.1 E-10	2.1 E-3	4.0 E-11	1.4 E-4
88.005	5.1	6.0	5.7 E-10	5.6 E-3	9.5 E-11	9.3 E-4
	5.2	12.0	1.2 E-10	6.9 E-4	1.0 E-11	5.8 E-5
	5.3	20.0	7.5 E-11	2.7 E-5	3.8 E-12	1.4 E-6

Intervals of shear zone:

Borehole	Interval	length [m]	T [m^2/s]	S	K [m/s]	S_s [m^{-1}]
88.002	2.2	11.0	2.3 E-9	1.7 E-3	2.1 E-10	1.5 E-4
88.003	3.2	13.5	2.7 E-9	3.0 E-3	2.0 E-10	2.2 E-4
88.004	4.2	15.2	2.8 E-9	3.5 E-3	1.8 E-10	2.3 E-4
	4.3	11.3	6.0 E-9	6.9 E-4	5.3 E-10	6.1 E-5
88.005	5.4	10.5	9.9 E-10	7.7 E-5	9.4 E-11	7.3 E-6

Parameters:

T	=	transmissivity	[m^2/s]
K	=	hydraulic conductivity (K=T/L)	[m/s]
S	=	storativity	[-]
S_s	=	coefficient of specific storage (S_s=S/L)	[m^{-1}]
L	=	length of interval	[m]

Table 6: Summary of results of the hydraulic parameters

The accuracy of these parameters, which are determined on the basis of "simple" methods, requires to be assessed critically for the following reasons:

- The interpretation methods used are restricted to the case of an infinite, isotropic homogeneous aquifer.
- Interpretation of pressure recovery according to Horner assumes a constant flow rate for the preceding injection phase, as well as radially symmetric flow from the formation to the borehole during pressure recovery.

These boundary conditions relating to the aquifer are not fulfilled for the transmissivity measurement in the present case since there is a heterogeneous open pore-space.

In addition to this, the evaluation of pressure recovery following constant head tests was based on the flow measured at the end of the injection phase. This does not fulfil the model concept of "constant flow during the injection phase".

Despite these reservations, the transmissivity values obtained can be used as first approximations because

- the values obtained using different test and interpretation methods (constant head/flow injection tests, "steady-state" estimate, pressure recovery) show a good correlation.
- a comparison with the results of evaluation using CURE (1990) showed an agreement in the order of factor 10 to 15.

However, the storage coefficients determined on the basis of constant head/flow injection tests had to be looked at critically because, similarly to the case of the transmissivity measurement, the boundary conditions regarding the aquifer were not fulfilled.

In addition to this, it has to be assumed that the upward dipping boreholes cannot be completely ventilated. Enclosed volumes of air falsify the measurement of the storage coefficient due to the increased, but unknown, "wellbore storage" component.

4.4 Discussion of results

The permeabilities (K) of the matrix are not significantly different from those of the shear zone. This slight difference can be explained by the existing pore-space geometry:

- The flow path geometry of the matrix is characterized by a network of grain boundary pores (Figure 7). Depending on the rock fabric, the permeability of the granodiorite matrix can thus be quite high in places. The pore-spaces of the matrix are also linked in some locations with the pore-spaces of the shear zone (cf. Figure 8).

- The flow geometry of the shear zone was characterized as a pore-space consisting of fault gouges and sheet silicate pores. The mean permeability K of the shear zone intervals is influenced strongly by the frequency of these fault gouges per interval (K = T/L). If a large number of fault gouges is determined for a particular interval, the permeability of this interval can exceed that of the matrix by up to two orders of magnitude. If, on the other hand, no fault gouges are identified for an interval, the permeability can actually be lower than that of the matrix (qualitative statement).

In addition to measuring hydrogeological parameters, the hydrotests were also designed to detect hydraulic links between the individual boreholes. Of particular interest is whether there are clear links between the shear zone intervals, and whether there are reactions between matrix and shear zone intervals.

The interference reactions measured during the constant head injection tests in phase I are summarized in Table 7, while the temporal pressure evolution is shown in Figure 24.

Test in Borehole	Interval	Testtyp	Interference reaction Borehole	Interval	Pressure reaction [Pa]	Injection time [h]
88.002	2.2 (Shear zone)	QCH 2.2	88.002	2.1 (Matrix)	5.8	~ 2
88.002	2.3 (Matrix)	QCH 2.3	88.002	2.1 (Matrix) 2.2 (Shear zone)	2.5 5.3	~ 2.50
88.003	3.2 (Shear zone)	QCH 3.2	88.003 88.005 88.005	5.3 (Matrix) 3.3 (Matrix) 5.4 (Shear zone)	13.1 13.7 70.4	~ 3.25
88.004	4.2 (Shear zone)	QCH 4.2	88.004	4.3 (Shear zone)	58.7	~ 2
88.004	4.3 (Shear zone)	QCH 4.31	88.004	4.2 (Shear zone)	24.1	~ 2.0
88.004	4.3 (Shear zone)	QCH 4.32	88.004 88.002 88.003	4.2 (Shear zone) 2.2 (Shear zone) 3.2 (Shear zone)	256.7 50.3 12.0	~ 66.0

Table 7: Interference reactions in Shear zone intervals

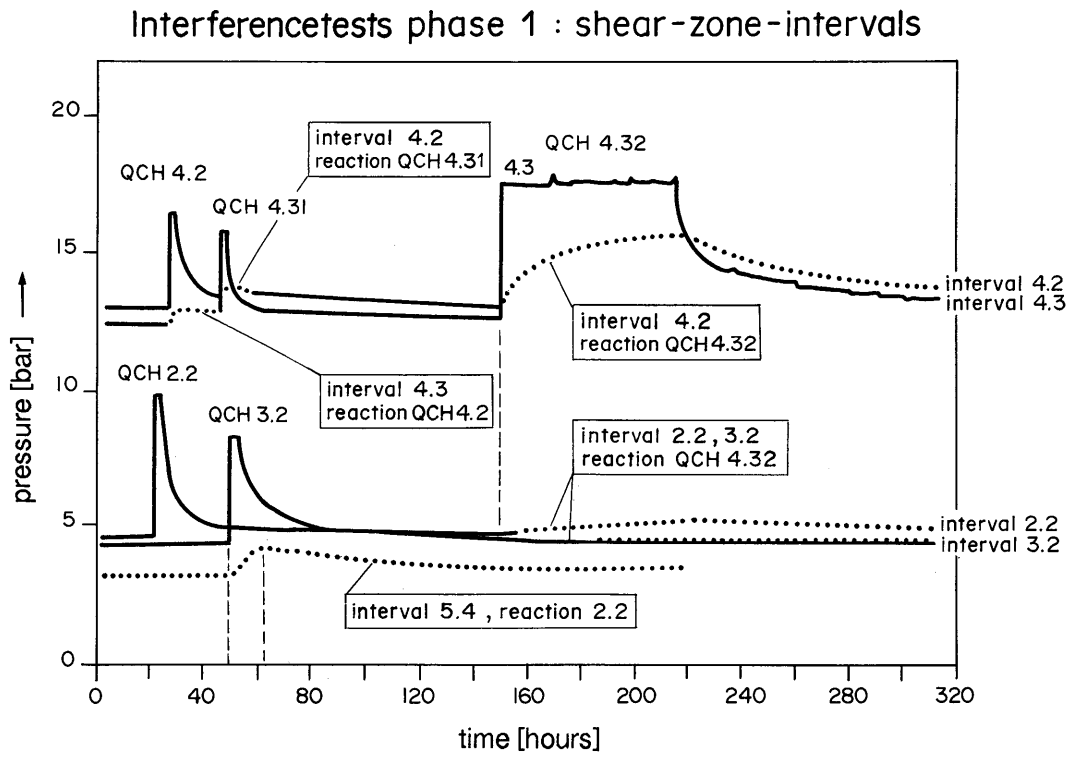

Figure 24: Interference reactions in Shear zone intervals

All observed interference reactions between the different borehole intervals, matrix and shear zone, during this testing campaign are summarized in the following:

- **Matrix --> matrix reactions** were not observed between the different boreholes
- **Shear zone --> shear zone reactions** between the different boreholes could be measured clearly during both the short-term injection test in shear zone interval BOVE 88.003, interval 3.2, and in the long-term injection test in shear zone interval BOVE 88.004, interval 4.3; this was expected on the basis of the flow path geometry of the shear zone.
- **Shear zone --> matrix reactions** between the different boreholes could not be detected. The pressure reaction in BOSB 80.005, interval 5.3 could be explained by the direct hydraulic link BOVE 88.003, interval 3.3 <--> BOSB 80.005, interval 5.3 (QCH 3.2).
- **Matrix --> matrix reactions** between the different boreholes were not detected. The injection tests in the matrix intervals in boreholes BOVE 88.002 and 88.003 did however show slight pressure reactions in the directly adjacent matrix intervals.

5 MODELING STUDIES

C. Gmünder (Simultec AG, Meilen)

5.1 Validation experiment

5.1.1 Introduction

One main problem in modeling the seepage flow in fractured rock arises from the fact, that information about the water pressure distribution can only be optained by drilling boreholes. In the first place such boreholes are expensive and in the second place they influence the seepage flow by creating additional flow paths along open borehole sections. The number of observation boreholes must therefore be minimized.

To aquire experience on the amount of head measurements needed to build up a model of the ventilation test, a validation experiment was performed. The head measurements done by GSF (BRASSER & KULL, 1987) were used to calibrate different model variants. Using these model variants, predictions of the head distribution along the planned boreholes BOVE 88.001 to BOVE 88.004 were done. After completion of the head measurements in these boreholes (see chapter 4) the measured head data was compared with the predicted head distribution (chapter 5.1.7).

5.1.2 Concept of "macropermeability"

The original configuration of the ventilation test is based on the assumption that the inflow to the ventilation drift can be explained using a homogeneous, isotropic continuum model. The aim of the test was thus to determine the sole permeability parameter of such a continuum model, the so -called "macropermeability" (BREWITZ & PAHL, 1986).

Macropermeability (= k_{macro}) is determined by one inflow rate (ventilated amount of water) and one head gradient (between the two parallel boreholes BOVE 84.011 and BOVE 84.018) for radial inflow.

For:	Q	=	2,0 [l/h.] = 5.5E-7	[m^3/s]
	Φ_R	=	23 by R = 5,25	[m]
	Φ_r	=	9 by r = 3,5	[m] (Φ_R and Φ_r: averages of head measurements)
	b	=	80	[m] (length of ventilation test drift)

$$k_{macro} = \frac{Q \cdot \ln (R/r)}{2 \cdot \pi \cdot b \cdot (\Phi_R - \Phi_r)} = 3E\text{-}11 \quad [m/s] \quad \text{(THIEM, 1906)}$$

Using this model, the head at the tunnel surface would be -15 m; at a distance of 30 m from the ventilation drift it would be 80 m.

The following observations show that a homogeneous, isotropic continuum model is too simple for describing inflow to the ventilation drift:

- A large component of the inflowing water arises in a fractured zone of the drift (see chapter 2). The measured quantity of water would therefore be strongly affected by shifting or rotating the drift.
- In borehole BOSB 83.001, at a distance of approx. 30 m from the ventilation drift, heads of 300 m in relation to the tunnel axis were measured (BRASSER & KULL, 1986).
- Injection tests in boreholes gave permeabilities which were up to 1000 times higher than k_{macro} (see chapter 4).

Describing flow into the ventilation drift at this scale therefore requires models which take into account the principal local hydrogeological structures.

5.1.3 Process of model validation

The scheme shown in Figure 25 shows the procedure selected for constructing a model of inflow to the ventilation drift. It was not possible to perform all the steps in the sequence shown here, particularly since responsibility for performing the tests and for the modeling lay in separate hands. Unfortunately it was not possible to continue the process up to the stage of producing a model capable of making predictions. The steps performed by the authors are indicated with heavy arrows.

5.1.4 Sensitivity analysis

To assist in determining the model geometry, the scope of the model and the boundary conditions, a sensitivity analysis was carried out (GMÜNDER, 1988). The modeling assumptions were varied systematically and subdivided according to their influence on the heads in the modelled domain:

- Modeling assumptions with a small influence can be held fixed for all modeling exercises.
- Modeling assumptions with a large influence are further subdivided into three categories:
  - those which can be defined more accurately by measurements, either directly or following a change in the test configuration (e.g. heads at the model boundary, inflows in individual shear zones)
  - those which can be eliminated by changing the test configuration (e.g. tunnel climate, effect of open sections of borehole)
  - those which can not be directly measured (e.g. most inhomogeneities).

The last assumptions must, for the meantime, be considered as variable and can be used to construct different model variants.

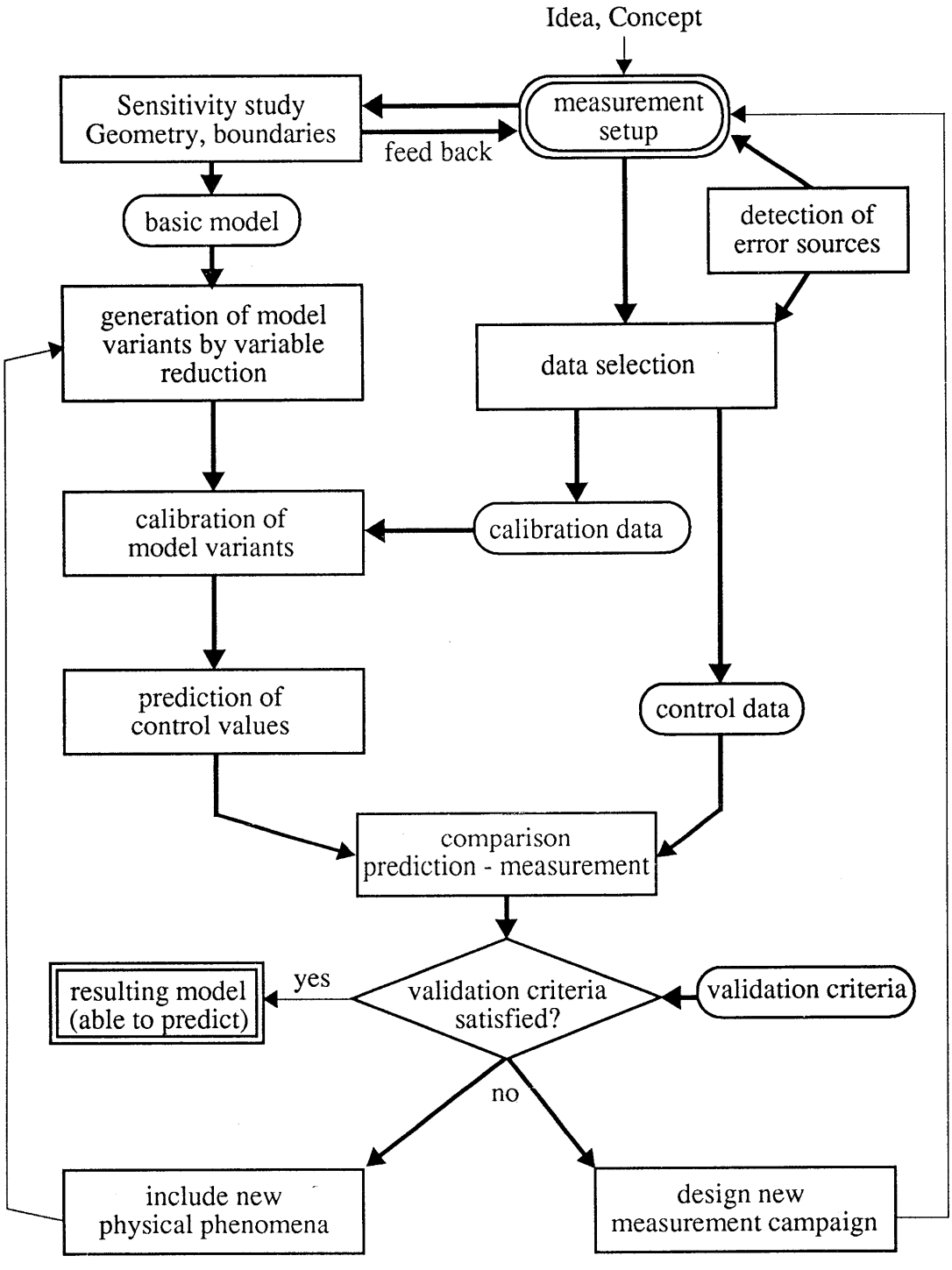

Figure 25: The performance of model validation

With the structural model shown in Figure 26 a series of sensitivity analysis were performed. Table 9 shows the results of the sensitivity analysis.

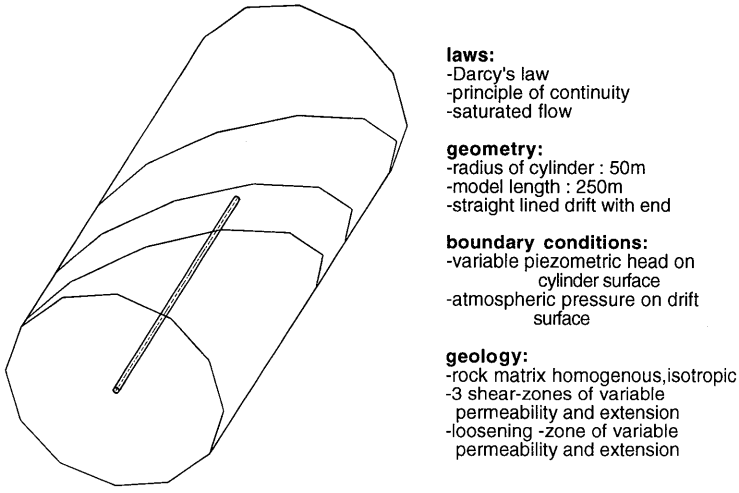

Figure 26: The basic conceptual model

5.1.5 Mathematical formulation

The AQUA-ROCK program, which was developed at the ETH-Zürich, was used to calculate the seepage; this program uses the finite element method. For the purposes of the present application, it is sufficient to say that 1-, 2- and 3-dimensional elements with linear arrangement of heads can be used. Further information on the program can be found in ARN (1989) and ARN & GMÜNDER (1991).

Two possible discretizations into finite elements are shown in Figure 27. A comparison with the analytical solution for radially symmetric inflow gave significantly smaller discretization errors for network B and this network was therefore used.

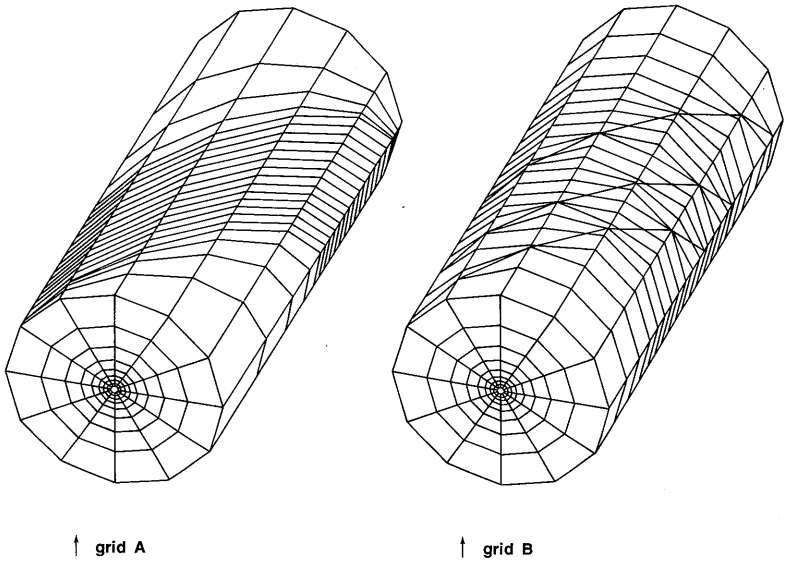

Figure 27: Finite element discretization

Model assumptions and their variations	**Influence or hydraulic head**		**Suggestion for further treatment of the assumptions**	
	near-field	far-field		
Boundary Conditions (B.C)				
Model radius	+	+	**fixed**	
B.C. surface of cylinder				
constant flow/head	0	o.a.	**fixed**	
value of head	++	++	**variable**	(measurements in complementary boreholes)
Total inflow	0	0	**fixed**	(measurements of discrete inflows)
Drift climate	+?	0	**elimination**	(100% relative humidity)
Test configuration				
Neighbouring drifts	0	o.a.	**fixed**	(negligible)
End of drift	+	+	**fixed**	
Measurement cavern	+	0	**fixed**	(negligible)
Open section of boreholes	o.a.	o.a.	partially **variable**, partially **fixed**	(negligible)
Geology				
Shear zone extent	++	++	**variable**	(further
Inhomog. matrix	++	++	**variable**	geological
Inhomog. shear zone	++	++	**variable**	investigation)
Disturbed zone	++	0	**variable**, partially **fixed**	(negligible)
Anisotropy	+	+	**fixed**	(negligible)
Flow model				
No-stationary flow	0	+	**fixed**	(negligible)

Legend:
0 = Influence negligible
\+ = Influence small
++ = Influence large
o.a. = Influence spatially variable

Table 9: Sensitivity analysis: assumptions and their variations

5.1.6 Selection of measured data

As can be seen from the scheme in Figure 25, measured data are required for two different purposes:

- For calibrating the parameters of the model variants (calibration data)
- For selecting the best model variants and testing their predictive ability (control data).

The measured data used for calibration will be presented once again here since they make up a very small component of the original data (Figure 28). Selection was made on the basis of an investigation of errors/uncertainties in data acquisition and data transmission (GMÜNDER, 1988). Three measured values for pressure and two for inflow were used to calibrate the model. The pressures were measured in borehole intervals which were 29, 32 and 19 m long. An element of uncertainty must therefore be taken into account in the spatial assignment of these pressures.

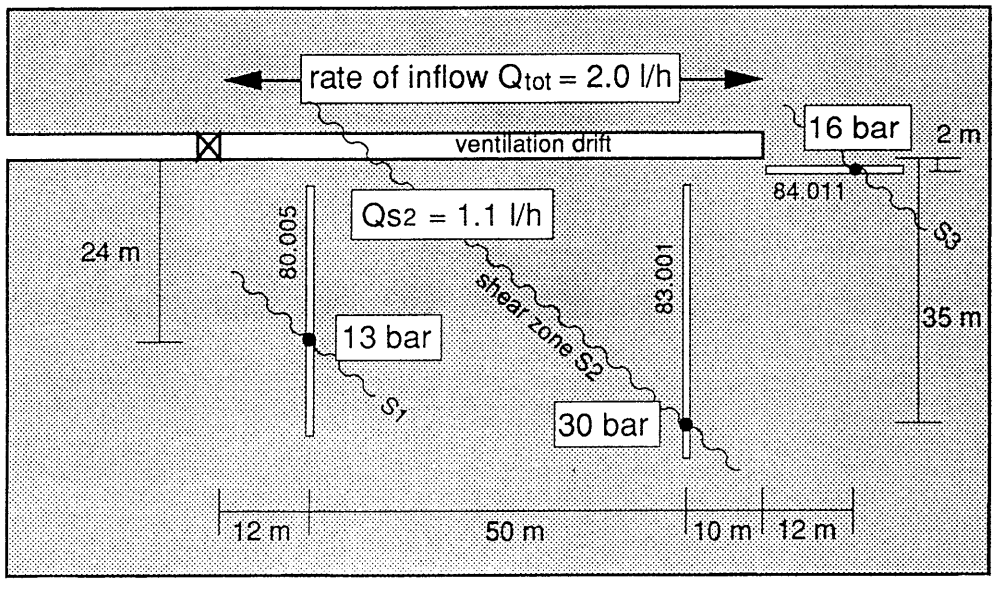

Figure 28: Measurements used for model calibration

5.1.7 Prediction calculations

5.1.7.1 Constructing model variants

The values of the unknown variables of a model comprising three shear zones of differing extent, varying groundwater table and varying decompressed zone cannot be determined using five measured parameters. The number of variables must therefore be (meaningfully) reduced by means of geological observation. Since there are several different approaches to this, several model variants have to be constructed. Each model variant is first calibrated using the measured calibration data (Figure 28) and is then used to predict control parameters. The different model variants can then be compared with one another using the measured control data. A selection of investigated model variants is given in Table 10.

5.1.7.2 Calibration

When carrying out the calibration, it is necessary to minimize the differences between model variant and calibration data (see table 11). Inflows and heads are handled separately since they do not have the same units. The least-squares method was used for the evaluation (HAHN & SHAPIRO, 1967).

5.1.7.3 Comparison of predictions and control measurements

The water pressures in the modelled domain are predicted using the calibrated model variants and are compared with pressures measured along 4 control boreholes with a total of 14 borehole intervals. The comparison is done visually as shown in Figure 29 and takes into account the fact that the water pressures are measured in borehole intervals and cannot therefore be assigned to any single point (KOVARI et al., 1989).

The interpretation of the comparative presentation (Figure 29) shows that:

- The observed control pressures can not be correctly predicted by any of the chosen model variants.
- The agreement between prediction and measurement is better away from the drift than in near-drift areas.
- The agreement is worse in borehole BOVE 88.003 and in the sections of borehole BOSB 80.005 lying on the side of the main access tunnel than in the other boreholes.

These deviations can be explained by the following:

- The discrepancy in the number of calibration data (3) and the number of measured control data (14), i.e. ratio of 1:5.
- Physical phenomena not being taken into account (GMÜNDER, 1990), for example the behaviour of head measurement boreholes in a fracture network, drying-out of the rock due to ventilation, etc.
- Measurement errors (e.g caused by enclosures of air in BOVE 88.003).

Table 10: Definition of the model variants

Model variants	**1**	**2**	**3**	**4**
Model structure SZ: shear zone BH: borehole DZ: disturbed zone	matrix homogeneous isotropic 1 infinite extended SZ SZ: parallel plates	matrix homogeneous isotropic 1 externally limited SZ 1 infinite extended SZ Disturbed zone Open sections of boreholes SZ: parallel plates	matrix homogeneous isotropic 2 infinite extended SZ SZ divided into 42 sub-zones and 5 transmis-sivity classes	matrix homogeneous isotropic 3 infinite extended SZ SZ: parallel plates
Boundary conditions Surface of cylinder	constant on surface	constant on surface	constant on surface	one constant head per SZ between shear zones: linear head values
Reason	most simplified geology	Considering effect of test configuration on rock permeability	Modelling observed inhomogeneity of SZ (channel flow)	Different water tabel levels in the SZ's which divide the rock mass
expected results	k_M, T_{SZ}, Φ_R	k_M, k_{DZ}, T_{SZ1}, T_{SZ2}, Φ_R, L_{SZ}	k_M, 84 T_{SZ}, Φ_R	k_M, T_{SZ1}, T_{SZ2}, T_{SZ3}, Φ_{R1}, Φ_{R2}, Φ_{R3},
Reduction of variables		$k_{DZ} = 5\ k_M$ $L_{SZ} = 25$ m	distribution T_{SZ} lognormal $\mu(\log T) = -10,3$ $\sigma(\log T) = 1,5$	$T_{SZ2} = T_{SZ1}$ $T_{SZ3} = T_{SZ1}$

Table 11: Calibration of model variants

Model variants	**1**	**2**	**3**	**4**
RELATIONSSHIP UNKNOWN PARAMETERS / MEASUREMENTS	**OVERDETERMINED**	**DETERMINED**	**UNDERDETERMINED (see chap. 5.1.6.4)**	**DETERMINED**
Calibration (see Figure 28)	Head: [m] calc. Meas. diff. 197 130 +67 231 300 -69 193 160 +33 Inflow: [l/h] calc. Meas. diff.	Head: [m] calc. Meas. diff. 127 130 -3 300 300 0 166 160 6 Inflow: [l/h] calc. Meas. diff.	Head: [m] calc. Meas. diff. 133 130 +3 275 300 -25 235 160 +75 Inflow: [l/h] calc. Meas. diff.	Head: [m] calc. Meas. diff. 131 130 +1 299 300 -1 162 160 +2 Inflow: [l/h] calc. Meas. diff.
Shear zone	1,1 1,1 0	1,1 1,1 0	1,1 1,1 0	1,1 1,1 0
Matrix	0,9 0,9 0	0,9 0,9 0	0,9 0,9 0	0,9 0,9 0
Resulting information	$-K_M$ = 6.8E-12 m/s $-T_{SZ}$ = 5.6E-10 m^2/s $-\Phi_R$ = 250 m	$-K_M$ = 3.2E-12 m/s $-K_{DZ}$ = 1.6E-11 m/s $-T_{SZ1}$ = 7.0E-10 m^2/s $-T_{SZ2}$ = 4.6E-10 m^2/s $-\Phi_R$ = 340 m	$-K_M$ = 5.0E-12 m/s -possible distribution of T_{SZ} in S_{Z1} and S_{Z2} (Figure 31a) $-\Phi_R$ = 280 m	$-K_M$ = 7.2E-12 m/s $-T_{SZ1,2,3}$ = 8.6E-10 m^2/s $-\Phi_{R1}$ = 130 m $-\Phi_{R2}$ = 345 m $-\Phi_{R3}$ = 155 m
Abbreviations	K_M = Hydraulic conductivity of rock matrix [m/s] L_{SZ} = Shear zone extent (max. radial distance relative to drift) [m] T_{SZ} = Shear zone transmissitity [m^2/s] Φ_R = Head at cylinder surface [bar] K_{DZ} = Hydraulic conductivity of Disturbed zone [-]			

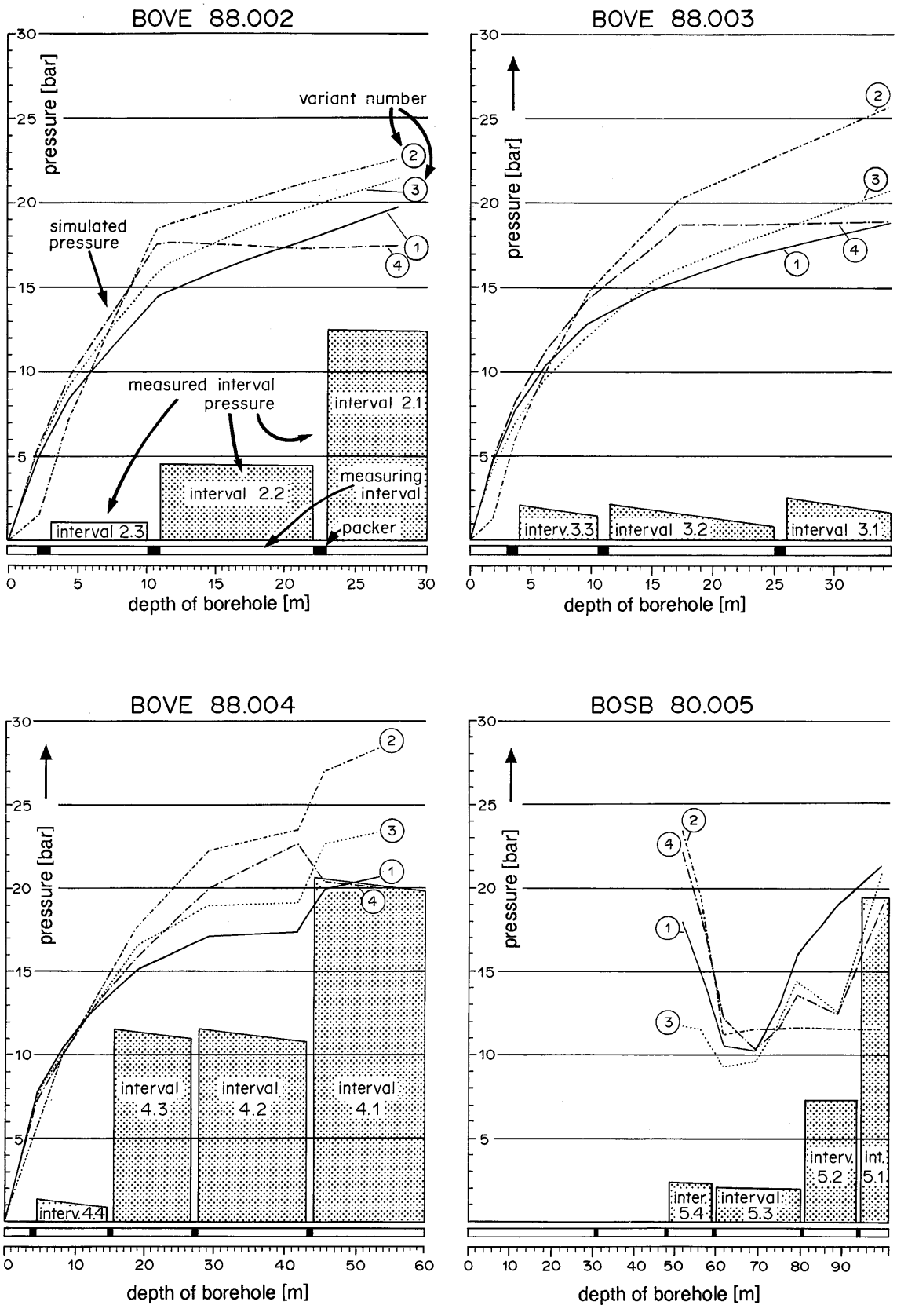

Figure 29: Comparison of the performed prediction calculation in 1988 and the borehole interval

5.1.7.4 Geostatistical shear zone model

In order to be understandable, model variant 3 (Table 10) requires some further explanation of geostatistical methods.

It is assumed that a shear zone is divided into numerous small subzones and that a mean permeability can be assigned to each of these subzones. If all these permeabilities are known, a shear zone model can be constructed which exactly reproduces the inhomogeneity of the shear zone.

However, the permeabilities of these subzones are not known and cannot in fact be measured. In the field of geostatistics, one therefore turns to models which give a "possible" allocation of permeabilities to the subzones. If all "possible" allocations are considered, then the true allocation must be included in these.

Calculating through all allocations would however exceed the capacity of any computing system - if the shear zone is subdivided into 42 subzones (according to Figure 31) which can have 5 independent permeabilities, then 5^{42} calculations would have to be carried out. This is dealt with by randomly picking out a small number of these combinations and calculating the unknown parameters (heads along the control boreholes) for these cases. This procedure is called the Monte-Carlo method. If enough calculations are carried out, the statistical distribution of the unknown parameters of the selected combinations will agree approximately with that of all possible combinations.

The question then arises as to which allocations of permeabilities to the subzones should be considered as "possible". In geostatistics, an allocation is termed "possible" if it fulfils the following conditions (NEUMAN, 1987):

- The statistical distribution (histogram) of the permeabilities should agree with that of reality.
- The change in permeability when moving from one location to another should agree on average (variogram) with that of reality.

Insufficient statistical material on shear zone transmissivities was available for geostatistical simulation of the shear zones in the ventilation test. At the time of the prediction calculations, the results of the injection tests in the control boreholes were not yet available. The following assumptions are therefore based on data on quantities of water arising when boreholes 80.005 and 83.001 were drilled:

- shear zone divided into 42 subzones
- transmissivity distributed log-normally with a mean value of (log T) equal -10.3 and variance of (log T) equal 1.5 (T in [m^2/s])
- transmissivities of individual surfaces are independent of one another (variogram horizontal for the selected surface area)
- number of performed realisations: 100.
- no restrictions were applied to the total flux into the drift and to the head at the calibration measurement points.

In order to obtain a log-normal permeability distribution in the shear zones, the distribution was divided into 5 classes of equal frequency. The allocation of the class frequency to the subzones can then be done using an equally distributed random number.

The results of the geostatistical simulation take the form of statistical distributions of the heads at each point of the model. Figure 30a shows the distribution at a calibration measurement point, while Figure 30b shows the 5, 30, 70 and 95% quantiles of the distribution along a control borehole. Figure 31a shows the distribution of transmissivity in shear zone S2 for the combination which gave the best fit with the measured calibration data. Figure 31b shows the resulting head distribution in the shear zone. Figure 30b shows that the geostatistical shear zone model can not describe the measured head data, even if one assumes the allocation which produced the lowest heads to be the true one.

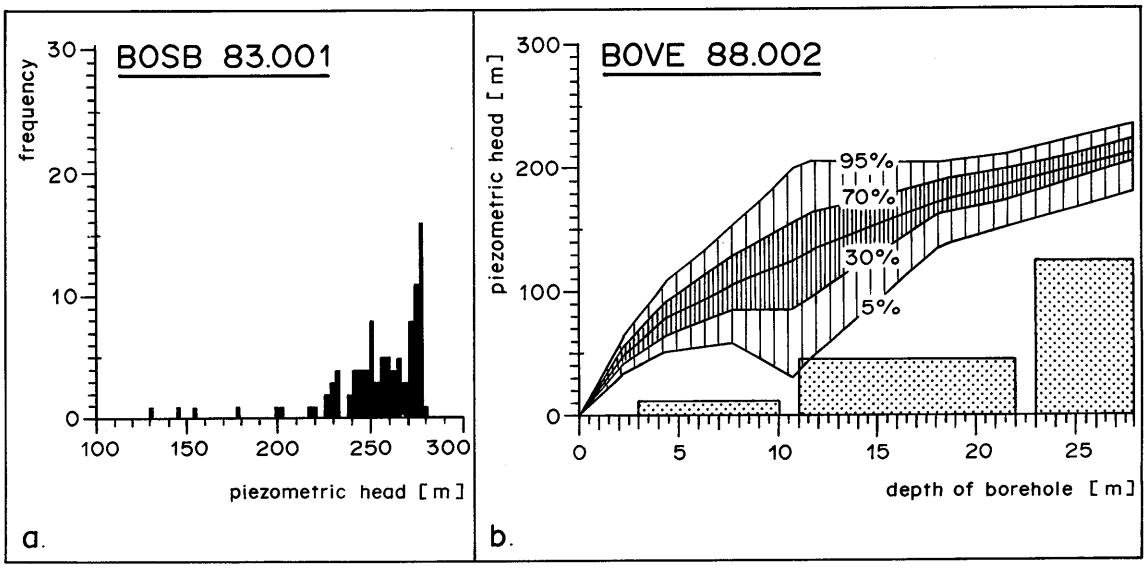

Figure 30: Results of the geostatistical calculations

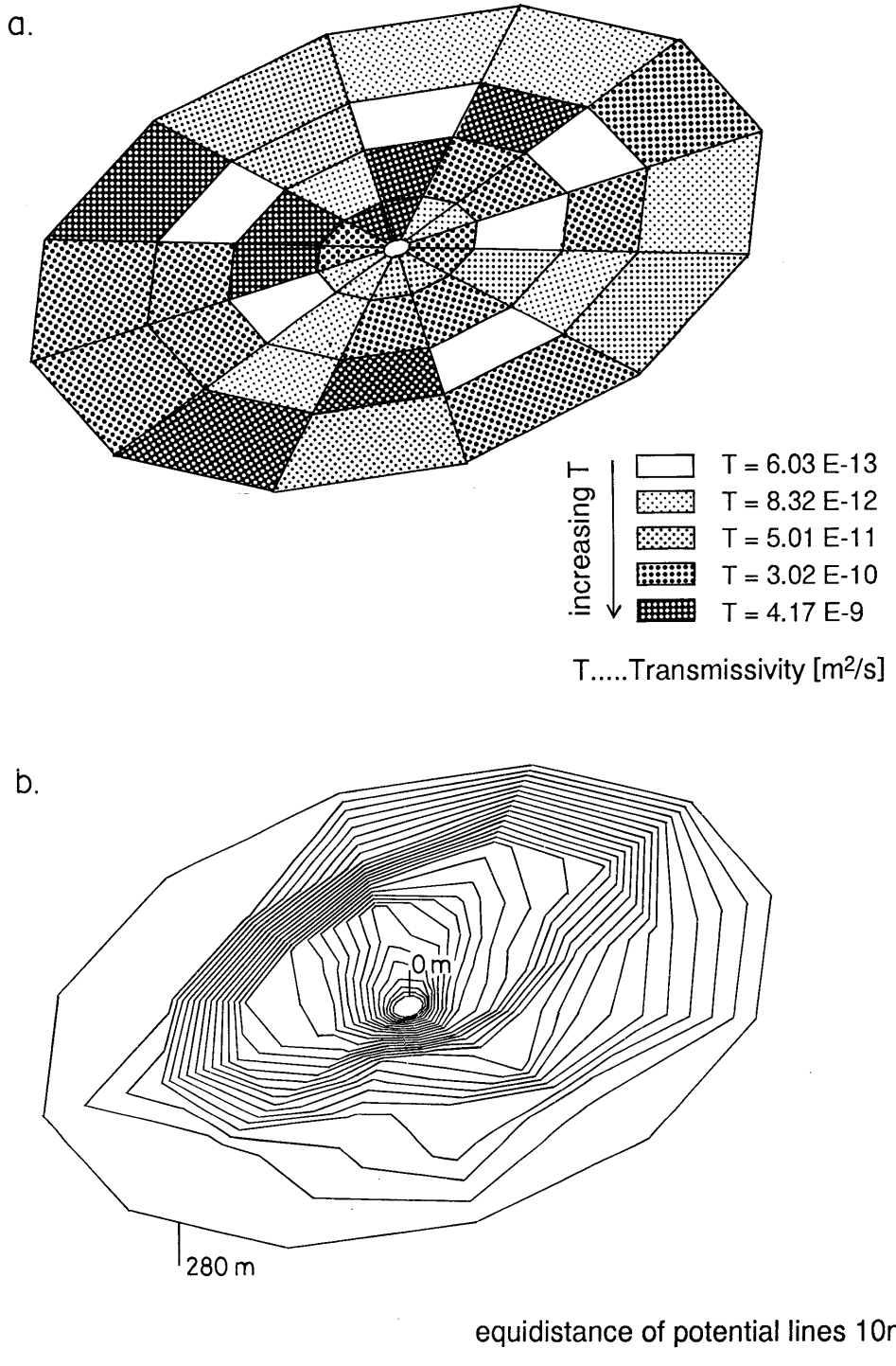

Figure 31: Realization with best agreement to calibration measurements

5.2 Estimation of the macro-permeability of a shear zone by inverse modeling

O. Jaquet (Colenco AG, Dättwil)

5.2.1 Conceptual model

The aim of the present modeling study is the calculation of the macro-permeability of the discontinuity intersecting the ventilation drift. The amount and quality of geologic and hydrogeologic information is sufficient for an inverse modeling approach to be used. Such an approach uses geostatistical methods to obtain a priori estimates of hydrogeological parameters and their uncertainties. Various conceptual models of the shear zone are considered and comparisons are made of the consistency of each one with relevant available data.

The final result is an improved characterization of the shear zone permeability that will facilitate a better description of the surrounding matrix properties.

The main discontinuity in the ventilation (VE) drift is the ductile shear zone between 465 and 475 m (see Figures 1 and 5, chapter 2). The water inflow into the drift from this shear zone - which is 10 m thick and possibly several hundred meters in extent - is approximately 1 liter per hour, this velocity corresponds to about 50% of the total inflow into the 80 m long ventilation drift. The main flow path in the shear zone consists of connected fractures filled with a porous breccia material (fault gouge; BOSSART & MAZUREK, 1991). The shear zone was hydraulically characterized by head measurements (see chapter 4). Since the VE drift is more than six years old, steady-state flow conditions are assumed to prevail within the shear zone, which is considered as a saturated porous medium. The amount of water flowing in or out of the plane of the shear zone is assumed to be negligible. It is further assumed that the shear zone can be adequately represented by a plane in the area of the VE drift. These assumptions allow the analysis to be performed with a 2-D finite element representation of the shear zone. The shear zone cuts the VE drift obliquely (Figure 32) and consequently the generated finite element mesh of the shear zone model has an elliptical geometry.

5.2.2 Inverse modeling approach

The inverse problem involves estimating model parameters from head measurements and appropriately weighted prior information on the medium properties. Adequate solutions to the inverse problem will improve the fit between the model and reality.

The approach used in this study was developed by CARRERA & NEUMAN (1986a, 1986b, 1986c). They posed the inverse problem in the context of the maximum likelihood (ML) theory, taking into account head measurements as well as prior information about model parameters. The choice of this probabilistic method is linked to the uncertainties that affect the parameters of the model. The quantification of these uncertainties is carried out using geostatistical methods.

ML theory leads to optimum parameters for a given model structure. Optimum parameterization can be achieved for various conceptual models of the aquifer. The criterion of Kashyap (CARRERA & NEUMAN, 1986c), derived from the ML concept, is used to select, from alternative conceptual models the one that is most consistent with available information regarding the shear zone.

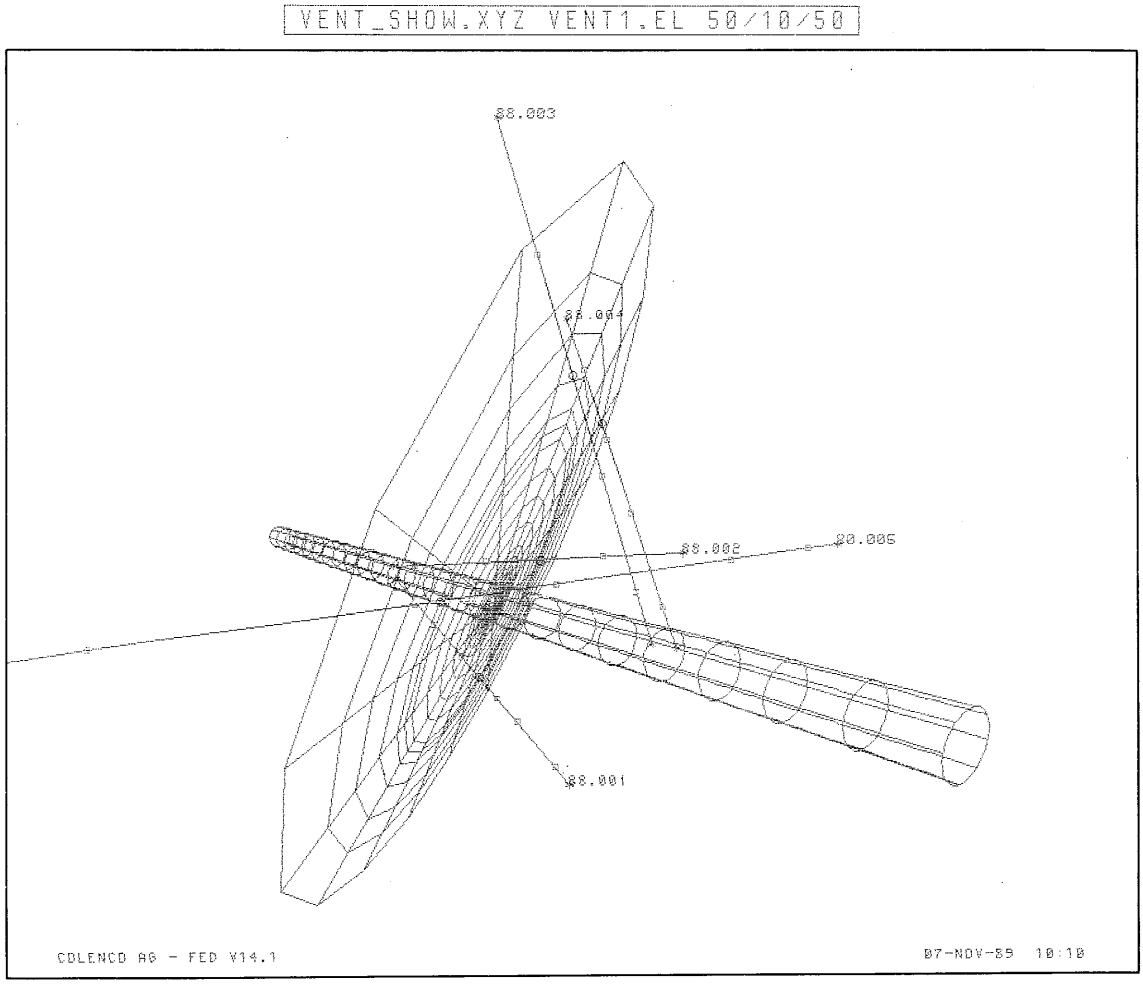

Figure 32: View of Mesh, VE Tunnel and Boreholes (red zone: shear zone, red circle: intersection of model plane with shear zone, blue square: packer position)

5.2.3 Objective function

To estimate the value of the transmissivity that best represents the overall hydraulic properties of the entire shear zone, the following objective function **J** is minimized:

$$J = (h^*-h^\circ)^T V_h^{-1} (h^*-h^\circ) + (y^*-y^\circ)^T V_y^{-1} (y^*-y^\circ) + (q^*-q^\circ)^T V_q^{-1} (q^*-q^\circ) + (H^*-H^\circ)^T V_H^{-1} (H^*-H^\circ)$$

where:

h^*, h°	=	head observations and computed head vectors (T: transposed vector)
y^*, y°	=	a priori estimated and computed log-transmissivity vectors
q^*, q°	=	a priori estimated and computed flow vectors
H^*, H°	=	a priori estimated and computed prescribed head vectors
V_h^{-1}, V_y^{-1}	=	inverse of variance matrices: head, log-transmissivity
V_q^{-1}, V_H^{-1}	=	flow and prescribed head respectively.

The calibration phase, i.e. the minimization of the objective function with respect to head observations and model parameters, leads to an improved estimation of the transmissivity of the shear zone. The minimization is carried out using the program INVERT developed by CARRERA & NEUMAN (1986b). An iterative approach is required due to the nonlinearity of the objective function with respect to all the parameters.

Prior estimates of the parameters together with their estimation variance are required as input for the inverse model. The estimation variances of the parameters are the relative weights of the different types of prior information regarding the shear zone.

5.2.4 Input parameters

5.2.4.1 Head observations

The head observations are the main source of information required for inverse modeling. These head data are taken from four boreholes (HEINIGER, 1989b) that intersect the shear zone and from sixteen measurements made in the drift. In order to calibrate the shear zone model, the uncertainty attached to the head observations is required. The **total variance of head errors** Σ_h^2, which includes the following squared errors terms, is expressed as follows:

$$\Sigma_h^2 = \sigma_o^2 + \sigma_h^2 + \sigma_m^2$$

where:

σ_o = **measurement error** associated with the measurement instruments and the extrapolation error associated with the analysis of the pressure bildup curve [m]

σ_h = **interpretation or unmodeled heterogeneity error** [m]

σ_m = **numerical or computational error** [m]

A detailed description and discussion regarding the head errors shown in table 12 is given in JAQUET & THOMPSON (1991).

h_z^* [m]	Σ_{hz} [m]	h_i^* [m]	Σ_{hi} [m]
1765	22	1732.45	0.13
1782	"	⋮	⋮
1770	"	⋮	⋮
1867	"	1735.95	0.13

Parameters:

h_z^* = head observation (shear zone) [m asl.]

Σ_{hz} = total head error (shear zone) [m]

h_i^* = head observation (inner boundary); the range of values is given [m asl.]

Σ_{hi} = total head error (inner boundary) [m]

Table 12: Head information for the shear zone model

5.2.4.2 A priori estimation of the transmissivity

Three conceptual models (given in table 13), relating to different medium or geometrical properties can be considered for the shear zone (JAQUET & THOMPSON, 1991). The a priori determination of the parameters of each conceptual model is required for inverse modeling.

MODEL	CONCEPTUAL CHARACTERISTICS	RUNS
A	one isotropic transmissivity zone	IVA04
B	one anisotropic transmissivity zone	IVB01
C	two isotropic transmissivity zones including a near-drift disturbed zone	IVC01

Table 13: Shear zone conceptual models

One isotropic transmissivity zone

An a priori estimate of the log-transmissivity and its error of estimation are required to fully parameterize the shear zone, which is then modelled as a single transmissivity zone.

Hydraulic tests were conducted in packed-off intervals in 4 boreholes (HEINIGER, 1989b) that intersect the shear zone to obtain hydraulic parameters. An estimate of the variogram cannot be obtained from the four log-transmissivity values available. Common variogram models for log-transmissivity are the linear and spherical variograms (DE MARSILY et al., 1984). Guided by the principle of parsimony, the linear variogram model $\gamma(h)$ was chosen, which is expressed as:

$$\gamma(h) = w\,h$$

where:

w = slope

h = Euclidean distance.

Assuming a 3-D isotropic transmissivity field with some homogeneous statistical properties allows one to derive by analogy, the slope at the origin from the variogram of the log-transmissivities taken from the Leuggern borehole (BELANGER et al., 1987).

The zone of influence of the hydraulic test is not negligible relative to the dimensions of the shear zone. Therefore, to estimate the log-transmissivity value of the shear zone, a variogram model that describes the spatial variability of the point log-transmissivity values is required. A change of scale is needed to obtain the point variogram model $\gamma(h)$ of the log-transmissivities. This operation, i.e. the deconvolution of the variogram $\gamma(h)$, can be carried out with the following approximate relation (ARMSTRONG, 1981):

$$\gamma(h) \approx \gamma(h) + \gamma(v,v) \qquad h >> v$$

where $\bar{\gamma}(v,v)$ is the mean variogram for the surface v, the zone of influence of the hydraulic test. The point linear variogram, resulting from the deconvolution, is then expressed as (JAQUET & THOMPSON, 1991):

$$\gamma(h) = 0.004 \cdot h$$

The estimation of the mean transmissivity value over a given zone is carried out by kriging, using the variogram and the four log-transmissivity data:

$$y_V^* = \sum_{\alpha=1}^{n} k^\alpha \, y_v(x_\alpha)$$

where:

y_V^* = mean log-transmissivity over the zone V

k^α = kriging weight

$y_v(x_\alpha)$ = log-transmissivity data at location x_α.

The kriging results for the transmissivity zone are as follows:

$$y^*_V = -8.51 \quad \sigma_y^2 = 0.02$$

where σ_y^2 is the estimation variance, and the back-transformed transmissivity value with its 95% confidence interval (assuming gaussian error) for the zone V is:

$$t_V^* = 10^{y_V^* \pm 2\sigma_y} \qquad [m^2/s]$$

$$t_V^* = 3.1E\text{-}9 \qquad [m^2/s]$$

$$1.6E\text{-}9 < t_V^* < 5.9E\text{-}9 \qquad [m^2/s]$$

<u>One anisotropic transmissivity zone</u>

The description of different deformed rock fabrics in the Grimsel crystalline is presented in chapter 2. The high cleavage intensity in the ventilation shear zone is responsible for the distinct anisotropic rock fabric. In the cleavage plane, a subvertically oriented stretching lineation is developed. It is suggested by BOSSART & MARTEL (1990) that the fabric anisotropy (axes of the finite strain ellipsoid) corresponds to the hydraulic anisotropy (axes of conductivity or transmissivity tensor).

Using the stochastic analysis of flow developed by BROWN (1984) for a two-dimensional anisotropic medium, the principal values for the components of the effective transmissivity tensor can be derived. These formulae are expressed as follows:

$$t_{Vxx}^* = t_{Va}^* \cdot \exp[(-\sigma_f^{*2}/2) \cdot (\Phi^* - 1/\Phi^* + 1)]$$

$$t_{Vyy}^* = t_{Va}^* \cdot \exp[(\sigma_f^{*2}/2) \cdot (\Phi^* - 1/\Phi^* + 1)]$$

where:

t_{Vxx}^* = principal value of effective transmissivity tensor (direction of X-axis of strain ellipsoid, see Figure 6)

t_{Vyy}^* = principal value of effective transmissivity tensor (direction of Y-axis)

t_{Va}^* = mean transmissivity value of the shear zone (3.2E-9 m^2/s)

σ_f^{*2} = variance of the ln-transmissivities (= 0.43)

Φ^* = ratio of the correlation scales (= 3).

The detailed description of the determination of the parameters required for the calculation of the components of the effective transmissivity tensor are given in JAQUET & THOMPSON (1991). The mean transmissivity value for the shear zone is obtained by kriging, as in the isotropic case, but this time the estimation is carried out with an anisotropic linear variogram. The variance of the transmissivities is calculated from the borehole data (see chapter 5.2.4.2), and the ratio of the correlation scales is derived from geological information. The following values of the components and their confidence intervals are obtained:

$$t_{Vxx}^* = 2.9E\text{-}9 \quad [m^2/s]$$

$$2.2E\text{-}9 < t_{Vxx}^* < 3.8E\text{-}9 \quad [m^2/s]$$

$$t_{Vyy}^* = 3.6E\text{-}9 \quad [m^2/s]$$

$$2.7E\text{-}9 < t_{Vyy}^* < 4.7E\text{-}9 \quad [m^2/s]$$

Two transmissivity zones

During excavation of the drift, a disturbed zone with hydraulic properties different from that of the shear zone can develop around the drift. The transmissivity of the disturbed zone is assumed to be one order of magnitude larger (ADANK & VOBORNY, 1989) than the mean transmissivity value obtained for the shear zone using the borehole data. Therefore the a priori value of the transmissivity of the disturbed zone and its confidence interval are:

$$3.1E\text{-}9 < 3.1E\text{-}8 < 3.1E\text{-}7 \quad [m^2/s]$$

The confidence interval is assumed by setting the lower limit of the interval to the mean value of the transmissivity of the shear zone. The calibrated value for the transmissivity of the disturbed zone can thereby take the same value as the shear zone, which would show the nonexistence of the disturbed zone. The thickness r_{DZ} of the disturbed zone is assumed to be equal to the radius of the drift:

$$r_{DZ} = 1.75 \quad [m]$$

The transmissivity value of the remaining part of the shear zone, which forms the second transmissivity zone of the model, is set to the same value as in the isotropic case (see part 5.2.4.2).

5.2.4.3 A priori estimation of the prescribed flow

At the inner boundary of the model, i.e. the intersection of the shear zone with the drift, the outflow from the shear zone was measured and monitored for a given time period. The measured flow rate from the shear zone is specified as a boundary condition on the inner boundary of the model.

The flow rate from the shear zone into the VE drift was measured over a five-month period. The test used plastic sheets to cover the shear zone and to collect all of the out-flowing water (BOSSART & HUFSCHMIED, 1989). The time interval between consecutive flow measurements was irregular, ranging from one measurement a week to four a day. The flow rate history and the histogram of the flow measurements are displayed in Figure 33.

The temporal variability of flow is analyzed using the approach developed by ROUHANI & WACKERNAGEL (1990). The experimental variogram is calculated using flow measurements sampled at different time intervals. A gaussian variogram model $\gamma(\Omega)$ provides the best fit with the experimental variogram for the flow (Figure 33):

$$\gamma(\Omega) = C_o + C_1 \cdot [1 - \exp(-\Omega^2/a^2)]$$

where:

Ω	=	time interval	[h.]
C_o	=	nugget effect (= 2.65E-3)	$[(l/h.)^2]$
C_1	=	sill (= 1.30E-3)	$[(l/h.)^2]$
$1.73 \cdot a = a_p$	=	practical range corresponding to 95% of the sill (= 600)	[h.]

The hypothesis of temporally stationary flow, considered in this geostatistical model, is equivalent to statistically homogeneous **steady state conditions** for the flow out of the shear zone during the time period considered. This assumption is supported by the absence of a clear trend in the data or in the experimental variogram.

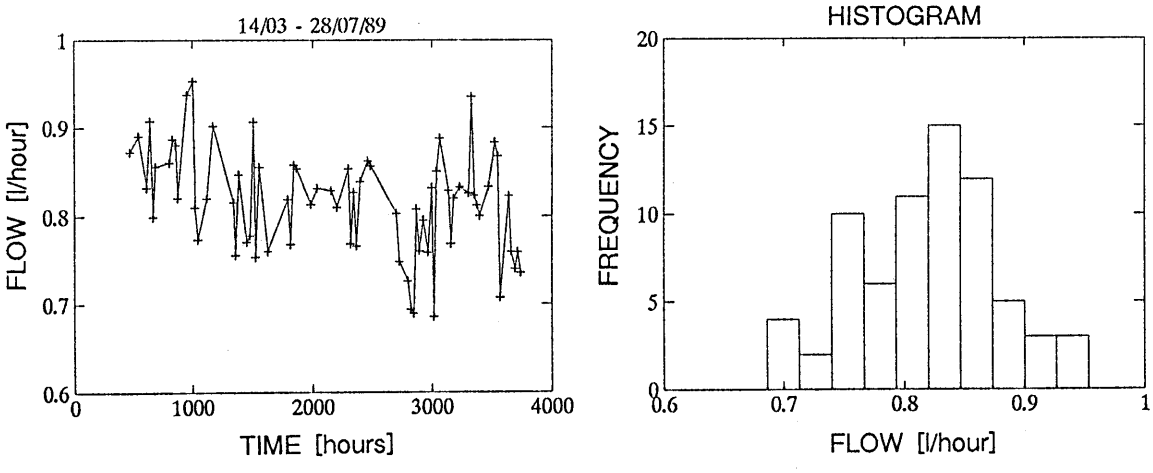

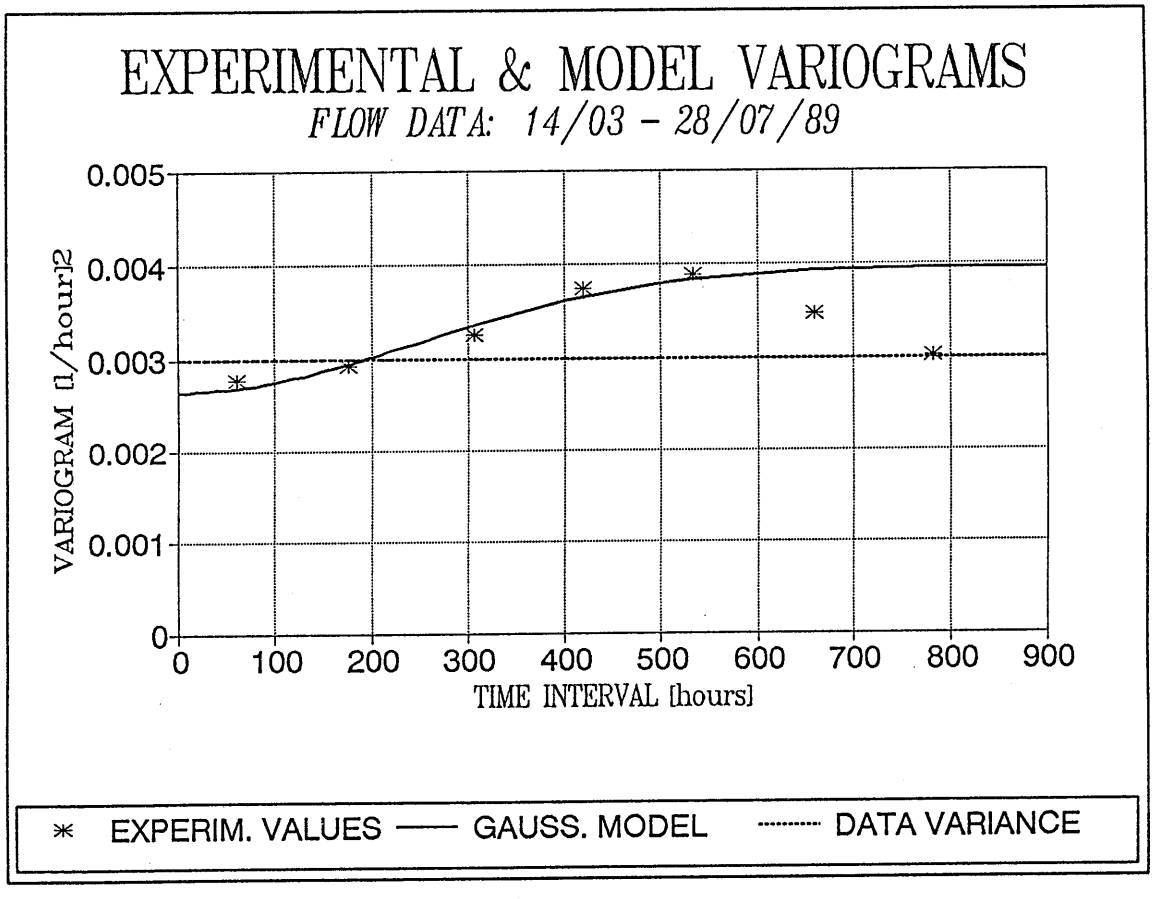

Figure 33: Statistics of the Flow Data

The estimation of the mean flow over the time period considered is made by kriging (JAQUET & THOMPSON, 1991) using the variogram and the measured data, and can be written as follows:

$$q_T^* = \sum_{\alpha=1}^{m} p^\alpha q(t_\alpha)$$

where:

q_T^*	=	mean flow over period T	[l/h.]
p^α	=	kriging weight	[-]
$q(t_\alpha)$	=	flow measurement at time t_α	[l/h.]

For the considered time period, the kriging results for the flow are:

$$q_T^* = 0.814 \quad [l/h.]$$
$$\sigma_q^2 = 1.19E\text{-}4 \quad [(l/h.)^2]$$

where:

σ_q^2	=	estimation variance	$[(l/h.)^2]$

5.2.4.4 A priori prescribed heads

The prescribed head values for the outer boundary of the shear zone model are taken from the GTS local model (ADANK & VOBORNY, 1989). The prescribed head error σ_{Ho^*} is derived from an estimation of the gradient error (JAQUET & THOMPSON, 1991) and is equal to:

$$\sigma_{Ho^*} = 14 \quad [m]$$

5.2.5 Model calibration

The three conceptual models of the shear zone, considered under part 5.2.4.2 (see table 13) are taken into consideration for calibration. The calibration phase, i.e. the minimization of the objective function with respect to head observations and model parameters, is carried out for four different runs (see table 14). The minimization of the objective function provides estimated values for the given parameters. As many as nineteen parameters (see table 14) can be estimated when calibrating the shear zone models using the program INVERT.

The input parameter values, obtained under part 5.2.4, for the reference run IVA04 are given in table 15. For the reference run IVA04, based on comparison runs with selected parameter sets, the number of eighteen is chosen. A sensitivity study has shown that the value of the computed log-transmissivity for the model A is almost insensitive to parameter variations (JAQUET & THOMPSON, 1991).

In the case of anisotropic conditions in the transmissivity field, the distribution of the flow around the drift should be variable. Therefore, the prescribed flow boundary at the inner boundary of the model is replaced by a fixed prescribed head boundary formed by the head observations, made on the drift wall (see table 12). After calibrating the model, the flow is calculated at each node of the inner boundary of the model and the total outflow to the drift is obtained. This then allows rescaling of the estimated components of the transmissivity tensor using the a priori flow rate q_T^*. This approach is also applied to a variant of run IVA04 of model A. The run IVA04 (var.) allows a better comparison with the results of run IVB01, because the introduction of anisotropic conditions increases the number of parameters only by one (see table 14 and 16).

RUN	ESTIMATED PARAMETER	NUMBER
IVA04 (ref.)	log-transmissivity flow rate prescribed heads (outer b.)	1 1 16
IVA04 (var.)	log-transmissivity prescribed heads (outer b.)	1 16
IVB01	log-transmissivity prescribed heads (outer b.)	2 16
IVC01	log-transmissivity flow rate prescribed heads (outer b.)	2 1 16

Table 14: Parameter sets of model A, B and C

y_V^*	σ_{y^*}	q_T^*[l/h.]	σ_{q^*}[l/h.]	H_o^*[m]	σ_{Ho^*}[m]
-8.51	0.14	0.814	1.09E-2	1780	14
				1886	14

Parameters:

y_V^*	=	log-transmissivity	[-]
σ_{y^*}	=	kriging error of y_V^*	[-]
q_T^*	=	flow rate (inner boundary)	[l/h.]
σ_{q^*}	=	kriging error of q_T^*	[l/h.]
H_o^*	=	prescribed head range (outer boundary)	[m asl.]
σ_{Ho^*}	=	estimation error of H_o^*	[m]

Table 15: Prior information relating to the parameters of run IVA04 (ref.)

In order to determine the effect of the addition of only one parameter on the calibration results, the results of run IVA04 (var.) are compared with those of run IVB01, and those of run IVA04 (ref.) with the results of run IVC01.

The values for the objective function and of the average squared head residual are the optimum results obtained through calibration using the maximum likelihood method. To each calibrated model corresponds the optimum computed parameters as given in table 18 and 19, and the resulting head fields are displayed on figures 34 and 35.

The computed values for the components of the log-transmissivity tensor of model B are similar to the computed value of log-transmissivity of model A (see table 18). The results of model B show that the a priori anisotropic conditions no longer persist after the model has been calibrated. If anisotropic conditions prevail within the shear zone, then the available data set does not allow their detection. The anisotropic conditions cannot be propagated from the outer boundary heads, because they were taken from the local GTS model, where no anisotropy was modelled.

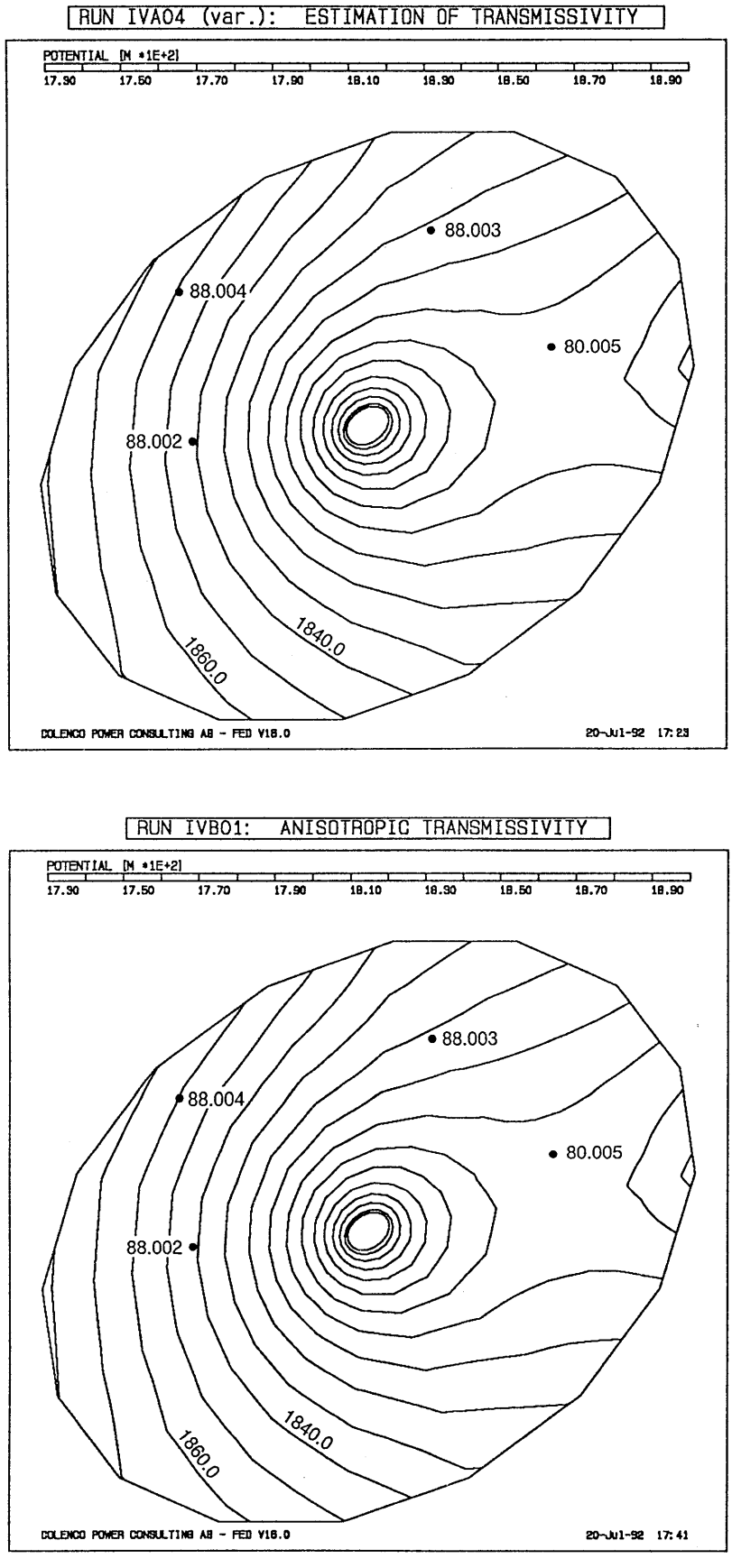

Figure 34: Head Fields of Models A and B

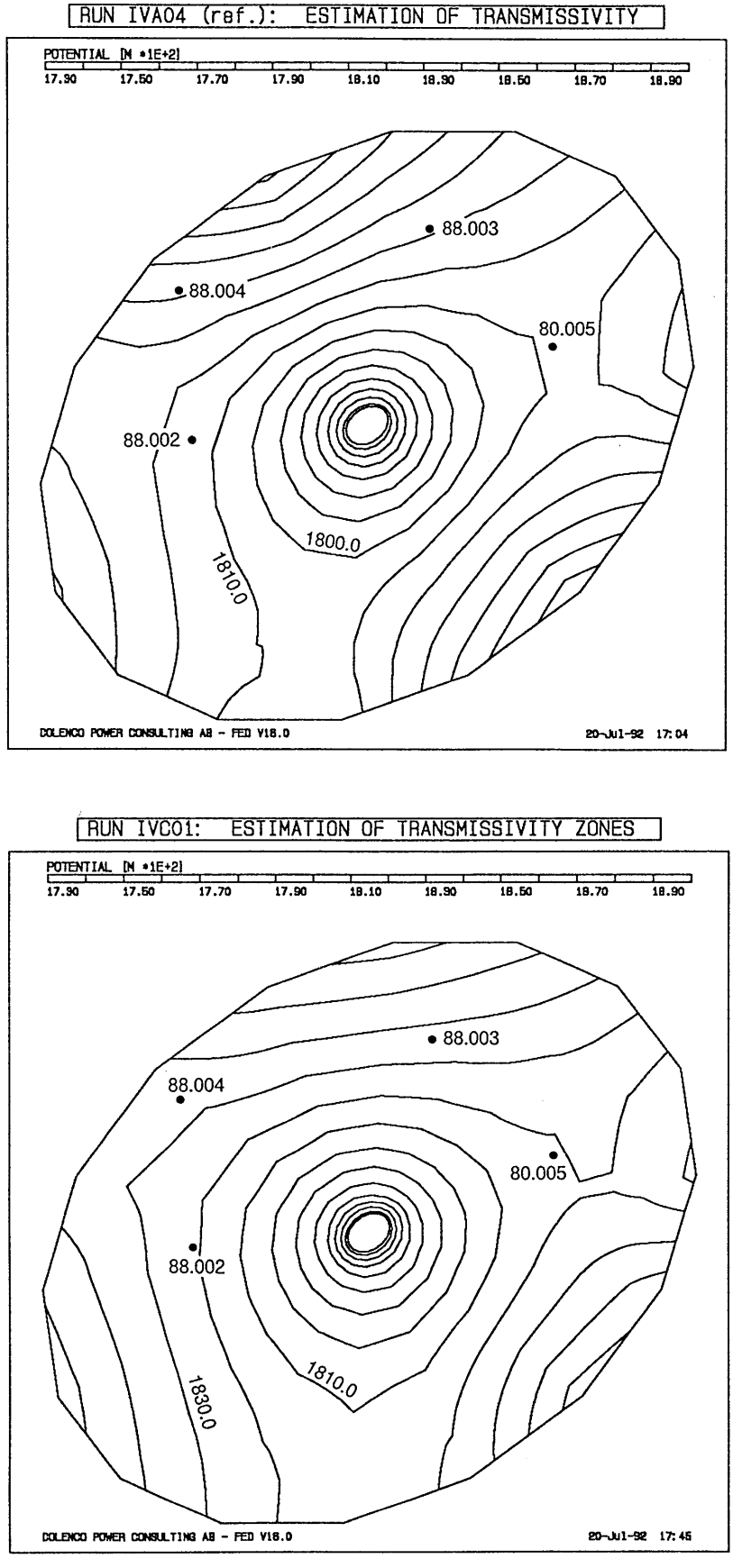

Figure 35: Head Fields of Models A and C

IVA04 (var.)		both runs			IVB01			
y_V^*	σ_{y^*}	q_T^*	H_o^*	σ_{Ho^*}	y_{Vxx}^*	σ_{xx^*}	y_{Vyy}^*	σ_{yy^*}
-8.51	0.14	0.814	1780	14	-8.54	0.12	-8.45	0.12
			1886	14				

Parameters:

y_V^*	=	log-transmissivity	[-]
σ_{y^*}	=	kriging error of y_V^*	[-]
q_T^*	=	flow rate (inner boundary)	[l/h.]
H_o^*	=	prescribed head range (outer boundary)	[m asl.]
σ_{Ho^*}	=	estimation error of H_o^*	[m]
y_{Vxx}^*	=	component of log-transmissivity tensor	[-]
σ_{xx^*}	=	estimation error of y_{Vxx}^*	[-]
y_{Vyy}^*	=	component of log-transmissivity tensor	[-]
σ_{yy^*}	=	estimation error of y_{Vyy}^*	[-]

Table 16: Prior information relating to the parameters of the shear zone model B

IVA04 (ref.)		both runs				IVC01			
y_V^*	σ_{y^*}	q_T^*	σ_{q^*}	H_o^*	σ_{Ho^*}	y_{DZ}^*	σ_{DZ^*}	y_V^*	σ_{y^*}
-8.51	0.14	0.814	1.09E-2	1780	14	-7.51	0.50	-8.51	0.14
				1886	14				

Parameters:

y_V^*	=	log-transmissivity of the shear zone	[-]
σ_{y^*}	=	kriging error of y_V^*	[-]
q_T^*	=	flow rate (inner boundary)	[l/h.]
σ_{q^*}	=	kriging error of q_T^*	[l/h.]
H_o^*	=	prescribed head range (outer boundary)	[m]
σ_{Ho^*}	=	estimation error of H_o^*	[m]
y_{DZ}^*	=	log-transmissivity of the disturbed zone	[-]
σ_{DZ^*}	=	estimation error of y_{DZ}^*	[-]

Table 17: Prior information relating to the parameters of the shear zone model C

For model C, the difference between the values for the computed log-transmissivity of the disturbed zone and the shear zone is small (see table 19). The disturbed zone presents a transmissivity value smaller than the value of the shear zone, which could indicate that the disturbed zone is behaving as a plug so as to match the flow at the inner boundary. This difference in the values of the transmissivity between the two zones is enhanced if the radius of the disturbed zone is increased (JAQUET & THOMPSON, 1991). Therefore, to obtain a log-transmissivity value for the disturbed zone that is smaller than the value of the shear zone, the thickness of the disturbed zone should be decreased. Thus, if a disturbed zone exists, its thickness is smaller than the radius of the drift.

MODEL A					
PARAM. / **RUN**	y_V°	$\sigma_{y^\circ}^2$	J	$\overline{(h^*-h^\circ)^2}$ [m^2]	d_k
IVA04 (var.)	-9.05	1.96E-2	14.9	354	72
MODEL B					
PARAM. / **RUN**	y_{Vxx}° / y_{Vyy}°	$\sigma_{xx^\circ}^2$ / $\sigma_{yy^\circ}^2$	J	$\overline{(h^*-h^\circ)^2}$ [m^2]	d_k
IVB01	-9.06 / -9.05	1.41E-2 / 1.41E-2	15.2	354	76

Parameters:

y_V°	=	log-transmissivity (isotropic)	[-]
$\sigma_{y^\circ}^2$	=	estimation variance of y_V°	[-]
y_{Vxx}°	=	component of log-transmissivity tensor	[-]
$\sigma_{xx^\circ}^2$	=	estimation variance of y_{Vxx}°	[-]
y_{Vyy}°	=	component of log-transmissivity tensor	[-]
$\sigma_{yy^\circ}^2$	=	estimation variance of y_{Vyy}°	[-]
J	=	objective function	[-]
$\overline{(h^*-h^\circ)^2}$	=	average square head residual	[m^2]
d_k	=	Kashyap criterion	[-]

Table 18: Results of calibration runs for model A and B

MODEL A					
PARAM. / **RUN**	y_V°	$\sigma_{y^\circ}^2$	J	$\overline{(h^*-h^\circ)^2}$ [m^2]	d_k
IVA04 (ref.)	-9.04	1.38E-4	143	380	186

MODEL C					
PARAM. / **RUN**	y_{DZ}° / y_V°	$\sigma_{DZ^\circ}^2$ / $\sigma_{y^\circ}^2$	J	$\overline{(h^*-h^\circ)^2}$ [m^2]	d_k
IVC01	-9.16 -9.00	2.67E-4 2.16E-4	119	503	191

Parameters:

y_V°	=	log-transmissivity of the shear zone	[-]
$\sigma_{y^\circ}^2$	=	estimation variance of y_V°	[-]
y_{DZ}°	=	log-transmissivity of the disturbed zone	[-]
$\sigma_{DZ^\circ}^2$	=	estimation variance of y_{DZ}°	[-]
J	=	objective function	[-]
$\overline{(h^*-h^\circ)^2}$	=	average square head residual	[m^2]
d_k	=	Kashyap criterion	[-]

Table 19: Results of calibration runs for model A and C

5.2.6 Model selection

The criterion of Kashyap (CARRERA & NEUMAN, 1986c) is used to select the appropriate conceptual model. This criterion, which consists of selecting the simplest model, allows more complexity to be built into the model as the amount of data increases. The model with the smallest value for the Kashyap criterion is the most adequate model regarding the available information. The results of the comparison of the value of the Kashyap criteria (see table 18 and 19) of models B and C with model A show that in both cases the addition of more parameters does not improve the consistency of the model with respect to the available information. To be able to detect anisotropic conditions within the shear zone or a disturbed zone around the drift, more head data would be necessary.

5.2.7 Conclusions

The results of the inverse modeling show that the conceptual model of the shear zone that is most consistent with the available data is the isotropic model with a single transmissivity zone.

The primary advantage of the inverse modeling approach is that it allows the linking of all the available quantitative information regarding a given model, and the improvement of the a priori estimates of the model parameters as well as the reduction of their uncertainty. Furthermore, alternative conceptual models can be tested and then selected using statistical criteria.

The quantification of the mean values of the parameters and their uncertainty as well as that of the head-information uncertainty are required before the calibration of the shear zone model. A methodology has been presented which allows the use of geostatistical and stochastic methods to quantify the various uncertainties related to the parameters and the head information.

The next step is to validate the inverse model of the shear zone. The validation of the shear zone model requires the definition of a validation experiment measuring one or more hydraulic properties of the shear zone, which then can be compared with the values predicted by the model. The value measured in the validation experiment should be within the interval defined by the estimation variance of the value predicted by the shear zone model. The scale of the validation experiment should be about the same size as the shear zone model.

The generalization of the inverse modeling approach to the calibration of numerical models is time saving with respect to calibration and, therefore, allows one to concentrate on testing and evaluation of a suite of conceptual models. The inverse modeling approach should then reduce conceptual uncertainty, i.e., the potential errors in the model structure or in the choice of relevant processes.

6 SUMMARY AND DISCUSSION

S. Vomvoris (Nagra)
B. Frieg (Nagra)
P. Bossart (Geotechnical Institute AG, Bern)

In the previous four chapters the Nagra activites within the VE-Test during the years 1988 -1990 were presented. In this chapter we summarize the activities, discuss some of the obtained results and conclude with the identification of areas where future investigations would be useful.

SUMMARY

Chapter 2: The geology in the ventilation test drift is dominated by tectonically deformed granodiorite gneisses (matrix) which are intersected by ductile mylonite shear zones of variable thickness. These ductile deformation structures can be linked with the Alpine greenschist metamorphism (20 Ma). During the course of regional uplift (5 Ma to recent) the ductile shear zones were reactivated and underwent brittle deformation. This lead to the formation of fault gouges, which are several mm thick particularly in areas of high deformation gradients. This brittle reactivation is also observed at the borders of lamprophyres. Concerning the flow path these fault gouges play the dominant role. In general, the fault gouges are hydrothermally not cemented, are highly porous (20 Vol%) and have practically no cohesion. The granodiorite gneisses have an interconnected network of grain boundary pores (porosity in the order of 1 Vol%). They provide a good hydraulic connection to the fault gouges in the shear zones. Visible water inflow into the drift is mostly bound to the shear zones which are brittely reactivated. One good example is the 10 m thick ventilation test shear zone. Ductile shear zones which are not reactivated seem to have a lower porosity than the granodiorites (in the order of 0.1 Vol%). Examples of such tight shear zones are found in the rear part of the ventilation drift. Due to the pore space geometry, the permeability in the shear zones is expected to vary considerably (reactivated-non reactivated shear zones), with permeability in the reactivated shear zones higher than in the matrix.

Chapter 3: The evaluation of macropermeability by performing a ventilation test is best suited for more or less homogeneous aquifers with simple initial hydraulic conditions around the drift. In the GTS the structures are heterogeneous (shear zones intercalated in the matrix) with a fabric anisotropy (cleavage planes). One useful approach is to evaluate the permeability of larger rock masses around the tunnel where the tectonic strains are uniform and the inflow does not vary substantially. This approach has been performed in the frontal part of the ventilation drift. A detailed water inflow balance into this frontal section (combination of ventilation test in the matrix with plastic sheeting in the shear zone) together with the pressure gradient of the parallel boreholes resulted in a matrix conductivity of 1.66E-11 m/s and a shear zone transmissivity (thickness 10 m) of 1.78E-9 m^2/s. The spatial and temporal variability of the evaporation rate was studied in the rear part of the drift. These rates vary between 0.1 $mg \cdot m^{-2} \cdot s^{-1}$ (limit of resolution) and about 6 $mg \cdot m^{-2} \cdot s^{-1}$. Zones of the highest permeability (fault gouges) show also the highest evaporation rates, which is confirmed by the flow path geometry.

Temporal variations were observed when the drift climate was changed (e.g. relative humidity). This is interpreted by removal and evaporation of the water stored close to the drift surface (e.g. water stored in the grain boundary pores of the granodiorite).

Chapter 4: The instrumentation of the boreholes with multipacker systems allowed the determination of the spatial distribution of the hydraulic heads around the ventilation drift. Based on simple test interpretation methods, it was possible to estimate approximate values of the hydrogeological parameters transmissivity, hydraulic conductivity, and storage coefficient of the matrix and the shear zone respectively. Additionally, it was possible to demonstrate hydraulic connections within the shear zones. The existing results are a basis for future field campaigns. Long-term injection tests, combined with a more detailed conceptual model for the test interpretation could help to confirm the assumptions made in Chapter 4.

Chapter 5, Section 1: Various observations show that a homogeneous, isotropic equivalent porous continuum model for the flow to the ventilation drift is oversimplified at this scale. A model which incorporates the local hydrogeologic structure provides, as expected, a much better representation. The methodological development of such a model was subject of this section. Several relatively simple models consistent with the geological investigation were used to predict the distribution of water pressure in a larger region around the ventilation drift. However, a comparison to control data collected afterwards in this region indicate the need to use the control data to recalibrate the models. Such validation studies are quite challenging because the collection of independent calibration and control data is very expensive and in low permeability rocks, the process of data collection may influence the actual values.

Chapter 5, Section 2: The results of the inverse modeling for the shear zone transmissivity show that for this scale the conceptual model of the shear zone most consistent with the available data is the isotropic model with a single transmissivity zone. The "macro"-transmissivity of the shear zone is 9.1E-10 m^2/s and its calculated confidence interval is 8.6 - 9.6E-10 m^2/s. The main purpose of this study was to develop an inverse modeling methodology combining the application of geostatistical and stochastic methods in order to estimate various model parameters and their uncertainties. The advantage of inverse modeling is that it locates the "optimal" parameter set for a given conceptual model and - through the error analysis - the confidence of the estimated values. It allows, thus, the modeler to concentrate on evaluating different conceptual models for interpreting the observations. A methodology has also been presented which allows the use of geostatistical and stochastic methods to quantify the a-priori mean values and the uncertainties related to the parameters and the head information. An application is illustrated in the text, albeit the obtained results should be taken with caution. For a more complete study, additional data and analysis could be used, e.g., transient head data in the shear zone and an assessment of the spatial distribution of the flow coming out of the shear zone (which might allow a characterization of the anisotropic conditions prevailing within the zone). In conclusion, the generalization of the inverse modeling approach to the calibration of flow and transport models is efficient (time saving) with respect to calibration and, therefore, allows one to concentrate on testing and evaluating a suite of conceptual models; it should therefore also reduce conceptual uncertainty, i.e., the potential errors in the model structure or the choice of relevant processes.

DISCUSSION

The calculation of macropermeability can be most successfully performed if there is a more or less homogeneous rock section around the tunnel drift and simple hydraulic conditions prevail. As the scale of the experiment increases it is harder to obtain these conditions. However, one could use the same principle and divide the tunnel into several slices of more or less homogeneous properties. In the ventilation tunnel five sections were initially selected, where more or less homogeneous tectonic strains were observed. In a further step these five sections were simplified into two different parts, a matrix- and a shear-zone part. It has been shown that the water inflow from the shear-zones is several times higher than in the matrix, if the shear-zones are brittlely reactivated (creation of predominant flow path). More important, under normal tunnel climate conditions the shear-zone inflows are liquid whereas the matrix inflows occur in the vapor phase (evaporation of water at or near the tunnel surface). This different hydraulic behaviour of shear-zones and matrix further justifies the division into quasi-homogeneous shear-zones- and matrix-parts respectively.

The methods for the derivation of the hydraulic poperties (transmissivity or hydraulic conductivity) were previously presented and the results of the four methods are shown in Figure 36 (method a: water balance; method b: hydrotests; method c and method d: modeling). The range of hydraulic conductivity in the matrix as determined by the hydrotest varies between 3.8E-12 and 2.2E-10 m/s. The hydrotests which were perfomed in matrix intervals lie close to the shear-zone and therefore seem to reflect partly the shear-zone permeability. Hydraulic conductivities which are higher than 1E-10 m/s in the matrix have to be interpreted with caution.

The range of transmissivity in the tested shear-zone is quite small (Figure 36). It varies between 4.6E-10 and 6.0E-9 m^2/s. The application of the inverse modeling (homogeneous shear-zone) results in smaller transmissivity range than the trial and error method. Both methods c) and d) provide an estimate of the effective or average transmissivity hydraulic conductivity valid at a much larger seale, which is expected to be less variable. Note that, both modeling methods are using field data of a) and especially b) as soft or hard (head values) input. If for example the packed off intervals of b) were deerased from between 10 and 15 m long to some decimeters long and covered only the relevant flow path zones (fault gouge networks in shear-zone), a much higher transmissivity would result in b); estimated local transmissivites for such zones could be two orders of magnitude higher. Consequently, the "error" around the "effective" mean calculated from method d) could potentially increase.

A slightly different method to calculate the permeability in different lithological units of the ventilation drift is to apply the discrete measured evaporation rates (Chapter 3.3) and to incorporate them either as deterministic or probabilistic boundary information at the tunnel surface. Reliable information on the hydraulic head distribution in the rock volume and at the outer model boundary, is of course still necessary. It is hoped to undertake such modeling in future phases of GTS.

One of the most significant observations of the Ventilation Test was the indication of "unsaturated" or "dryed-out" regions of the low permeability rocks. In the previous chapters this was coined as "removing water from storage" implying a transient and multiphase phenomenon. The extent of the unsaturated zone, its influence on the hydraulic properties estimated using simple models, and its reversibility are topics that have been planned for the following phases of the GTS. A better understanding of these effects will provide the basis for an improved design of ventilation experiments and for appropriate choice of interpretation models. Similar phenomena may have been observed elsewhere (e.g. Stripa), but our sensitivitiness can be considered one of the most beneficial accomplishments of the Phase 2 to the topic (VE-Test).

In conclusion, under the "Ventilation Test" during Phase 2 Nagra has, in cooperation with GSF, initiated a series of activites relating to the geological characterization of crystalline rocks, the measurements of inflows into drifts constructed in low-permeability rocks, the performance of hydraulic experiments in such rocks, as well as the development of methods and tools for the interpretation of the obtainded values. Areas for future applied research have been identified and provide the basis for designing experiments for the next GTS phases; the results will further improve our ability to characterize and predict groundwater flow in low permeability rocks in the vicinity of a drift , in particular with respect to deep geological radioactive waste disposal.

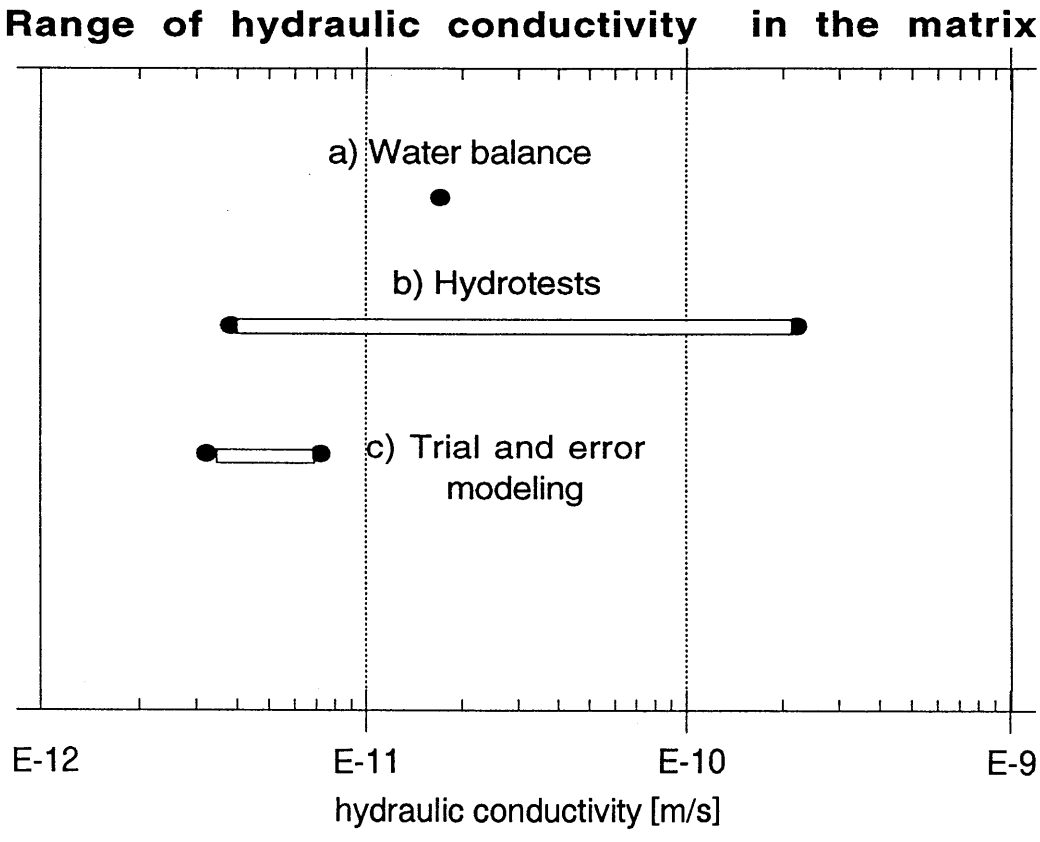

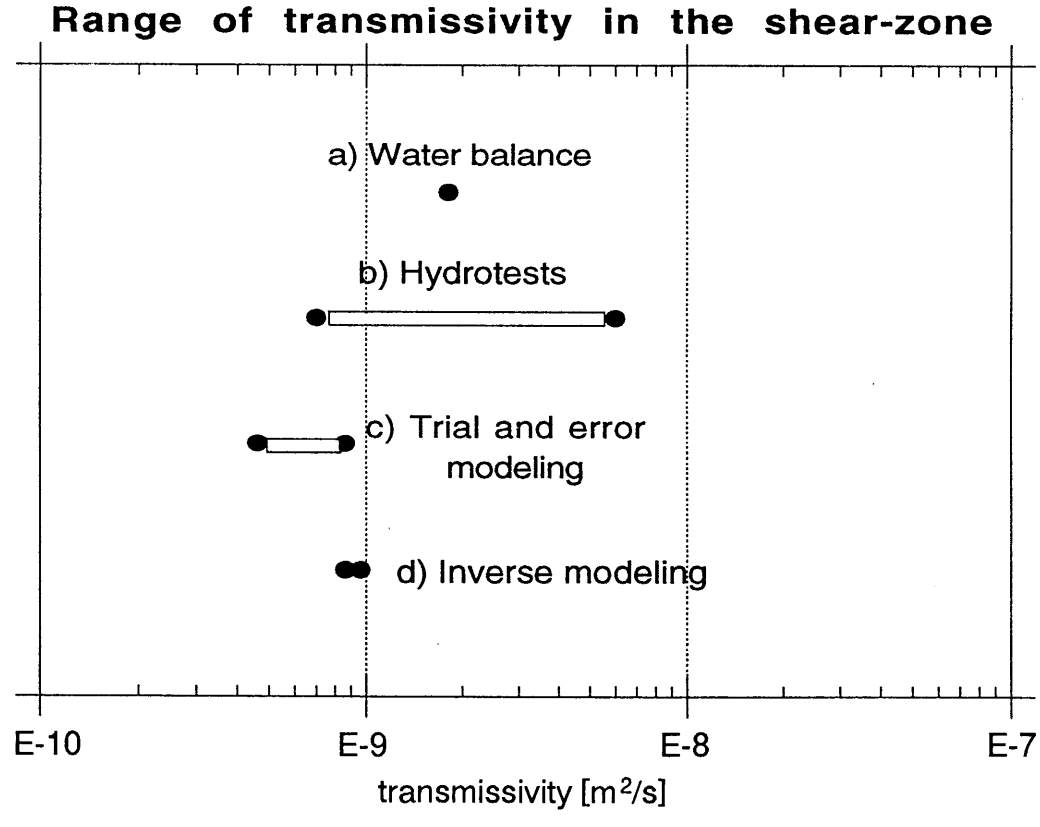

Figure 36: Hydraulic conductivity (matrix) and transmissivity derived by different methods

7 REFERENCES

ADANK, P. & VOBORNY, O. (1989): Modellierung der Grundwasserströmung im Gebirgskörper um das Felslabor Grimsel: Lokalmodell FLG 1989, Project MOD, Jahresbericht 1989. - Nagra Internal Report; Baden (Nagra).

AHMED, S. (1987): Estimation des Transmissivités des Aquifères par Méthodes Géostatistiques Multivariables et Résolution Indirecte du Problème Inverse. - Thèse, Ecole Nationale Supérieure des Mines de Paris.

ARMSTRONG, M. (1981): Basic Geostatistics Applied to Coal. - C-87, Centre de Géostatistique, Fontainebleau, France.

ARN, TH. (1989): Numerische Erfassung der Strömungsvorgänge im geklüfteten Fels. - Dissertation, IBETH, Fels- und Untertagebau, Mitteilung 1/89.

ARN, TH. & GMÜNDER, CH. (1991): Benutzeranleitung AQUA-ROCK. - Costra SA, 6900 Lugano-Cassarate.

BEAR, J. (1972): Dynamics of Fluids in Porous Media. - American Elsevier.

BELANGER, D.W., FREEZE, G.A., LOLCAMA, J.L. & PICKENS, J.F. (1987): Interpretation of Hydraulic Testing in Crystalline Rock at the Leuggern Borehole. - Nagra Technical Report, NTB 87-19.

BERTHE, D., CHOUKROUNE, P. & JEGOUZO, P. (1979): Orthogneiss, mylonite and non-coaxial deformation of granites: the example of the South Amorican Shear Zone. - J. Str. Geol. 1, p. 31 - 42.

BIDAUX, P. & TSANG, C.-F. (1991): Fluid Flow Patterns Around a Well Bore or an Underground Drift With Complex Skin Effects. - Water Resources Research, Vol. 27, No. 11, p. 2993 - 3008.

BOSSART, P. & HUFSCHMIED, P. (1989): Ermittlung von Kluftzuflüssen durch Folienabdeckung, Ventilationsstollen, FLG. - Nagra Internal Report; Baden (Nagra).

BOSSART, P. & MARTEL, S. (1990): Ductile and brittle deformations in the Grimsel Crystalline, Upper Aare Valley, Switzerland. - Nagra Internal Report; Baden (Nagra).

BOSSART, P. & MAZUREK, M. (1991): Structural geology and Geometry of Water Flow-path in the Migration Shear-Zone, Grimsel Test Site. - Nagra Technical Report, NTB 91-12; Wettingen (Nagra).

BRADBURY, M.H. (ed) (1989): Grimsel Test Site: Laboratory investigations in support of the migration experiments. - Nagra Technical Report, NTB 88-23; Baden (Nagra).

BRASSER, T. (1987): Der Ventilationstest, ein untertägiger Versuch zur Ermittlung der Gebirgspermeabilität. - Bergbau 12/87.

BRASSER, T. & KULL, H. (1986): Ventilationsversuch (VE) im Felslabor Grimsel. - Gesellschaft für Strahlen- und Umweltforschung mbH, München, Interner Bericht.

BRASSER, T. & KULL, H. (1987): Ventilationsversuch (VE) Phase 2 im Felslabor Grimsel. - Gesellschaft für Strahlen- und Umweltforschung mbH, München, Interner Bericht.

BREWITZ, W. & KULL, H. (1992), (in preparation): Der Ventilationstest zur Bestimmung der mittleren Gebirgsdurchlässigkeit (Makropermeabilität) von geklüftetem Kristallin. - Nagra Technical Report, NTB 91-02.

BREWITZ, W. & PAHL, A. (1986): German Participation in the Grimsel Test Site (GTS) in Switzerland - -Targets and Methods of in-situ Experiments in Granite for Radioactive Waste Disposal. - IAEA-SM-289, Int. Symp. on the Siting Design and Construction of Underground Repositories for Radioactive Wastes, Hannover, Germany, March 3 - 7.

BROWN, D.M. (1984): Stochastic Analysis of Flow and Transport in a Variable-Aperture Rock Fracture. - MSc Thesis, MIT.

CARRERA, J. & NEUMAN, S. (1986a): Estimation of Aquifer Parameters Under Transient and Steady State Conditions: 1. Maximum Likelihood Method Incorporating Prior Information. - Water Resources Research, Vol. 22, No. 2, p.199 - 210.

CARRERA, J. & NEUMAN, S. (1986b): Estimation of Aquifer Parameters Under Transient and Steady State Conditions: 2. Uniqueness, Stability and Solution Algorithms. - Water Resources Research, Vol. 22, No. 2, p.211 - 227.

CARRERA, J. & NEUMAN, S. (1986c): Estimation of Aquifer Parameters Under Transient and Steady State Conditions. 3. Application to Synthetic and Field Data. - Water Resources Research, Vol. 22, No. 2, p.228 - 242.

CHOUKROUNE, P. & GAPAIS, D. (1983): Strain pattern in the Aar granite (Central Alps): Orthogneiss developed by bulk inhomogeneous flattering. - J. Struct. Geol. 5: 411 - 418.

COOPER, H.H. & JACOB, C.E. (1946): A generalized graphical method for evaluating formation constants and summarizing well field history. - Am. Geophys. Union Trans., Vol. 27, No. 4, p. 526 - 534.

CURE-CLAUSTHALER UMWELT UND RESERVOIR ENGINEERING GMBH (1990): Auswertung hydraulischer Tests, Felslabor Grimsel. - GSF Interner Bericht; Braunschweig (GSF).

DE MARSILY, G., LAVEDAN, G., BOUCHER, M. & FASANINO, G. (1984): Interpretation of Interference Tests in a Well Field using Geostatistical Techniques to Fit the Permeability Distribution in a Reservoir Model. - Geostatistics for Natural Resources Characterization, Part. 2, Reidel Publishing Company.

FLINN, D. (1962): On folding during three-dimensional progressive deformation. - Q.J. Geol. Soc. London, 118, p. 385 - 428.

GMÜNDER, CH. (1988): FLG, Modellierung Ventilationstest. - Nagra Internal Report; Baden (Nagra).

GMÜNDER, CH. (1990): FLG: Modellierung Ventilationstest, Vergleich Prognosen-Messungen. - Nagra Internal Report; Baden (Nagra).

GOODMAN, R.E. et al. (1965): Groundwater inflows during tunnel driving. - Ing. Geol., Vol. 2, page 39-56.

HAHN, G.J. & SHAPIRO, S.S. (1967): Statistical Models in Engineering. - John Wiley & Sons.

HEINIGER, P. (1989a): FLG, Ventilationstest, Hydraulische Tests Phase 1, Funktionskontrolle der Packersysteme BOVE 88.001, 88.002, 88.003 (BOVE 88.004). - Nagra Internal Report, Juni 1989.

HEINIGER, P. (1989b): FLG, Ventilationstest, Hydrogeologische Untersuchungen in den Bohrungen BOVE 88.001, 88.002, 88.003, 88.004 und in der Bohrung 80.005. - Nagra Internal Report; Baden (Nagra).

HORNER, D.R., (1951): Pressure build-up in wells. - Third World Pet. Congress Sect. II, E.J. Bull., Leiden, p. 503 - 521.

IROUSCHEK, A. & BOSSART, P. (1989): Ventilationstest, geologischer Bericht der vier Validierungsbohrungen BOVE 88.001 - 88.004.- Nagra Internal Report; Baden (Nagra).

JACOB, C.E. & LOHMANN, S.W. (1952): Nonsteady flow to a well of constant drawdown in an extensive aquifer. - Transactions, Am. Geoph. Union, Volume 33, No. 4, p. 559 - 570.

JAQUET, O. & THOMPSON, B. (1991): Inverse Modelling in the Macro-permeability Experiment at the Grimsel Test Site. - Nagra Internal Report; Wettingen (Nagra).

JOB, D., RESELE, G. & WACKER, C. (1988): Hydrogeologic Modelling of the Chalk River Block. - Colenco report, Baden-Switzerland (Colenco).

KEUSEN, H.R., GANGUIN, J., SCHULER, P. & BULETTI, M. (1989): Felslabor Grimsel, Geologie. - Nagra Technical Report, NTB 87-14; Baden (Nagra).

KOVARI, K., ARN, TH. & GMÜNDER, CH., (1989): Groundwater Flow through Fissured Rock: Field Investigations and Interpretaiton in the Albigna Dam Area, Graubünden, Switzerland. - Nagra Technical Report, NTB 90-10; Baden (Nagra).

KRALIK, M., CLAUER, N., HOLNSTEINER, R., HUEMER, H. & KAPPEL, F. (in preparation): Recurrent fault activity in the Grimsel Test Site (GTS, Switzerland): revealed by Rb-Sr, K-AR and Tritium isotope techniques. - Nagra Technical Report.

KULL, H. (1988): Ventilationsversuch (VE) Phase 2 im Felslabor Grimsel. - Gesellschaft für Strahlen- und Umweltforschung mbH, München, Interner Bericht.

KULL, H. (1989): Ventilationsversuch (VE) Phase 2 im Felslabor Grimsel. - Gesellschaft für Strahlen- und Umweltforschung mbH, München, Interner Bericht.

LOHMANN, S.W. (1972): Groundwater Hydraulics. - United States Government Printing Office, Geological Survey professional paper 708, p. 23 - 27.

MARQUER, D., GAPAIS, D. & CAPDEVITA, R. (1985): Comportement chimique et orthogneissification d'une granodiorite en faciès schistes verts (Massif de l'Aar, Alpes Centrales). - Bull. Minéral. 108: 209 - 221.

MARTEL, S.J. & PETERSON, J.E. Jr. (1991): Interdisciplinary Characterization of Fracture Systems at the US/BK Site, Grimsel Laboratory, Switzerland. -Int. J. Rock Mech. Min. Sci. Geomech. Abstr. 28/4: 295 - 323.

MOYE, D.G. (1967) Diamond Drilling for Foundation Exploration. - Civil Eng. Trans., Inst. Eng. Australia, April 1967, pp. 95 - 100.

NAGRA, (1985): Grimsel Test Site - Overview and Test Programs. - Nagra Technical Report, NTB 85-46; Baden (Nagra).

NEUMANN, S.P. (1987): Stochastic Continuum Representation of Fractured Rock Permeability as an Alternative to the REV and Fracture Network Concepts. - 28th US Symposium on Rock Mechanics, Tucson.

RAMSAY, J.G. & HUBER, M.I. (1987): The techniques of modern structural geology. - Academic Press, London (2 vol.), 700 pp.

ROUHANI, S. & WACKERNAGEL, H. (1990): Multivariate Geostatistical Approach to Space-Time Data Analysis. - Water Resources Research, Vol. 26, No. 4, p. 585 - 591.

SCHNEEBELI, M., BAER, T., WYDLER, H. & FLUEHLER, H. (1991): In situ measurements of water potential and water content in unsaturated granitic rock. - Proceedings of NEA-OECD " workshop on Gas and Release from Radioactive Waste Repositories, Aix-en-Provence, France, 23rd - 26th September 1991". at al., 1991.

SNOW, D.T. (1965): A Parallel Plate Model of Fractured Media. - ph. d. thesis, Berkley.

THIEM, G. (1906): Hydrologische Methoden. - Gebhardt, Leipzig, 56 p.

UEDA, M. (1956): Measurement of the gradient of water-vapor pressure and the diffusion coefficient. - Japan J. Applied Physics, pp 144 - 149.

WATANABE, K. (1991a): Evaporation Measurements at the Grimsel Test Site - Nagra Internal Report; Wettingen/Switzerland (Nagra).

WATANABE, K. (1991b): Evaporation Measurements in the Validation drift - Part 1. - Stripa Technical Report, TR 91-06.

WATANABE, K., AIZAWA, T., ONO, M., YANAGISAWA, K., SAKUMA, H., YAMAMOTO, H. & KANDA, N. (1989): Evaporation measurement for mapping the groundwater discharge over a tunnel wall of low permeability. - Journal of the Japan Society of Engineering Geology, Vol. 30, No. 4 pp 189 - 196.

WATANABE, K. & OSADA, M. (1991): Evaporation Measurements in the Ventilation drift - Part 2. - Stripa Technical Report, TR 91-27.

WOODCOCK, N.H. (1979): Specification of fabric shapes using an eigenvalue method. - Geol. Soc. Amer. Bull. 88: 1231 - 1236.

ZIEGLER, B.P. (1976): Theory of Modelling and Simulation. - Wiley & Sons.